Aspects of Brushless Doubly-Fed Induction Machines

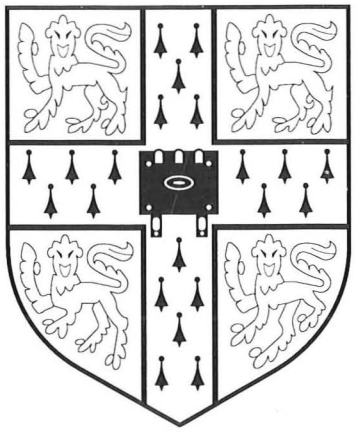

DISSERTATION SUBMITTED TO THE
UNIVERSITY OF CAMBRIDGE
FOR THE DEGREE OF
DOCTOR OF PHILOSOPHY

Michael Stephen Boger
St. John's College
August 1997

Indexing terms

Brushless Doubly-Fed Induction Machine (BDFM)

Cascaded Induction Machine

Induction Motor

Harmonic Analysis

DQ Analysis

Inter-bar Currents

Declaration

The author wishes to declare that, except for commonly understood and accepted ideas or where reference is made to the work of others, the work in this dissertation is his own and includes nothing which is the outcome of work done in collaboration. It has not been submitted in part, or in whole, to any other university for a degree, diploma or other qualification.

M. S. Boger
St. John's College
September 1997

Acknowledgements

This work could not have been so easily completed without the moral and financial support of others. I am eternally grateful to my parents who have always given me love and encouragement.

I thank my former supervisor, Professor Alan Wallace of Oregon State University, who first introduced me to the complexities of electrical machines and, over the past ten years, has become a good friend.

I thank my current supervisor, Professor Stephen Williamson, who has enabled this research financially and given me the opportunity to study at Cambridge. With his inspiration and guidance I've been able to understand harmonic analysis and gain more insight into the operation of the BDFM.

I also thank my friends here at Cambridge who have always been there to discuss ideas with. Special thanks to Douglas Carter and Benjamin Gordon, who have given me inspiration and the knowledge that engineering can be fun.

Finally I wish to thank the technicians who have assisted in configuration of the laboratory apparatus and in the administration of the lab. Special thanks to John Grundy who has borne the brunt of this work.

May I always keep learning.

Summary

This dissertation, composed of two parts, studies the brushless doubly-fed induction machine (BDFM)—an electric machine with two stator windings, a modified cage-rotor, and, when run synchronously, the electrical properties of a synchronous machine, i.e. precise speed and power-factor control.

The first part of this dissertation is dedicated to the development of a two axis (dq) model to aid in design of the BDMF. It improves on the properties of similar models by allowing for the determination of the individual rotor-bar currents and the components of electromagnetic torque produced by each of the two stator windings. The model has the ability to predict both dynamic and steady-state behaviour, the latter verified by experiment and by comparison to predicted results of a different model of the BDFM.

The second part of this dissertation, which is the primary focus of this dissertation, is concerned with the phenomenon of inter-bar rotor currents, those which flow between the rotor bars through the rotor iron. Experiments have shown that these currents, present in virtually all die-cast rotors for all types of induction-based machines, seriously degrade the performance of the BDFM by causing increased rotor losses, reduced efficiency, increased stator input power, and increased stator currents, especially when used as a motor. To understand this phenomenon and predict its effect on machine performance, a coupled-circuit model is developed based on harmonic analysis. It is verified through experiments using a specially fabricated rotor in which the rotor bar to rotor iron contact has been promoted. Investigations are conducted using the model to determine the minimum level of insulation needed to obtain satisfactory performance. Results show that the rotor bars must be insulated to an order of magnitude greater than that achieved in the normal die-casting process.

List of Principal Symbols

Symbols in boldface signify vector or matrix quantities (e.g. $\mathbf{Z}$. Variables with an over-bar (e.g. $\bar{V}$) are complex phasors and those with an arrow over them (e.g. $\vec{c}$) are vectors.

dq Model

Primary Symbols

Primed variables (R'), unless specified otherwise, refer to quantities in the rotor reference frame.

$\mathbf{C}$	Transformation matrix.
I, i	Current (A).
L	Inductance (H).
L_l	Leakage inductance (H).
L_m	Magnetising inductance (H).
M	Mutual inductance (H).
N_l	Number of rotor loops.
N_n	Number of rotor nests.
P	Number of pole-pairs.
R, r	Resistance (Ω).
T, T_e	Electromagnetic torque ($\mathrm{N} \cdot \mathrm{m}$).
V, v	Voltage (V).
Z	Impedance (Ω).
$\Im$	Signifies the "imaginary part of" operator.

$\Re$	Signifies the "real part of" operator.
α	Displacement angle between the magnetic axis of the second winding and the reference axis (rad).
β	Electrical separation angle between rotor nests (rad).
γ	Phase angle of the second winding voltage (rad).
ω	Angular velocity (rad/s).
ϕ	Phase angle of a current (rad).
θ	Angle (rad).
f	Frequency (Hz).
j	$\sqrt{-1}$.
l'	Leakage inductance of a common rotor bar in a Type III rotor (H).
r'	Resistance of a common rotor bar in a Type III rotor (Ω).
t	Time (s).

Subscripts

1	Winding 1 quantity.
2	Winding 2 quantity.
0	Zero sequence quantity.
A	First phase of a three-phase quantity.
B	Second phase of a three-phase quantity.
C	Third phase of a three-phase quantity.
R	Rotor quantity.
d	d axis quantity.
q	q axis quantity.

Superscripts

T	Transpose.
$*$	Complex conjugate.

Inter-bar Current Model

Primary Symbols

B, b	Flux density (Wb/m^2).
C	Conductor density function coefficient (1/m).
E, e	Electric field (V/m).
I, i	Current (A).
J, j	Current density (A/m).
K_b	Slot width factor.
K_d	Distribution factor.
K_p	Pitch factor.
K_{sk}	Skew factor.
L_l	Leakage inductance (H).
N_c	Number of cuts made in the rotor.
N_{eq}	Number of independent rotor loop circuits.
N_l	Number of rotor loops within each nest.
N_n	Number of rotor nests.
N_{ph}	Number of series turns per phase.
N_s	Number of stator slots.
P	Number of pole-pairs.
R	Resistance (Ω).
$\vec{R}, \vec{r}$	Position vector.
T	Torque (N $\cdot$ m) or turns per coil.
U, u	Voltage (induced) (V).
V, v	Voltage (V).
W	Axial length of the motor (m).
Z	Impedance (Ω).
$\Im$	Signifies the "imaginary part of" operator.
$\Re$	Signifies the "real part of" operator.
α	Span of a stator coil (m).
γ	Skew angle of the rotor (rad).
κ, λ, μ	Harmonic number.

μ_0	Permeability of free space (H/m).
ω	Angular velocity (rad/s).
ω'	Angular velocity of the currents in the rotor (rad/s).
ω''	Angular velocity of the voltages induced in the stator by currents flowing in the rotor (rad/s).
σ	Span of a rotor current-loop (m).
$\hat{a}$	Direction vector.
b_s, b_R	Slot width of the stator or rotor (m).
c	Conductor density function (1/m).
d	Machine diameter to the air-gap (m).
f	Force (N).
g	Air-gap length (m).
j	$\sqrt{-1}$.
k, l, m	Harmonic wave number (1/m).
t	Time (s).
v	Velocity of the rotor (m/s).
w'	Distance between adjacent cuts (m).
x	Axial coordinate in the SRF.
x'	Axial coordinate in the RRF.
x''	Axial coordinate in the skewed RRF.
y	Circumference coordinate in the SRF.
y'	Circumferential coordinate in the RRF.
y''	Circumferential coordinate in the skewed RRF.
z	Radial coordinate.

Subscripts

0	Initial position or reference quantity.
1	Winding 1 quantity.
2	Winding 2 quantity.
A	First phase of a three-phase quantity.
B	Second phase of a three-phase quantity.
C	Third phase of a three-phase quantity.

R	Rotor quantity.
S	Stator quantity.

Superscripts

T	Transpose.
κ, λ, μ	Harmonic number.
$*$	Complex conjugate.

List of Figures

List of Tables

Contents

Chapter 1

Introduction

Many industrial processes have a need for variable speed operation. This need is met by different variable-speed drives composed of a motor and some method of control. Historically this control was performed using rheostats connected to either the drive motor or other auxiliary motors needed to obtain variable speed operation. Resistance control was inherently inefficient and has been virtually superseded by power-electronic converters capable of providing a more efficient method of control. With the cost of electronics falling constantly, more companies are using power-electronic based variable-speed drives instead of resistance based drives. However, the cost of the power-electronic converter still represents a significant portion of the total cost of the drive. Wallace, Speé and Lauw, researchers at Oregon State University, have proposed a drive based on the brushless doubly-fed machine (BDFM) which uses a converter rated at a fraction of the output power of the drive [1]. The drive system has the following properties which make it a strong candidate for many applications:

- low power rating converter
- precise speed control
- power factor control
- robust construction
- free from brushes and slip rings

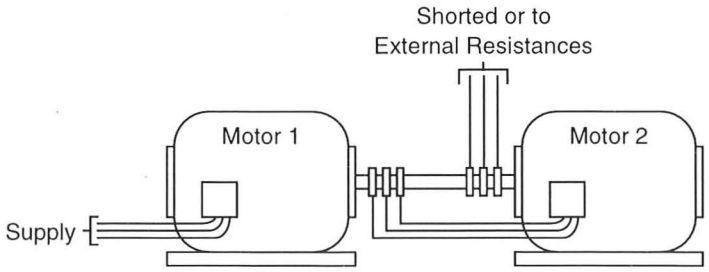

Figure 1.1: Cascaded connection of two wound-rotor induction machines.

1.1 Background

The origins of the BDFM lie in work done on cascaded induction machines. The cascade connection of two induction machines has been recognised as one method of obtaining low-speed operation since the turn of the century. In this configuration, shown in Fig. 1.1, two wound-rotor induction machines are mechanically connected to the same shaft and load, with the stator winding of the first machine connected to the mains (supply) and the rotor winding of the first machine connected to the stator winding of the second machine. The rotor winding of the second machine may be either short-circuited or connected to external resistances for speed control. If the first machine has $2P_1$ poles and the second $2P_2$ poles, the cascaded configuration will behave like a $2(P_1 + P_2)$ induction machine.

Louis Hunt, in a 1907 meeting of the Institute of Electrical Engineers held in Manchester, described the operation of the cascade induction machine [2] with a more detailed description following in his second paper read in the same venue in 1914 [3].

> "At the synchronous speed of an induction motor no energy is transmitted to the rotor, and if we assume that the distribution of flux follows a sine law, there will be no currents in the secondary windings. If, then, the mains are connected to the rotor of a machine the latter will revolve in a direction opposite to that of its magnetic field, so that at synchronous speed the field will be stationary in space and no electromotive force will be generated in the stator windings which now form the secondary of the motor. Instead of connecting the rotor windings of the first motor to the stator windings of the second machine, we may connect them to the second rotor windings, taking care to reverse two of the connections so that

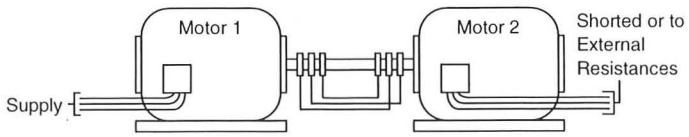

Figure 1.2: The modified cascaded connection of two wound-rotor induction machines.

> with currents circulating in both windings the magnetic fields produced will rotate in opposite directions. The stator winding of the second motor now becomes the secondary, and the rotor windings may be permanently connected without slip rings."

The speed of this motor, as well as its starting torque, was controlled by external resistances connected to the stator windings of the second machine. This modified connection of two wound-rotor induction machines is shown in Fig. 1.2

Hunt, combining the two machines into a single frame, sought to reduce both the cost and the complexity as well as improve the operating characteristics [2]. His new motor did not need slip rings and utilised multiple rotor windings. The stator consisted of a single, parallel-connected, three-phase winding which, depending on the connection points used, behaved like two different windings with different pole numbers. In his subsequent paper he gave greater detail of the design, construction, and operation of the machine based on its performance record during seven years of industrial use from 1907–1914 [3].

In 1921 Creedy followed up Hunt's paper by describing the theory behind the single stator winding as well as providing innovations in the design of the stator and rotor windings [4]. His work on the rotor windings provided the groundwork for the replacement of the complicated multiple rotor windings with a series of bars formed into nested loops [4]. Creedy also presented further refinements to Hunt's analysis with examples of situations where cascaded machines were being used: "collieries, quarries, etc., for driving all classes of machines, particularly haulage gears, crushers, etc., and for many other purposes, including printing presses, paying-out gear in cable ships, etc."

The research effort on the single-frame cascaded induction machine lay dormant for 45 years until in 1966 B. H. Smith, a professor at a university in Australia, conducted research into this machine, renaming it a "twin stator induction machine," [5] and developed a steady-state performance model based on induction

motor equivalent circuits. In 1967 he showed that the machine could also operate synchronously by exciting the second stator winding with a variable frequency supply [6]. When doubly-fed, the speed of the machine was precisely dictated by the frequencies of the applied voltages and the pole numbers of the stator windings.

Smith verified his results on a test apparatus that consisted of a concatenation of two wound-rotor induction machines. The shafts of the two motors were connected to a chain and sprocket assembly, allowing the effects of the relative angular displacements between the rotors to be investigated during synchronous operation. This established the existence of an internal torque angle during synchronous operation similar to that of a synchronous machine. In fact, by ignoring the resistance of the stator windings and rotor, an equivalent circuit of the form voltage-behind-reactance results, just like that of the simplified synchronous machine model. Smith et al. continued their research with investigations of stability in 1979 [7] and development of refined equivalent models [8, 9] with the last paper being published in 1993[1].

In 1970 Broadway and Burbridge, researchers at the University of Bristol, began conducting research into the single-frame cascaded induction machine developed by Hunt [10]. The research conducted was not related to the work by Smith, and indeed, Broadway and Burbridge were unaware of his work. They investigated both asynchronous and synchronous operation. The synchronous operation was concerned solely with dc excitation applied to the second winding unlike the variable frequency excitation investigated by Smith.

Broadway and Burbridge's motor used a single three-phase winding with multiple parallel paths which, depending on the way in which the coils were supplied, appeared as a winding with 18 poles and one with 12 poles simultaneously. The published paper contained a comprehensive analysis based on induction-motor theory as well as some fundamental design guidelines concerning the selection of stator-winding pole numbers and rotor configuration. In particular, they paid particular attention to the rotor design and recommended the use of rotor bars instead of windings for the rotor, backing up Creedy's findings.

[1] Curiously, Smith's work has mostly gone unnoticed. This is probably due to calling the machine a twin stator induction machine—a name not normally used in literature searches.

It is worth noting that the performance characteristics of the single-frame cascaded induction machine could also be achieved by using a single, large pole-number wound-rotor induction machine. However, such a machine would have the disadvantages of being much larger than the single-frame cascaded machine and would use slip rings—not desirable for some applications, especially those related to the mining industry.

In 1978 Kusko and Somuah analysed a single-frame cascaded machine that used two separate stator windings [11]. The first winding was connected to the mains and the second to the mains via a thyristor based inverter-rectifier, with the power-electronic converter allowing synchronous operation over a varied speed range. Results showed that the power factor could be controlled by varying the firing angle of the thyristors. Below the speed corresponding to dc excitation of the second winding ($f_1/(P_1+P_2)$, f_1 the supply frequency), the power flowed from the second winding to the supply when the machine was used as a motor. Above that speed, the power flow was reversed.

In 1989, A. K. Wallace et al. published results of research into a detailed equivalent circuit developed for the motor capable of modelling the transient behaviour of the machine [12, 13]. Their single-frame machine consisted of a single stator winding and a rotor similar to that described by both Hunt and Broadway and Burbridge. The stator winding consisted of both a six-pole system and a two-pole system depending on the connection points used[2]. A bi-directional power-electronic converter was used to allow power flow to and from the two pole winding system. At this time, the motor began to be referred to as a brushless doubly-fed induction machine (BDFM). The research effort continued with the development of a *dq* (two axis) model presented in 1991 [14, 15]. The utility of the model was further demonstrated in [16].

Experiments and simulations showed both the speed and power factor of the BDFM could be controlled with the level of desired control dictated by the size of converter necessary. For many perceived applications the rating of the converter could be greatly reduced (e.g. 20% of the total power output of the machine) [13]. The research was funded by a consortium of government and private organisations

[2]Later prototypes used two separate stator windings.

keen on transferring the technology to industry[3] for the following applications:

- limited or wide speed range pump drives, especially those operating in environments not suited for slip rings, commutators or brushes [11];
- brushless synchronous motors and generators where slip rings and brushes cannot meet environmental or mean time between failure (MTBF) requirements [11];
- variable-speed generators for use in wind-power generation [17] or automotive alternators [18];
- propulsion system for mass transit vehicles [19];
- stand-alone or stand-by diesel powered generator systems;
- high voltage applications where a lower voltage converter can be used [20].

The models presented by Wallace et al. were specific to a BDFM with stator winding systems of six and two poles, severely limiting their applicability to other combinations of pole numbers on the stator. The limitations were removed when Boger, Wallace, Speé and Li presented a general pole-number model in [21]. Based on *dq* analysis, it allowed for both dynamic and steady-state simulations. However, like its predecessor in [14], the effects of all the rotor loops were modelled by a single pair of coils. This simplification reduced the complexity of the model but at the expense of the identification of the individual rotor loop currents.

The overall performance of the machine could now be predicted. However, without knowledge of the actual rotor-loop currents, informed decisions about the rotor design could not be made, e.g. balancing of the rotor losses between the different rotor loops. To determine the rotor currents and aid design, another model was developed by this author based on the work in [21]. The development of this model is one aspect of this thesis and is presented in Chapter 2, a summary of which was presented in [22].

[3]This was motivated by a patent secured by the consortium and Oregon State University in 1989 for a BDFM using a power-electronic converter.

Subsequent to this development, Ferreira, Williamson, and Wallace published work describing another model in 1997 [23, 24]. This model provided greater accuracy between predicted and measured results as well as more insight into the electromagnetic mechanism that produces synchronous operation. The model's strength derives from its treatment of the spatial harmonics due to the non-sinusoidal distribution of the stator and rotor windings. It is based on harmonic analysis, an analysis technique developed by Williamson [25, 26]. The model is currently only able to predict steady-state performance. However, it does provide a very flexible, though slightly more complicated model suitable for machine design. It can be shown that the *dq* model and this harmonic model are equivalent when the fundamental (principal) spatial harmonics alone are considered in the harmonic model.

Significant cost savings can be made in mass production if the rotor of the BDFM is die-cast instead of being hand-fabricated. With commercialisation in mind, in 1994 the Oregon State University (OSU) research team ordered a die-cast rotor for the BDFM from a major motor manufacturer. The rotor was constructed using the same techniques used in the casting of squirrel cage rotors. Upon receipt, the rotor was placed into a BDFM and tested. The resulting performance was disastrous. The stator currents were far greater than expected with the result that the BDFM had difficulty synchronising, if at all, and suffered from poor efficiency. Through collaborative work with the University of Cambridge, it became apparent that inter-bar currents may be a possible cause of the problem—something never considered previously in the analyses.

These currents are always present in die-cast rotors to some extent. However, their effect is mitigated by the fact that the resistance of the rotor bars is significantly less than that between the bars so that the current is primarily constrained within the rotor bars themselves. However, the inter-bar current phenomenon is still not thoroughly understood though some insight was provided by two papers investigating the effect of inter-bar currents in single phase motors [27, 28]. Although partially understood in single-phase motors, the effects of inter-bar currents on the BDFM were not known. This lack of understanding, and a desire to produce a better design and possible industrially viable motor, motivated research into this phenomenon.

In order to understand the effects of inter-bar currents, a coupled-circuit model was developed based on the harmonic model presented in [23] and using a similar method to describe the rotor as that proposed in [27]. The result was the coupled-circuit harmonic model, described in Chapter 3, which allowed for the flow of inter-bar currents between adjacent rotor bars. The majority of this dissertation is concerned with this model, developed to answer three questions,

- What effects do inter-bar currents have on a BDFM?
- Are inter-bar currents the cause of the observed performance degradation?
- If inter-bar currents are detrimental to machine performance, how well should the bar be insulated from the rotor iron? i.e. what threshold level of resistance must be achieved?

The answers to these questions as well as a verification of the model are discussed in Chapter 4.

In summary, this dissertation presents both a *dq* model and a harmonic inter-bar current model. The *dq* model facilitates design and represents an improvement over existing *dq* models by allowing the rotor loop currents to be determined. It allows for prediction of both transient and steady-state performance, although the primary focus is on the latter. The inter-bar current model provides insight into the practical problems realised when using a die-cast rotor. It enables the performance of a BDFM under the influence of inter-bar currents to be predicted and investigates the level of resistance necessary to mitigate this problem. To provide a foundation for these analyses, a more detailed description of the BDFM is provided.

1.2 Description of the BDFM

A BDFM is a single-frame cascaded induction machine consisting of two three-phase stator windings. The first winding, referred to as the power winding, has P_1 pole-pairs and the second winding, referred to as the control winding, has P_2 pole-pairs. Two constraints exist for the set of pole-pair numbers for both windings. Firstly, both windings must not have the same pole-pair number in order to avoid

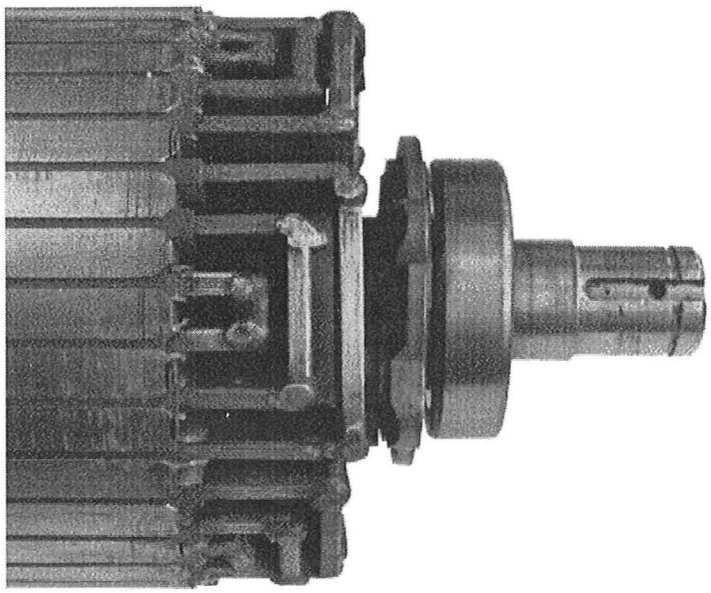

Figure 1.3: Picture of a BDFM cage rotor with six nests (three shown), each with three loops.

transformer-type coupling [2, 3, 4]. Secondly, the difference in pole-pair numbers must be greater than one to prevent unbalanced magnetic pull [3, 4, 10].

The rotor of the BDFM is unique and is critical to synchronous operation. It is a modified form of induction motor cage rotor with the simplest form of rotor being a squirrel-cage rotor with $N_n = P_1 + P_2$ bars. However, in order to reduce the referred rotor leakage inductance [10], electrically isolated loops may be placed between the cage bars forming a *nest*. The bars forming the cage of the rotor need not be present. Fig. 1.3 shows a picture of one end of an actual rotor with six nests, each containing three loops. The rotor illustrated does not contain a cage, only one nest and most of its two adjacent nests being shown. The figure clearly shows how the inner loops are isolated from each other; the opposite end of the rotor shown is identical.

The BDFM has two modes of operation, asynchronous and synchronous and can be either singly or doubly-fed. When singly-fed, the first winding is connected to the mains (supply) and the second may be either short-circuited or connected to external resistors for speed control. When connected in this way, only asyn-

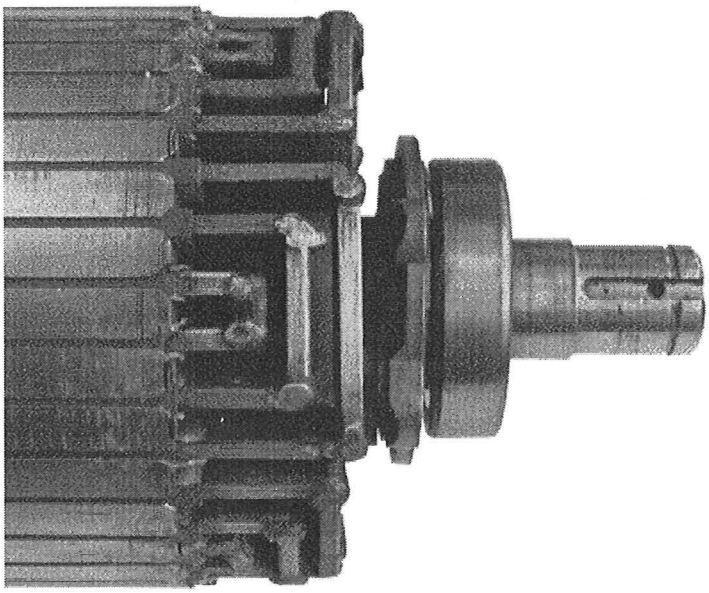

Figure 1.3: Picture of a BDFM cage rotor with six nests (three shown), each with three loops.

transformer-type coupling [2, 3, 4]. Secondly, the difference in pole-pair numbers must be greater than one to prevent unbalanced magnetic pull [3, 4, 10].

The rotor of the BDFM is unique and is critical to synchronous operation. It is a modified form of induction motor cage rotor with the simplest form of rotor being a squirrel-cage rotor with $N_n = P_1 + P_2$ bars. However, in order to reduce the referred rotor leakage inductance [10], electrically isolated loops may be placed between the cage bars forming a *nest*. The bars forming the cage of the rotor need not be present. Fig. 1.3 shows a picture of one end of an actual rotor with six nests, each containing three loops. The rotor illustrated does not contain a cage, only one nest and most of its two adjacent nests being shown. The figure clearly shows how the inner loops are isolated from each other; the opposite end of the rotor shown is identical.

The BDFM has two modes of operation, asynchronous and synchronous and can be either singly or doubly-fed. When singly-fed, the first winding is connected to the mains (supply) and the second may be either short-circuited or connected to external resistors for speed control. When connected in this way, only asyn-

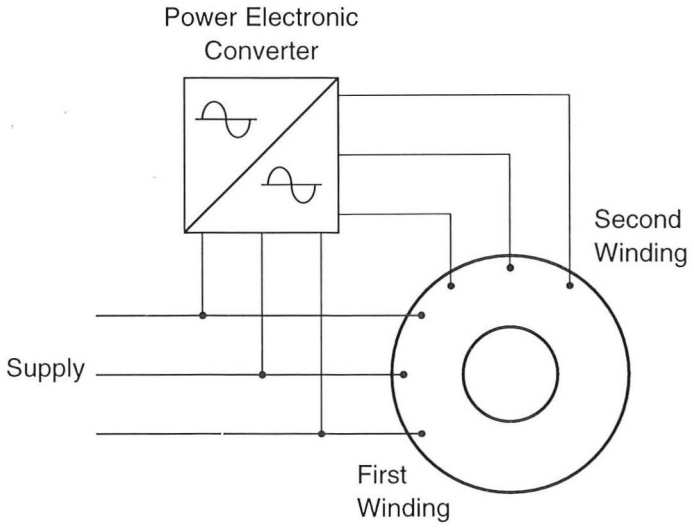

Figure 1.4: Doubly-fed configuration of the BDFM showing the the power-electronic converter connected to the second stator winding.

chronous operation results and the motor performs like an induction machine of $2(P_1 + P_2)$ poles with a synchronous speed given by the ratio $f_1/(P_1 + P_2)$, where f_1 is the mains frequency. This method of operation is well documented in the literature [2, 4, 10].

When doubly-fed, both windings are connected to power sources. Conventionally, the first winding is connected to the mains and the second to the mains via a variable-frequency power-electronic converter[4], as shown in Fig. 1.4. However, alternative configurations can also be considered where the second winding is excited with dc.

Asynchronous operation while doubly-fed is not desirable. In this situation, the BDFM behaves like two independent induction machines, each with a different synchronous speed, working against each other. Large torque and speed pulsations occur as well as pulsations in the supply currents. Conversely, synchronous operation when doubly-fed is highly desirable. It results in a motor that exhibits precise speed and power factor control. The BDFM has a well defined torque

[4]The variable-frequency excitation need not be supplied by a power-electronic converter. For example, the experiments performed in Chapter 4 use a controlled synchronous machine to provide the variable frequency and excitation level.

angle in this situation and behaves similarly to a synchronous machine. It is this mode of operation which is considered in this dissertation.

Synchronous operation occurs when the two stator windings induce rotor fields which interlock and produce supply frequency voltages in each other. This interlocking is called *cross coupling*. If an induction motor with a sinusoidally-distributed, three-phase stator winding is excited with balanced, three-phase currents then the currents will establish a rotating magnetic field. This field will induce currents in the rotor bars at a frequency proportional to slip. These rotor currents, in turn, set up a magnetic field which will couple with the stator winding and induce voltages at supply frequency. This coupling is called *direct coupling*. When a second winding of a different pole number is placed on the stator it will also couple directly with the rotor. However, if the rotor currents induced by one winding induce voltages in the other stator winding at its own supply frequency, *cross coupling* is said to occur. In other words, cross coupling is the coupling that occurs between the two stator windings via the rotor. This concept is illustrated in Fig. 1.5.

The synchronous speed, ω_R, is the speed at which cross coupling occurs between the fundamental spatial harmonics of the two windings (pole-pair numbers of the windings) and is given by the expression

$$\omega_R = \frac{\omega_1 \pm \omega_2}{P_1 + P_2} \tag{1.1}$$

where ω_R is the shaft speed (in rad/s), ω_1 is the frequency of the power-winding voltage, and ω_2 is the frequency of the control-winding voltage. The sum of the two supply frequencies is used if the windings are connected in the same phase sequence, and the difference is used for an opposing phase sequence. For dc excitation, $\omega_2 = 0$.

The power factor of the power winding can be changed by varying the level of excitation applied to the control winding. The range of power factors achievable is dependent both on the design of the motor and the kVA rating of the converter. If the converter uses a synchronous rectifier, the power factor of the complete drive system can be potentially controlled to achieve unity—or even leading—power-factor operation (as viewed from the mains).

angle in this situation and behaves similarly to a synchronous machine. It is this mode of operation which is considered in this dissertation.

Synchronous operation occurs when the two stator windings induce rotor fields which interlock and produce supply frequency voltages in each other. This interlocking is called *cross coupling*. If an induction motor with a sinusoidally-distributed, three-phase stator winding is excited with balanced, three-phase currents then the currents will establish a rotating magnetic field. This field will induce currents in the rotor bars at a frequency proportional to slip. These rotor currents, in turn, set up a magnetic field which will couple with the stator winding and induce voltages at supply frequency. This coupling is called *direct coupling*. When a second winding of a different pole number is placed on the stator it will also couple directly with the rotor. However, if the rotor currents induced by one winding induce voltages in the other stator winding at its own supply frequency, *cross coupling* is said to occur. In other words, cross coupling is the coupling that occurs between the two stator windings via the rotor. This concept is illustrated in Fig. 1.5.

The synchronous speed, ω_R, is the speed at which cross coupling occurs between the fundamental spatial harmonics of the two windings (pole-pair numbers of the windings) and is given by the expression

$$\omega_R = \frac{\omega_1 \pm \omega_2}{P_1 + P_2} \tag{1.1}$$

where ω_R is the shaft speed (in rad/s), ω_1 is the frequency of the power-winding voltage, and ω_2 is the frequency of the control-winding voltage. The sum of the two supply frequencies is used if the windings are connected in the same phase sequence, and the difference is used for an opposing phase sequence. For dc excitation, $\omega_2 = 0$.

The power factor of the power winding can be changed by varying the level of excitation applied to the control winding. The range of power factors achievable is dependent both on the design of the motor and the kVA rating of the converter. If the converter uses a synchronous rectifier, the power factor of the complete drive system can be potentially controlled to achieve unity—or even leading—power-factor operation (as viewed from the mains).

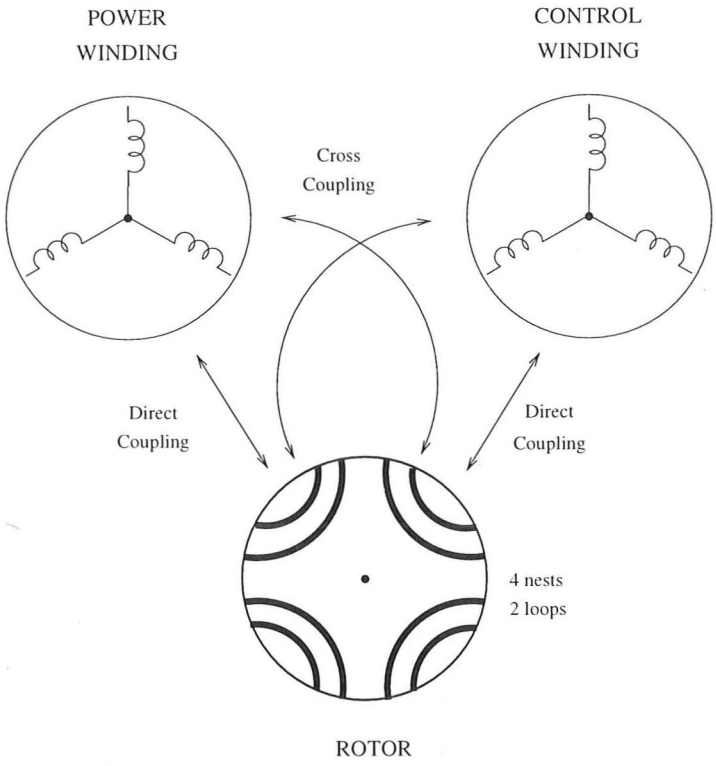

Figure 1.5: Representation of direct and cross coupling of the stator fields with the rotor fields.

Chapter 2

dq Model

2.1 Introduction

For the purposes of this analysis, the BDFM is assumed to consist of two balanced, sinusoidally distributed, three-phase stator windings and a rotor composed of a number of circuits. The electrical performance of the machine can be described, in the stationary (stator) reference frame (SRF), by the matrix voltage equation,

$$\mathbf{V} = \mathbf{ZI} \tag{2.1}$$

where $\mathbf{V}$ is a vector of applied voltages to each of the stator windings and rotor circuits, $\mathbf{I}$ is a vector of the currents, and $\mathbf{Z}$ is the impedance matrix which incorporates the effects that the different windings and circuits have on each other. Both the voltages and currents are functions of time. The impedance matrix, as will be shown, is dependent on the rotor position and contains the differential operator $\frac{d}{dt}$. Finding the solution to this equation is non-trivial, as was demonstrated by Wallace et al. in [12]. However, a change of variables can be performed which will reduce the complexity of the equations, thus making it easier to solve them.

In general, any set of equations can undergo a change of variables which will transform them into another reference frame. For instance, Park's Transformation [29, pg. 134] was used in the analysis of synchronous machines to transform the stator voltage equations into the rotor reference frame (RRF). Krause showed

that Park's transformation is just a special case of a general transformation that transforms the equations into an arbitrary reference frame with angular velocity ω [29].

Reference frame theory is also used by Jones to present a unified theory of electric machinery based on the application of, at most, three transformations, each performing a particular function [30]. The combination of the three transformations he presents is similar to the transformation of Krause.

Jones' transformation is power invariant which means that the sum of the voltage-current products in both reference frames, the original and transformed, is the same, as opposed to Krause's transformation which requires a factor of 3/2 in order to balance the powers in the two reference frames. A benefit to using a power invariant transformation is that the transformation is orthogonal, which means that the inverse of the transformation matrix is its transpose[1].

The analysis of the BDFM presented in this chapter, like that presented by Li et al. in [14] and by Boger et al. in [21], uses a power invariant form of the rotor reference frame transformation presented in Krause, which is equivalent to the cascaded RRF transformations of Jones. The RRF is used because, as was shown by Li et al. in [14], it is the only reference frame where the rotor position dependent inductances become constant. In order to simplify the analysis, the following assumptions are made:

- balanced, sinusoidally distributed stator windings of different pole numbers
- infinitely permeable iron (no saturation)
- cylindrical, smooth air-gap surfaces

[1]This is true only if the matrix is real. If it is complex, the inverse is its conjugate transpose.

2.2 Voltage Equation in the SRF

The generalised voltage equation for the BDFM in the stator reference frame can be written as [21]

$$\begin{bmatrix} \mathbf{v_1} \\ \mathbf{v_2} \\ \mathbf{0} \end{bmatrix} = \begin{bmatrix} \mathbf{Z_{11}} & \mathbf{0} & \mathbf{Z_{1R}} \\ \mathbf{0} & \mathbf{Z_{22}} & \mathbf{Z_{2R}} \\ \mathbf{Z_{1R}^T} & \mathbf{Z_{2R}^T} & \mathbf{Z_{RR}} \end{bmatrix} \begin{bmatrix} \mathbf{i_1} \\ \mathbf{i_2} \\ \mathbf{i_R} \end{bmatrix} \tag{2.2}$$

where the vectors $\mathbf{v_1}$ and $\mathbf{v_2}$ represent the stator voltages of the first and second windings, $\mathbf{i_1}$ and $\mathbf{i_2}$ the respective stator phase currents, and $\mathbf{i_R}$ the rotor loop currents. The remaining elements represent the self impedance of and the coupling impedance between the different circuits. Since the two stator windings are of different pole numbers, there is assumed to be no coupling between them, signified by the $\mathbf{0}$ elements in the matrix.

2.2.1 Stator Impedances

The time-varying voltage vectors are defined,

$$\mathbf{v_1} = \begin{bmatrix} v_{1A}(t) & v_{1B}(t) & v_{1C}(t) \end{bmatrix}^T \tag{2.3}$$

$$\mathbf{v_2} = \begin{bmatrix} v_{2A}(t) & v_{2B}(t) & v_{2C}(t) \end{bmatrix}^T \tag{2.4}$$

where the letter in the subscript of the elements, (A, B, C), refers to the phase of the voltage. Similarly, for the current vectors

$$\mathbf{i_1} = \begin{bmatrix} i_{1A}(t) & i_{1B}(t) & i_{1C}(t) \end{bmatrix}^T \tag{2.5}$$

$$\mathbf{i_2} = \begin{bmatrix} i_{2A}(t) & i_{2B}(t) & i_{2C}(t) \end{bmatrix}^T \tag{2.6}$$

For a balanced three phase winding, it can be assumed that each phase has the same resistance and self inductance, and the same mutual inductance with the other phases. Furthermore, the mutual inductance, M, and magnetising inductance, L_m, are related such that $M = -\frac{1}{2}L_m$. These relationships are used in

the self impedance matrix for the first winding [21, 29],

$$Z_{11} = \begin{bmatrix} R_1 + (L_{l1} + L_{m1})\frac{d}{dt} & -\frac{1}{2}L_{m1}\frac{d}{dt} & -\frac{1}{2}L_{m1}\frac{d}{dt} \\ -\frac{1}{2}L_{m1}\frac{d}{dt} & R_1 + (L_{l1} + L_{m1})\frac{d}{dt} & -\frac{1}{2}L_{m1}\frac{d}{dt} \\ -\frac{1}{2}L_{m1}\frac{d}{dt} & -\frac{1}{2}L_{m1}\frac{d}{dt} & R_1 + (L_{l1} + L_{m1})\frac{d}{dt} \end{bmatrix} \quad (2.7)$$

where R_1 is the resistance of a phase, L_{l1} is the leakage inductance per phase and L_{m1} is the magnetising inductance per phase of the first winding. Likewise for the second winding,

$$Z_{22} = \begin{bmatrix} R_2 + (L_{l2} + L_{m2})\frac{d}{dt} & -\frac{1}{2}L_{m2}\frac{d}{dt} & -\frac{1}{2}L_{m2}\frac{d}{dt} \\ -\frac{1}{2}L_{m2}\frac{d}{dt} & R_2 + (L_{l2} + L_{m2})\frac{d}{dt} & -\frac{1}{2}L_{m2}\frac{d}{dt} \\ -\frac{1}{2}L_{m2}\frac{d}{dt} & -\frac{1}{2}L_{m2}\frac{d}{dt} & R_2 + (L_{l2} + L_{m2})\frac{d}{dt} \end{bmatrix} \quad (2.8)$$

The differential operator, $\frac{d}{dt}$, operates on the product of the inductance and the current (flux linkage), its placement being very important when the inductances are rotor position dependent (time varying). However, for the stator self-impedance matrix, the operator may be placed after the inductances because the inductances are constant under the assumptions made in Section 2.1, i.e. ignoring slotting and saturation effects.

2.2.2 Rotor Impedances

There are three different configurations of rotor bars, all of which have the same basic structure. The first configuration, which is the simplest to analyse, is attributed to Creedy [4] and is composed of groups of concentric, isolated loops forming nests, with each nest equally spaced around the circumference of the rotor. This rotor configuration is denoted Type I and is shown in Fig. 2.1. The second configuration, attributed to Broadway [10], has a common end-ring on one end of the rotor, as shown in Fig. 2.2, and is denoted a Type II rotor. The third configuration, the Type III rotor, is a modification of the original Broadway rotor. There is still a common end-ring, however, adjacent outer loops share a common rotor bar. In fact, the set of outer loops forms a squirrel cage rotor of $N_n = P_1 + P_2$ bars. This rotor configuration is depicted in Fig. 2.3.

The rotor can be considered to consist of N_l loops within N_n nests, thus forming a total of $N_n N_l$ individual rotor circuits. In this analysis, each loop within a nest

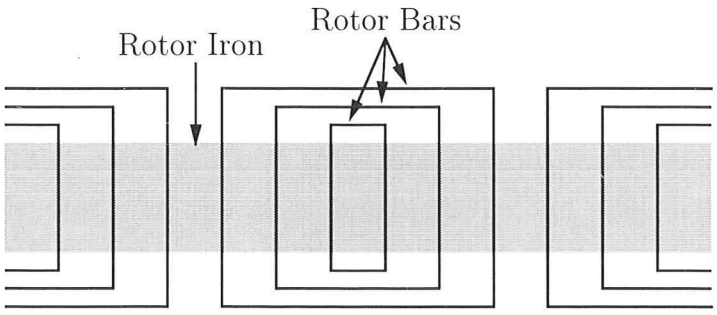

Figure 2.1: Rotor configuration of the Type I rotor showing three loops within one nest as well as portions of the adjacent nests.

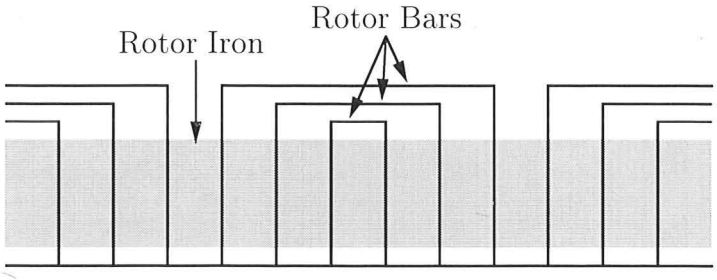

Figure 2.2: Rotor configuration of the Type II rotor showing three loops within one nest as well as portions of the adjacent nests.

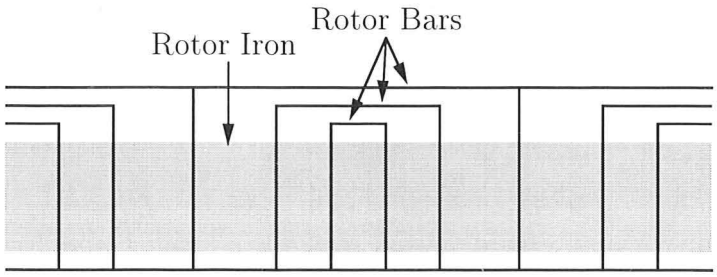

Figure 2.3: Rotor configuration of the Type III rotor showing three loops within one nest as well as portions of the adjacent nests.

is arbitrarily numbered from the inside out, with each nest numbered sequentially. The rotor circuits are notionally divided into a set of N_l systems, each with N_n elements. Each of the sets is a group of similar rotor loops, one loop from each nest. In effect, this forms an N_n phase rotor system, there being N_l such systems in the rotor. For example, the first rotor loop system would be composed of the inner loop of the first nest, the inner loop of the second nest, and so on until all inner loops of the nests were counted.

In all three rotor configurations, there will be coupling between loops i and j in the same nest, denoted L_{ij} and mutual inductance between loops i and j in different nests, M_{ij}. For the case when $i = j$, L_{ij} is the self inductance of the rotor loop. In addition to the inductances, each rotor loop has a resistance. For the i-th rotor loop, the resistance is denoted R_{ii}. For both the Type II and Type III rotors (not the Type I rotor), there will be shared resistance elements between loops in the same nest due to the common end ring. This resistance will be designated R_{ij} for the common resistance between loops i and j.

All of the loop impedances are incorporated into the rotor impedance matrix (of dimension $N_l N_n \times N_l N_n$),

$$\mathbf{Z_{RR}} = [\mathbf{Z_{R_i R_j}}] \tag{2.9}$$

where each sub-matrix $\mathbf{Z_{R_i R_j}}$, of dimension $N_n \times N_n$, is the rotor impedance matrix which couples rotor loop system i with rotor loop system j and is given as

$$\underset{i,j\in\{1,\ldots,N_l\}}{\mathbf{Z_{R_i R_j}}} = \begin{bmatrix} R_{ij} + L_{ij}\frac{d}{dt} & M_{ij}\frac{d}{dt} & \cdots & M_{ij}\frac{d}{dt} \\ M_{ij}\frac{d}{dt} & R_{ij} + L_{ij}\frac{d}{dt} & \cdots & M_{ij}\frac{d}{dt} \\ \vdots & \vdots & \ddots & \vdots \\ M_{ij}\frac{d}{dt} & M_{ij}\frac{d}{dt} & \cdots & R_{ij} + L_{ij}\frac{d}{dt} \end{bmatrix} \tag{2.10}$$

It is assumed that the rotor is symmetrical so that $\mathbf{Z_{R_i R_j}} = \mathbf{Z_{R_j R_i}}$.

For the Type III rotor, the outer loops share a common rotor bar of resistance $r'_{N_l N_l}$ and leakage inductance $l'_{N_l N_l}$ which must be taken into account. The shared components, already present in the loop resistance and self-impedance elements, must be subtracted from the impedance elements of adjacent nests. This is a result of writing implicit mesh-current equations for each rotor loop in the rotor loop system. Specifically, for the m-th row and n-th column element of $\mathbf{Z_{R_{N_l} R_{N_l}}}$,

the impedance is given as

$$\left(\mathbf{Z}_{\mathbf{R_{N_l}R_{N_l}}}\right)_{mn} = R_{N_l N_l} - r'_{N_l N_l} + (M_{N_l N_l} - l'_{N_l N_l})\frac{d}{dt} \tag{2.11}$$

provided nests m and n are adjacent.

2.2.3 Stator-Rotor Coupling Impedances

The mutual impedance between the rotor and the stator will be rotor position dependent [29, 21]. In order for the mutual inductance relationships to be derived, a common reference from which to define the rotor angle must therefore be established. The axis of the first phase of the power winding is arbitrarily chosen as this reference, which will also correspond to the axis of the first rotor nest. The mechanical angle of the rotor shaft, θ_R, is measured with respect to this reference. The second winding reference axis is assumed to be displaced a mechanical angle α from this reference.

Because the stator windings are sinusoidal, it can be assumed that the mutual inductance between the stator and the rotor will be sinusoidal in nature. The mutual inductance that relates the voltages in the stator winding with currents in the rotor systems can be written in a row-matrix form, where each sub-matrix refers to the coupling between a set of rotor loop currents and the particular stator winding system being considered. For both stator windings,

$$\mathbf{Z_{1R}} = \frac{d}{dt}\begin{bmatrix}\mathbf{L_{1R_1}} & \cdots & \mathbf{L_{1R_{N_l}}}\end{bmatrix} \tag{2.12}$$

$$\mathbf{Z_{2R}} = \frac{d}{dt}\begin{bmatrix}\mathbf{L_{2R_1}} & \cdots & \mathbf{L_{2R_{N_l}}}\end{bmatrix} \tag{2.13}$$

where $\mathbf{L_{1R_i}}$ and $\mathbf{L_{2R_i}}$ are mutual inductance matrices that represent the coupling between that particular stator winding and the i-th rotor loop system. Each of these sub-matrices is of dimension $3 \times N_n$, each row corresponding to a particular stator phase. Tersely,

$$\mathbf{L_{1R_i}} = \left[(M_{1R_i})_{mn}\right] \tag{2.14}$$

$$\mathbf{L_{2R_i}} = \left[(M_{2R_i})_{mn}\right] \tag{2.15}$$

where $(M_{1R_i})_{mn}$ and $(M_{2R_i})_{mn}$ represent the mutual coupling between the m-th stator phase and the n-th rotor loop of the i-th rotor loop system.

Adjacent rotor nests are separated by a mechanical angle $\frac{2\pi}{N_n}$. For a stator winding of P pole-pairs, the electrical angle between adjacent rotor nests seen by the stator windings is $\beta = \frac{2\pi}{N_n}P$. Each of the phases of a stator winding are electrically $\frac{2\pi}{3}$ apart. Hence, by proper substitution, the mutual impedance elements in (2.14) and (2.15) can be written

$$(M_{1R_i})_{mn} = M_{1R_i}\cos\left(P_1\theta_R + (n-1)\beta_1 - (m-1)\frac{2\pi}{3}\right) \tag{2.16}$$

$$(M_{2R_i})_{mn} = M_{2R_i}\cos\left(P_2\theta_R - P_2\alpha + (n-1)\beta_2 - (m-1)\frac{2\pi}{3}\right) \tag{2.17}$$

where $m \in \{1,2,3\}$ and $n \in \{1,2,\ldots,N_n\}$; M_{1R_i} and M_{2R_i} are the peak values of the mutual inductance (assumed sinusoidal) between the respective stator winding and i-th rotor loop system; and

$$\beta_1 = P_1\frac{2\pi}{N_n} \tag{2.18}$$

$$\beta_2 = P_2\frac{2\pi}{N_n} \tag{2.19}$$

are the electrical angles between the rotor nests.

As indicated in (2.2), the mutual impedance between the rotor and the stator is symmetrical so that $\mathbf{Z_{R1}} = \mathbf{Z_{1R}^T}$ and $\mathbf{Z_{R2}} = \mathbf{Z_{2R}^T}$.

2.3 Voltage Equation in the RRF

In order to aid in the analysis and properly include the effects of both windings on the rotor, the rotor current in each bar will be considered to consist of two components. One component is that induced by the first stator winding, $\mathbf{i_{R1}}$, and the other is that induced by the second stator winding, $\mathbf{i_{R2}}$, such that $\mathbf{i_R} = \mathbf{i_{R1}} + \mathbf{i_{R2}}$. The effect of this decomposition is to modify the voltage equation in (2.2) so that

the new voltage equation becomes,

$$\begin{bmatrix} \mathbf{v_1} \\ \mathbf{v_2} \\ \mathbf{0} \\ \mathbf{0} \end{bmatrix} = \begin{bmatrix} \mathbf{Z_{11}} & \mathbf{0} & \mathbf{Z_{1R}} & \mathbf{Z_{1R}} \\ \mathbf{0} & \mathbf{Z_{22}} & \mathbf{Z_{2R}} & \mathbf{Z_{2R}} \\ \mathbf{Z_{1R}^T} & \mathbf{0} & \mathbf{Z_{RR}} & \mathbf{0} \\ \mathbf{0} & \mathbf{Z_{2R}^T} & \mathbf{0} & \mathbf{Z_{RR}} \end{bmatrix} \begin{bmatrix} \mathbf{i_1} \\ \mathbf{i_2} \\ \mathbf{i_{R1}} \\ \mathbf{i_{R2}} \end{bmatrix} \tag{2.20}$$

where the direct and cross-coupled components of the stator induced voltages are made more apparent. For example, the product $\mathbf{Z_{1R}i_1}$ corresponds to direct coupling with the rotor and $\mathbf{Z_{1R}i_2}$ to cross-coupling with the rotor.

By a change of variables, this equation can be transformed into the RRF, eliminating the time varying inductances in the impedance matrix. The transformation of variables, either voltages or currents, is given by the transformation equation

$$\mathbf{f'} = \mathbf{Cf} \tag{2.21}$$

where $\mathbf{f'}$ is an arbitrary transformed quantity (voltage or current), $\mathbf{f}$ is the original quantity, and $\mathbf{C}$ is the transformation matrix. The basic voltage equation in (2.1),

$$\mathbf{V} = \mathbf{ZI} \tag{2.22}$$

is transformed by left-multiplying both sides of (2.22) by the system transformation matrix, $\mathbf{C}$, to obtain

$$\mathbf{CV} = \mathbf{CZI} \tag{2.23}$$

Using (2.21), the following substitutions are made,

$$\mathbf{V'} = \mathbf{CV} \tag{2.24}$$

$$\mathbf{I} = \mathbf{C^{-1}I'} \tag{2.25}$$

to obtain the transformed voltage equation

$$\mathbf{V'} = \mathbf{Z'I'} \tag{2.26}$$

where the impedance, $\mathbf{Z'}$, is the transformed impedance matrix which is related to the original impedance matrix by the relationship

$$\mathbf{Z'} = \mathbf{CZC^{-1}} \tag{2.27}$$

the new voltage equation becomes,

$$\begin{bmatrix} \mathbf{v_1} \\ \mathbf{v_2} \\ 0 \\ 0 \end{bmatrix} = \begin{bmatrix} \mathbf{Z_{11}} & 0 & \mathbf{Z_{1R}} & \mathbf{Z_{1R}} \\ 0 & \mathbf{Z_{22}} & \mathbf{Z_{2R}} & \mathbf{Z_{2R}} \\ \mathbf{Z_{1R}^T} & 0 & \mathbf{Z_{RR}} & 0 \\ 0 & \mathbf{Z_{2R}^T} & 0 & \mathbf{Z_{RR}} \end{bmatrix} \begin{bmatrix} \mathbf{i_1} \\ \mathbf{i_2} \\ \mathbf{i_{R1}} \\ \mathbf{i_{R2}} \end{bmatrix} \tag{2.20}$$

where the direct and cross-coupled components of the stator induced voltages are made more apparent. For example, the product $\mathbf{Z_{1R}i_1}$ corresponds to direct coupling with the rotor and $\mathbf{Z_{1R}i_2}$ to cross-coupling with the rotor.

By a change of variables, this equation can be transformed into the RRF, eliminating the time varying inductances in the impedance matrix. The transformation of variables, either voltages or currents, is given by the transformation equation

$$\mathbf{f'} = \mathbf{Cf} \tag{2.21}$$

where $\mathbf{f'}$ is an arbitrary transformed quantity (voltage or current), $\mathbf{f}$ is the original quantity, and $\mathbf{C}$ is the transformation matrix. The basic voltage equation in (2.1),

$$\mathbf{V} = \mathbf{ZI} \tag{2.22}$$

is transformed by left-multiplying both sides of (2.22) by the system transformation matrix, $\mathbf{C}$, to obtain

$$\mathbf{CV} = \mathbf{CZI} \tag{2.23}$$

Using (2.21), the following substitutions are made,

$$\mathbf{V'} = \mathbf{CV} \tag{2.24}$$

$$\mathbf{I} = \mathbf{C^{-1}I'} \tag{2.25}$$

to obtain the transformed voltage equation

$$\mathbf{V'} = \mathbf{Z'I'} \tag{2.26}$$

where the impedance, $\mathbf{Z'}$, is the transformed impedance matrix which is related to the original impedance matrix by the relationship

$$\mathbf{Z'} = \mathbf{CZC^{-1}} \tag{2.27}$$

2.3.1 Transformation Matrices

The transformation matrix, $\mathbf{C}$, must be block diagonal in order to be able to identify the particular rotor and stator systems. It is composed of the stator and rotor transformation matrices such that

$$\mathbf{C} = \begin{bmatrix} \mathbf{C_1} & 0 & 0 & 0 \\ 0 & \mathbf{C_2} & 0 & 0 \\ 0 & 0 & \mathbf{C_{R1}} & 0 \\ 0 & 0 & 0 & \mathbf{C_{R2}} \end{bmatrix} \tag{2.28}$$

where $\mathbf{C_1}$ and $\mathbf{C_2}$ are the stator transformation matrices for the first and second stator windings, respectively, and $\mathbf{C_{R1}}$ and $\mathbf{C_{R2}}$ are the rotor transformation matrices for the two rotor components.

Stator Transformation Matrices

The stator transformation matrix converts a set of three phase voltages into a set of two orthogonal coils fixed on the rotor. The two coils are the quadrature axis (q) and direct axis (d) coils. The stator transformation matrices used in this analysis are modified from those given by Krause in [29], using information given in Jones [30] in order to make them power invariant, and were used in Li and Boger [14, 21]. For the first stator winding, the transformation matrix is given as

$$\mathbf{C_1} = \sqrt{\frac{2}{3}} \begin{bmatrix} \cos(P_1\theta_R) & \cos\left(P_1\theta_R - \frac{2\pi}{3}\right) & \cos\left(P_1\theta_R + \frac{2\pi}{3}\right) \\ \sin(P_1\theta_R) & \sin\left(P_1\theta_R - \frac{2\pi}{3}\right) & \sin\left(P_1\theta_R + \frac{2\pi}{3}\right) \\ \frac{1}{\sqrt{2}} & \frac{1}{\sqrt{2}} & \frac{1}{\sqrt{2}} \end{bmatrix} \tag{2.29}$$

The second winding is displaced by an angle α from the first winding. In order to maintain consistency, this angle must be included in the transformation matrix, yielding

$$\mathbf{C_2} = \sqrt{\frac{2}{3}} \begin{bmatrix} \cos(P_2\theta_R - P_2\alpha) & \cos\left(P_2\theta_R - P_2\alpha - \frac{2\pi}{3}\right) & \cos\left(P_2\theta_R - P_2\alpha + \frac{2\pi}{3}\right) \\ \sin(P_2\theta_R - P_2\alpha) & \sin\left(P_2\theta_R - P_2\alpha - \frac{2\pi}{3}\right) & \sin\left(P_2\theta_R - P_2\alpha + \frac{2\pi}{3}\right) \\ \frac{1}{\sqrt{2}} & \frac{1}{\sqrt{2}} & \frac{1}{\sqrt{2}} \end{bmatrix} \tag{2.30}$$

Since the transformation matrix maps the three phases onto two orthogonal phases, the effect of including the displacement angle is to align both of the stator systems on the same q and d axes. The angle, because it is a mechanical angle, is translated into an electrical angle through multiplication by the pole-pair number. The factor $\sqrt{2/3}$, which is an equivalent turns ratio, accounts for the transformation of the three phases into two, the radical a result of the power invariance.

The last row of both matrices refers to the zero sequence quantity. The zero sequence current, physically, is that which would flow through the neutral of a star connected system, if present, or circulate in delta connected windings. If the system of applied voltages is balanced, there will be no zero sequence components.

Rotor Transformation Matrices

The rotor loops have been organised into N_l systems, each of N_n-phases. The rotor transformation must map each system onto two orthogonal coils fixed on the rotor. It can be derived from the general transformation matrix given by Krause [29] by setting Krause's arbitrary reference frame velocity to zero ($\omega = 0$) since only rotor quantities are being considered. This makes the transformation purely geometric. It may be written as

$$\mathbf{C} = \sqrt{\frac{2}{N_n}} \begin{bmatrix} 1 & \cos(-\beta) & \cdots & \cos(-(N_n-1)\beta) \\ 0 & \sin(-\beta) & \cdots & \sin(-(N_n-1)\beta) \end{bmatrix} \tag{2.31}$$

where it is assumed that the first rotor loop is aligned with the q axis (the reference) and that adjacent rotor phases are separated by an electrical angle β from each other. Each matrix is of dimension $2 \times N_l$.

Because the matrix is rectangular, it does not have a true inverse. However, it does have a pseudo-inverse such that multiplication of the matrix with its pseudo-inverse yields a unity matrix. The pseudo-inverse of the matrix is, because the transformation is power invariant (orthogonal), its transpose. Hence,

$$\mathbf{C}\mathbf{C}^{\mathbf{T}} = \mathbf{U_2} \tag{2.32}$$

and

$$\mathbf{C}^{\mathbf{T}}\mathbf{C} = \mathbf{U_{N_n}} \tag{2.33}$$

where $\mathbf{U_x}$ represents the identity matrix of order x.

Because there are two stator systems in the BDFM, there will be two different electrical separation angles, β_1 for the first winding (see (2.18)) and β_2 for the second winding (see (2.19)), and two different rotor transformation matrices, $\mathbf{C_{R1}}$ and $\mathbf{C_{R2}}$. specifically, for the transformation of the i-th rotor loop system,

$$\mathbf{C_{R1_i}} = \begin{bmatrix} 0 & \cos(-\beta_1) & \cdots & \cos(-(N_n-1)\beta_1) \\ 0 & \sin(-\beta_1) & \cdots & \sin(-(N_n-1)\beta_1) \end{bmatrix} \tag{2.34}$$

$$\mathbf{C_{R2_i}} = \begin{bmatrix} 1 & \cos(-\beta_2) & \cdots & \cos(-(N_n-1)\beta_2) \\ 0 & \sin(-\beta_2) & \cdots & \sin(-(N_n-1)\beta_2) \end{bmatrix} \tag{2.35}$$

Because the rotor loop systems are aligned axially,

$$\mathbf{C_{R1_1}} = \mathbf{C_{R1_2}} = \cdots = \mathbf{C_{R1_{N_l}}} \tag{2.36}$$

and

$$\mathbf{C_{R2_1}} = \mathbf{C_{R2_2}} = \cdots = \mathbf{C_{R2_{N_l}}} \tag{2.37}$$

There are two ways in which to assemble the set of N_l transformation matrices into a complete rotor transformation matrix. The first way organises each loop system transformation matrix into a row matrix so that for a non-specific rotor system,

$$\mathbf{C_R} = \begin{bmatrix} \mathbf{C_{R_1}} & \cdots & \mathbf{C_{R_{N_l}}} \end{bmatrix} \tag{2.38}$$

where the complete matrix has dimension $2 \times N_n N_l$.

Each sub-matrix maps one rotor loop system into a set of two coils. However, because a row matrix is used, the effects of each rotor loop system are combined into a single, equivalent set of dq coils. This is shown conceptually in Fig. 2.4. A reverse transformation of the equivalent set of coil currents will indicate that all loops in the same nest have the same current—a fact known to be false. Thus, this transformation results in the inability to predict the individual rotor loop currents. Nevertheless, this mapping was used in [14] and [21] because it reduced the number of necessary equations.

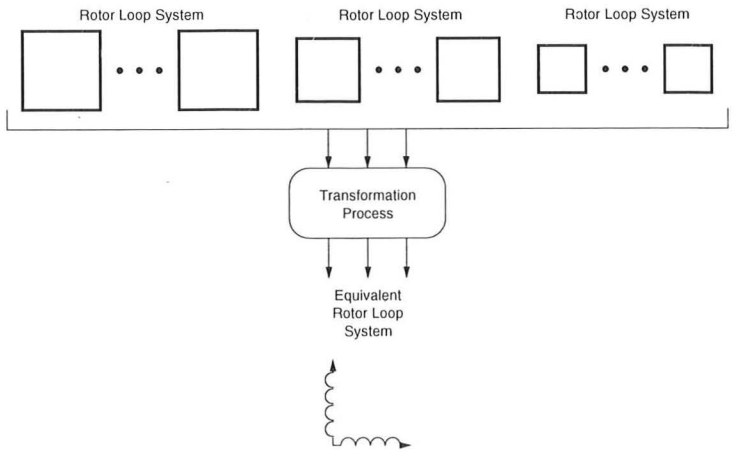

Figure 2.4: Conceptual representation of the rotor transformation process which maps each rotor loop system (three shown) into a single set of orthogonal coils.

The second way to assemble the matrix organises the individual transformation matrices into a block diagonal matrix,

$$\mathbf{C_R} = \begin{bmatrix} \mathbf{C_{R_1}} & \mathbf{0} & \cdots & \mathbf{0} \\ \mathbf{0} & \mathbf{C_{R_2}} & \cdots & \mathbf{0} \\ \vdots & \vdots & \ddots & \vdots \\ \mathbf{0} & \mathbf{0} & \cdots & \mathbf{C_{R_{N_l}}} \end{bmatrix} \tag{2.39}$$

which is of dimension $2N_l \times N_n N_l$. It results in the mapping of each rotor loop system into its own set of orthogonal coils, which is shown conceptually in Fig. 2.5. Since one set of coils is used for each rotor loop system, the identity of each of the individual rotor loop currents can be determined through the reverse transformation. For this reason, this transformation will be used in this analysis. Making the transformation matrices specific to the each stator winding yields

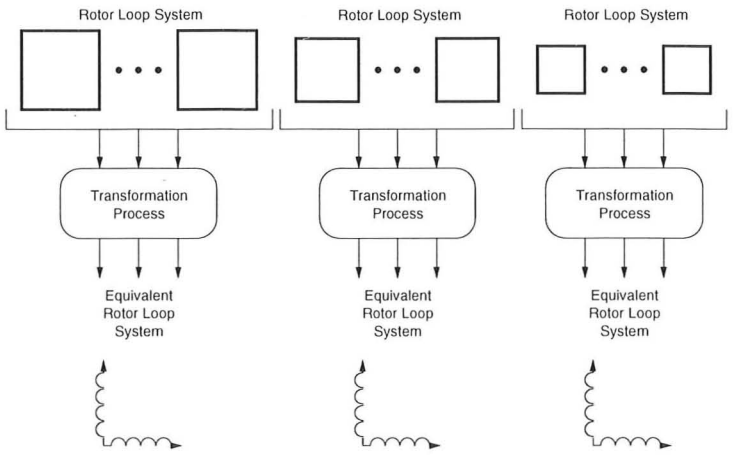

Figure 2.5: Conceptual representation of the rotor transformation process used in this thesis which maps each rotor loop system (three shown) into its own set of orthogonal coils.

$$\mathbf{C_{R1}} = \begin{bmatrix} \mathbf{C_{R1_1}} & \mathbf{0} & \cdots & \mathbf{0} \\ \mathbf{0} & \mathbf{C_{R1_2}} & \cdots & \mathbf{0} \\ \vdots & \vdots & \ddots & \vdots \\ \mathbf{0} & \mathbf{0} & \cdots & \mathbf{C_{R1_{N_l}}} \end{bmatrix} \tag{2.40}$$

$$\mathbf{C_{R2}} = \begin{bmatrix} \mathbf{C_{R2_1}} & \mathbf{0} & \cdots & \mathbf{0} \\ \mathbf{0} & \mathbf{C_{R2_2}} & \cdots & \mathbf{0} \\ \vdots & \vdots & \ddots & \vdots \\ \mathbf{0} & \mathbf{0} & \cdots & \mathbf{C_{R2_{N_l}}} \end{bmatrix} \tag{2.41}$$

where each of the sub-matrices are defined in (2.34) and (2.35). As mentioned earlier, each of the sub-matrices in the matrix is identical—the subscripts are only used to simplify bookkeeping.

2.3.2 Transformed Quantities

Voltage and Current Vectors

Equation (2.26), $\mathbf{V}' = \mathbf{Z}'\mathbf{I}'$, is the matrix voltage equation that describes the electrical performance of the BDFM in the RRF. The voltage vector,

$$\mathbf{V}' = \begin{bmatrix} v_{q1} & v_{d1} & v_{01} & v_{q2} & v_{d2} & v_{02} & \mathbf{v'_{R1}} = \mathbf{0} & \mathbf{v'_{R2}} = \mathbf{0} \end{bmatrix}^T \tag{2.42}$$

represents the applied voltages to the windings in the RRF. The vectors $\mathbf{v'_{R1}}$ and $\mathbf{v'_{R2}}$, each of dimension $1 \times N_n N_l$, are zero since no voltages are applied to the rotor. Since no slip rings are present, the voltages are zero. The subscripts $q, d, 0$ refer to the quantities on the q axis, d axis, or zero sequence components, respectively. Similarly, the current vector

$$\mathbf{I}' = \begin{bmatrix} i_{q1} & i_{d1} & i_{01} & i_{q2} & i_{d2} & i_{02} & \mathbf{i'_{R1}} & \mathbf{i'_{R2}} \end{bmatrix}^T \tag{2.43}$$

represents the currents in the stator windings and those in the rotor loops which are induced by each of the stator windings, i.e. the vectors $\mathbf{i'_{R1}}$ and $\mathbf{i'_{R2}}$. For the rotor current induced by the first stator winding,

$$\mathbf{i'_{R1}} = \begin{bmatrix} \mathbf{i'_{R1_1}} & \cdots & \mathbf{i'_{R1_{N_l}}} \end{bmatrix}^T \tag{2.44}$$

where the current in the i-th rotor loop system is given as

$$\mathbf{i'_{R1_i}} = \begin{bmatrix} i_{qR1_i} \\ i_{dR1_i} \end{bmatrix} \tag{2.45}$$

Similarly for the rotor currents induced by the second stator winding,

$$\mathbf{i'_{R2}} = \begin{bmatrix} \mathbf{i'_{R2_1}} & \cdots & \mathbf{i'_{R2_{N_l}}} \end{bmatrix}^T \tag{2.46}$$

where the current in the i-th rotor loop system is given as

$$\mathbf{i'_{R2_i}} = \begin{bmatrix} i_{qR2_i} \\ i_{dR2_i} \end{bmatrix} \tag{2.47}$$

Impedance Matrix

The impedance matrix must also be defined in order to solve the matrix equation. The elements are determined by performing the matrix product indicated in (2.27), which requires the inverse of the transformation matrix. Although the transformation matrix does not have a proper inverse because it is rectangular, it does have a pseudo-inverse equal to its transpose. This is a result of the orthogonality of the constituent matrices. By substituting $\mathbf{C^{-1}} = \mathbf{C^T}$, the impedance matrix can be written as

$$\begin{aligned}\mathbf{Z'} &= \begin{bmatrix} \mathbf{C_1 Z_{11} C_1^T} & \mathbf{0} & \mathbf{C_1 Z_{1R} C_{R1}^T} & \mathbf{C_1 Z_{1R} C_{R2}^T} \\ \mathbf{0} & \mathbf{C_2 Z_{22} C_2^T} & \mathbf{C_2 Z_{2R} C_{R1}^T} & \mathbf{C_2 Z_{2R} C_{R2}^T} \\ \mathbf{C_{R1} Z_{1R}^T C_1^T} & \mathbf{0} & \mathbf{C_{R1} Z_{RR} C_{R1}^T} & \mathbf{0} \\ \mathbf{0} & \mathbf{C_{R2} Z_{2R}^T C_2^T} & \mathbf{0} & \mathbf{C_{R2} Z_{RR} C_{R2}^T} \end{bmatrix} \\ &= \begin{bmatrix} \mathbf{Z'_{11}} & \mathbf{0} & \mathbf{Z'_{1R1}} & \mathbf{Z'_{1R2}} \\ \mathbf{0} & \mathbf{Z_{22}} & \mathbf{Z'_{2R2}} & \mathbf{Z'_{2R1}} \\ \mathbf{Z'_{R1}} & \mathbf{0} & \mathbf{Z'_{1RR}} & \mathbf{0} \\ \mathbf{0} & \mathbf{Z'_{R2}} & \mathbf{0} & \mathbf{Z'_{2RR}} \end{bmatrix} \end{aligned} \tag{2.48}$$

The calculation of this impedance is non-trivial because the differential operator, $\frac{d}{dt}$, is embedded within the impedance matrix. Even though present in the impedance matrix, it acts on the product of inductance and current (flux linkage), which necessitates using of the chain rule,

$$\frac{d}{dt}(Li) = \left(\frac{d}{dt}L\right) i + L\left(\frac{d}{dt}i\right) \tag{2.49}$$

where the inductance, L, is that formed *after* the post-multiplication by $\mathbf{C^T}$. Some of the impedance matrices include inductances which vary with the time-varying rotor angle $\theta_R = \omega_R t$. Differentiation of the rotor angle introduces the rotor speed, ω_R, giving rise to speed dependent terms.

After considerable simplification, and making use of the trigonometric identi-

ties in Appendix D, the stator impedance matrices may be expressed as

$$\mathbf{Z'_{11}} = \begin{bmatrix} R_1 + L_1\frac{d}{dt} & P_1\omega_R L_1 & 0 \\ -P_1\omega_R L_1 & R_1 + L_1\frac{d}{dt} & 0 \\ 0 & 0 & R_1 + L_{l1}\frac{d}{dt} \end{bmatrix} \tag{2.50}$$

$$\mathbf{Z'_{22}} = \begin{bmatrix} R_2 + L_2\frac{d}{dt} & P_1\omega_R L_2 & 0 \\ -P_1\omega_R L_2 & R_2 + L_2\frac{d}{dt} & 0 \\ 0 & 0 & R_2 + L_{l2}\frac{d}{dt} \end{bmatrix} \tag{2.51}$$

where

$$L_1 = \frac{3}{2}L_{m1} \tag{2.52}$$

$$L_2 = \frac{3}{2}L_{m2} \tag{2.53}$$

The transformation de-couples the zero sequence quantities from the dq quantities. The transformation also introduces the scaling factor $\frac{3}{2}$, a result of the three phase to two phase transformation. It also produces speed dependent terms which account for the relative motion between the rotor and the stator windings.

The RRF impedance matrix contains terms which represent both direct and cross coupling. Direct coupling is represented by the impedances

$$\mathbf{Z'_{1R1}} = \begin{bmatrix} \mathbf{Z'_{1R1_1}} & \cdots & \mathbf{Z'_{1R1_{N_1}}} \end{bmatrix} \tag{2.54}$$

$$\mathbf{Z'_{2R2}} = \begin{bmatrix} \mathbf{Z'_{2R2_1}} & \cdots & \mathbf{Z'_{2R2_{N_1}}} \end{bmatrix} \tag{2.55}$$

where, for the i-th rotor loop system,

$$\mathbf{Z'_{1R1_i}} = \begin{bmatrix} M'_{1R_i}\frac{d}{dt} & P_1\omega_R M'_{1R_i} \\ -P_1\omega_R M'_{1R_i} & M'_{1R_i}\frac{d}{dt} \end{bmatrix} \tag{2.56}$$

$$\mathbf{Z'_{2R2_i}} = \begin{bmatrix} M'_{2R_i}\frac{d}{dt} & P_1\omega_R M'_{2R_i} \\ -P_1\omega_R M'_{2R_i} & M'_{2R_i}\frac{d}{dt} \end{bmatrix} \tag{2.57}$$

for which the elements of equivalent mutual inductance are given as

$$M'_{1R_i} = \frac{\sqrt{3N_n}}{2}M_{1R_i} \tag{2.58}$$

$$M'_{2R_i} = \frac{\sqrt{3N_n}}{2}M_{2R_i} \tag{2.59}$$

The factor $\frac{\sqrt{3N_n}}{2}$, an equivalent turns ratio, results from resolving the N_n phases of the rotor-loop system into two phases. The transformation also produces speed dependent terms which not only account for the relative motion between the rotor and stator windings, but also represents the coupling between the q and d axes.

Described in Chapter 1, cross coupling is the coupling between a stator winding and the rotor currents produced by the other stator winding. The impedances

$$\mathbf{Z'_{1R2}} = \begin{bmatrix} \mathbf{Z'_{1R2_1}} & \cdots & \mathbf{Z'_{1R2_{N_1}}} \end{bmatrix} \tag{2.60}$$

$$\mathbf{Z'_{2R1}} = \begin{bmatrix} \mathbf{Z'_{2R1_1}} & \cdots & \mathbf{Z'_{2R1_{N_1}}} \end{bmatrix} \tag{2.61}$$

represent the cross coupling where, for the i-th rotor loop system,

$$\mathbf{Z'_{1R2_i}} = \begin{bmatrix} M'_{1R_i}\frac{d}{dt} & -P_1\omega_R M'_{1R_i} \\ -P_1\omega_R M'_{1R_i} & -M'_{1R_i}\frac{d}{dt} \end{bmatrix} \tag{2.62}$$

$$\mathbf{Z'_{2R1_i}} = \begin{bmatrix} M'_{2R_i}\frac{d}{dt} & -P_1\omega_R M'_{2R_i} \\ -P_1\omega_R M'_{2R_i} & -M'_{2R_i}\frac{d}{dt} \end{bmatrix} \tag{2.63}$$

The difference between the direct and cross-coupling impedances is the negation of some of the impedance elements. This is purely a mathematical result of the post multiplication by the rotor transformation matrix of the other winding ($\mathbf{C^T_{R2}}$ for the impedance $\mathbf{Z_{1R2}}$ and $\mathbf{C^T_{R1}}$ for the impedance $\mathbf{Z_{2R1}}$).

The effects the stator currents have on the rotor loops are represented by the impedance matrices

$$\mathbf{Z'_{R1}} = \begin{bmatrix} \mathbf{Z'_{R1_1}} & \cdots & \mathbf{Z'_{R1_{N_1}}} \end{bmatrix}^T \tag{2.64}$$

$$\mathbf{Z'_{R2}} = \begin{bmatrix} \mathbf{Z'_{R2_1}} & \cdots & \mathbf{Z'_{R2_{N_1}}} \end{bmatrix}^T \tag{2.65}$$

where for the i-th rotor loop system,

$$\mathbf{Z'_{R1_i}} = \begin{bmatrix} M'_{1R_i}\frac{d}{dt} & 0 & 0 \\ 0 & M'_{1R_i}\frac{d}{dt} & 0 \end{bmatrix} \tag{2.66}$$

$$\mathbf{Z'_{R2_i}} = \begin{bmatrix} M'_{2R_i}\frac{d}{dt} & 0 & 0 \\ 0 & M'_{2R_i}\frac{d}{dt} & 0 \end{bmatrix} \tag{2.67}$$

The product of these matrices and their respective stator currents yield the voltages induced in the equivalent rotor coils. Since the rotor, by definition, is already in the RRF, no speed dependent terms exist.

Equation (2.48) identifies two rotor impedance matrices, $\mathbf{Z'_{1RR}}$ and $\mathbf{Z'_{2RR}}$, each of dimension $2N_l \times 2N_l$. However, the calculations show that each is identical and given as

$$\mathbf{Z'_{RR}} = \left[\mathbf{Z'_{R_iR_j}}\right] \tag{2.68}$$

where each sub-matrix is given as

$$\underset{i,j\in\{1,\ldots,N_l\}}{\mathbf{Z'_{R_iR_j}}} = \begin{bmatrix} R'_{ij} + L'_{ij}\frac{d}{dt} & 0 \\ 0 & R'_{ij} + L'_{ij}\frac{d}{dt} \end{bmatrix} \tag{2.69}$$

in which the equivalent resistance and inductance elements are given as

$$R'_{ij} = R_{ij} \tag{2.70}$$

$$L'_{ij} = L_{ij} + M_{ij} \tag{2.71}$$

If a Type III rotor is used (see Fig. 2.3), the rotor resistance and inductance elements must be modified because of the presence of the common rotor bar. In this case, $i = j = N_l$ and

$$R'_{N_lN_l} = R_{N_lN_l} - 2r'_{N_lN_l}\cos\beta_1 \tag{2.72}$$

$$L'_{N_lN_l} = L_{N_lN_l} + M_{N_lN_l} - 2l'_{N_lN_l}\cos\beta_1 \tag{2.73}$$

2.3.3 Discussion

In expanded form, the RRF matrix voltage equation is

$$\begin{bmatrix} \mathbf{v'_1} \\ \mathbf{v'_2} \\ \mathbf{0} \\ \mathbf{0} \end{bmatrix} = \begin{bmatrix} \mathbf{Z'_{11}} & \mathbf{0} & \mathbf{Z'_{1R1}} & \mathbf{Z'_{1R2}} \\ \mathbf{0} & \mathbf{Z_{22}} & \mathbf{Z'_{2R2}} & \mathbf{Z'_{2R1}} \\ \mathbf{Z'_{R1}} & \mathbf{0} & \mathbf{Z'_{1RR}} & \mathbf{0} \\ \mathbf{0} & \mathbf{Z'_{R2}} & \mathbf{0} & \mathbf{Z'_{2RR}} \end{bmatrix} \begin{bmatrix} \mathbf{i'_1} \\ \mathbf{i'_2} \\ \mathbf{i'_{R1}} \\ \mathbf{i'_{R2}} \end{bmatrix} \tag{2.74}$$

where the voltages and currents are both time-varying quantities in the RRF. Transformation to the RRF eliminated the time-varying inductances present in the original impedance matrix, $\mathbf{Z}$, replacing some of the quantities with speed dependent terms. The rotor current in each loop system has been decomposed into two different components so that the effects of direct and cross coupling

can be easily identified. Alternatively, the components can be recombined into one equivalent current in order to reduce the number of equations; the details of this recombination are given in Appendix E. The matrix equations represent the electrical model of the BDFM which can be used to predict dynamic performance. However, the model is incomplete without an expression for the electromagnetic torque produced by the BDFM.

2.4 Torque Equation

The electromagnetic torque produced by an induction motor can be calculated using the following matrix equation [29],

$$T_e = \mathbf{i_S^T} \frac{\partial}{\partial \theta_R} \mathbf{Z_{SR}} \mathbf{i_R} \tag{2.75}$$

where $\mathbf{i_S}$ is the vector of stator currents, $\mathbf{Z_{SR}}$ is the mutual impedance matrix, and $\mathbf{i_R}$ is the vector of rotor currents.

For the BDFM there are two stator current vectors, $\mathbf{i_1}$ and $\mathbf{i_2}$. Likewise, there are two components of rotor current, $\mathbf{i_{R1}}$ and $\mathbf{i_{R2}}$[2]. In order to account for the cross coupling, the mutual impedance matrix must be arranged in the following manner,

$$\mathbf{Z_{SR}} = \begin{bmatrix} \mathbf{Z_{1R}} & \mathbf{Z_{1R}} \\ \mathbf{Z_{2R}} & \mathbf{Z_{2R}} \end{bmatrix} \tag{2.76}$$

where the off-diagonal matrices account for cross coupling with the rotor currents produced by the other stator winding and the diagonal ones to direct coupling. In expanded form,

$$T_e = \begin{bmatrix} \mathbf{i_1} & \mathbf{i_2} \end{bmatrix} \frac{\partial}{\partial \theta_R} \begin{bmatrix} \mathbf{Z_{1R}} & \mathbf{Z_{1R}} \\ \mathbf{Z_{2R}} & \mathbf{Z_{2R}} \end{bmatrix} \begin{bmatrix} \mathbf{i_{R1}} \\ \mathbf{i_{R2}} \end{bmatrix} \tag{2.77}$$

The torque equation is transformed to the rotor reference frame by substituting the dq currents for the actual currents. Using (2.25), the actual stator currents are related to the dq currents by the relationship

$$\mathbf{I_S} = \mathbf{C_S^T} \mathbf{I'_S} \tag{2.78}$$

[2]See Appendix E for the derivation of torque using an equivalent rotor current.

where

$$\mathbf{C_S} = \begin{bmatrix} \mathbf{C_1} & 0 \\ 0 & \mathbf{C_2} \end{bmatrix} \tag{2.79}$$

Taking the transpose of both sides of (2.78),

$$\mathbf{I_S^T} = \mathbf{I_S'^T C_S} \tag{2.80}$$

The actual rotor currents are obtained directly from (2.25),

$$\mathbf{I_R} = \mathbf{C_R^T I'_R} \tag{2.81}$$

By direct substitution,

$$T_e = \begin{bmatrix} \mathbf{i'_1} & \mathbf{i'_2} \end{bmatrix} \begin{bmatrix} \mathbf{C_1} & 0 \\ 0 & \mathbf{C_2} \end{bmatrix} \frac{\partial}{\partial \theta_R} \begin{bmatrix} \mathbf{Z_{1R}} & \mathbf{Z_{1R}} \\ \mathbf{Z_{2R}} & \mathbf{Z_{2R}} \end{bmatrix} \begin{bmatrix} \mathbf{C_{R1}^T} & 0 \\ 0 & \mathbf{C_{R2}^T} \end{bmatrix} \begin{bmatrix} \mathbf{i'_{R1}} \\ \mathbf{i'_{R2}} \end{bmatrix} \tag{2.82}$$

After considerable simplification, the electrical torque can be represented as the sum of four components,

$$T_e = T_{11} + T_{12} + T_{21} + T_{22} \tag{2.83}$$

where T_{11} and T_{22} are the conventional induction motor torque components due to direct coupling,

$$T_{11} = P_1 \sum_{i=1}^{N_l} M_{1R_i} \left(i_{q1} i_{dR1_i} - i_{d1} i_{qR1_i} \right) \tag{2.84}$$

$$T_{22} = P_2 \sum_{i=1}^{N_l} M_{2R_i} \left(i_{q2} i_{dR2_i} - i_{d2} i_{qR2_i} \right) \tag{2.85}$$

and T_{12} and T_{21} are the components due to the cross coupling,

$$T_{12} = -P_1 \sum_{i=1}^{N_l} M_{1R_i} \left(i_{q1} i_{dR2_i} + i_{d1} i_{qR2_i} \right) \tag{2.86}$$

$$T_{21} = -P_2 \sum_{i=1}^{N_l} M_{2R_i} \left(i_{q2} i_{dR1_i} - i_{d2} i_{qR1_i} \right) \tag{2.87}$$

By inspection, neither i_{01} nor i_{02} is present in the expressions for torque, which shows that the zero sequence quantities do not produce any torque.

2.5 Steady-State Voltage Model

The matrix voltage equation, (2.74), in conjunction with the expressions for the produced torque form the complete electromechanical model of the BDFM suitable for modelling the transient behaviour of the BDFM. The solution is determined using conventional time-stepping techniques and algorithms (e.g. the Runge-Kutta algorithm). However, in order to facilitate design and understanding, a voltage equation capable of predicting the steady-state performance needs to be developed. This can be achieved by assuming balanced, sinusoidal excitation and conducting an analysis similar to that performed by Boger et al. in [21].

2.5.1 Voltage Equation

Assume the first winding to be excited with balanced, positive sequence voltages of the form,

$$\mathbf{v_1(t)} = \sqrt{2}V_1 \begin{bmatrix} \cos(\omega_1 t) \\ \cos(\omega_1 t - \frac{2\pi}{3}) \\ \cos(\omega_1 t + \frac{2\pi}{3}) \end{bmatrix} \tag{2.88}$$

where $\sqrt{2}V_1$ is the amplitude of the voltages. Transforming this voltage set to the RRF using

$$\mathbf{v_1'} = \mathbf{C_1 v_1} \tag{2.89}$$

results in the RRF voltages,

$$\begin{bmatrix} v_{q1} \\ v_{d1} \\ v_{01} \end{bmatrix} = \sqrt{3}V_1 \begin{bmatrix} \cos(P_1\omega_R - \omega_1)t \\ \sin(P_1\omega_R - \omega_1)t \\ 0 \end{bmatrix} \tag{2.90}$$

where a substitution for the rotor phase angle, $\theta = \omega_R t$, has been made since the BDFM is assumed to be in a steady-state (constant speed). As shown, a balanced set of voltages do not produce a zero sequence component. Therefore, this component will be neglected in the ensuing analysis. Representing the voltage set as complex quantities yields

$$\mathbf{v_1'} = \sqrt{3} \begin{bmatrix} \Re\left\{V_1 e^{j(P_1\omega_R - \omega_1)t}\right\} \\ \Re\left\{-jV_1 e^{j(P_1\omega_R - \omega_1)t}\right\} \end{bmatrix} \tag{2.91}$$

The winding currents will also be sinusoidal and balanced. In the stationary reference frame,

$$\mathbf{i_1} = \sqrt{2}I_1 \begin{bmatrix} \cos(\omega_1 t + \phi_1) \\ \cos(\omega_1 t - \frac{2\pi}{3} + \phi_1) \\ \cos(\omega_1 t + \frac{2\pi}{3} + \phi_1) \end{bmatrix} \tag{2.92}$$

where $\sqrt{2}I_1$ is the amplitude of the current in one phase and ϕ_1 is the phase angle of the current with respect to the voltage. In the rotor reference frame, the currents can be expressed using complex notation as

$$\mathbf{i'_1} = \begin{bmatrix} i_{q1} \\ i_{d1} \end{bmatrix} = \sqrt{3} \begin{bmatrix} \Re\left\{\bar{I}_1^* e^{j(P_1\omega_R - \omega_1)t}\right\} \\ \Re\left\{-j\bar{I}_1^* e^{j(P_1\omega_R - \omega_1)t}\right\} \end{bmatrix} \tag{2.93}$$

where $\bar{I}_1^* = I_1 e^{-j\phi_1}$ is the conjugate of $\bar{I}_1 = I_1 e^{j\phi}$. The negative phase angle is a result of applying the transformation.

Since the voltage equations are in the RRF, the frequency of the rotor currents induced by the first winding will be that of the RRF voltages, i.e. $P_1\omega_R - \omega_1$. The induced rotor currents will have a form similar to the stator currents. For the i-th rotor loop system,

$$\mathbf{i'_{R1_i}} = \begin{bmatrix} i_{qR1_i} \\ i_{dR1_i} \end{bmatrix} = \sqrt{3} \begin{bmatrix} \Re\left\{\bar{I}_{R1_i}^* e^{j(P_1\omega_R - \omega_1)t}\right\} \\ \Re\left\{-j\bar{I}_{R1_i}^* e^{j(P_1\omega_R - \omega_1)t}\right\} \end{bmatrix} \tag{2.94}$$

where $\bar{I}_{R1_i} = I_{R1_i} e^{j\phi_{R1}}$ and $\bar{I}_{R1_i}$ is the rms value of rotor current in the first nest of the i-th rotor loop system.

The second winding may be excited with either a positive or negative sequence voltage set. For a positive sequence voltage set,

$$\mathbf{v_2(t)} = \sqrt{2}V_2 \begin{bmatrix} \cos(\omega_2 t + \gamma) \\ \cos(\omega_2 t + \gamma - \frac{2\pi}{3}) \\ \cos(\omega_2 t + \gamma + \frac{2\pi}{3}) \end{bmatrix} \tag{2.95}$$

where γ is an arbitrary phase angle. As will be shown later, this angle becomes significant in the steady-state equations despite being meaningless in the SRF dynamic equations.

The voltages are transformed into the RRF using the transformation

$$\mathbf{v_2'} = \mathbf{C_2 v_2} \tag{2.96}$$

which results in the complex RRF voltages (neglecting the zero sequence quantity),

$$\begin{bmatrix} v_{q2} \\ v_{d2} \end{bmatrix} = \sqrt{3} \begin{bmatrix} \Re\left\{\bar{V}_2^* e^{j(P_2\omega_R - \omega_2)t}\right\} \\ \Re\left\{-j\bar{V}_2^* e^{j(P_2\omega_R - \omega_2)t}\right\} \end{bmatrix} \tag{2.97}$$

where $\bar{V}_2 = V_2 e^{j\gamma}$. When the voltages are represented as phasors, the phase angle γ represents the internal torque angle of the machine during synchronous operation. Because the actual value of this angle is unimportant, the displacement angle α between the axis of the second stator winding and the reference axis can be arbitrarily set to $\alpha = 0$. The importance of the angle γ was recognised by Li in [14]; used and given further significance by Boger et al. in [21]; and thoroughly investigated, measured, and verified by Ferreira in [31].

The second winding currents in the RRF, using complex notation, will have a form,

$$\mathbf{i_2'} = \begin{bmatrix} i_{q2} \\ i_{d2} \end{bmatrix} = \sqrt{3} \begin{bmatrix} \Re\left\{\bar{I}_2^* e^{j(P_2\omega_R - \omega_2)t}\right\} \\ \Re\left\{-j\bar{I}_2^* e^{j(P_2\omega_R - \omega_2)t}\right\} \end{bmatrix} \tag{2.98}$$

where $\bar{I}_2 = I_2 e^{j\phi_2}$ and ϕ_2 is the phase angle of the currents. Once in phasor form, this angle will be given with respect to the phase angle of voltage of the first winding, which was chosen as the reference. The rotor currents induced by the second winding for the i-th rotor loop system will have a form,

$$\mathbf{i'_{R2_i}} = \begin{bmatrix} i_{qR2_i} \\ i_{dR2_i} \end{bmatrix} = \sqrt{3} \begin{bmatrix} \Re\left\{\bar{I}_{R2_i}^* e^{j(P_2\omega_R - \omega_2)t}\right\} \\ \Re\left\{-j\bar{I}_{R2_i}^* e^{j(P_2\omega_R - \omega_2)t}\right\} \end{bmatrix} \tag{2.99}$$

where $\bar{I}_{R2_i} = I_{R2_i} e^{j\phi_{R2}}$ and $\bar{I}_{R2_i}$ is the rms value of rotor current in the first nest of the i-th rotor loop system.

For negative sequence excitation, the second winding voltages are given as

$$\mathbf{v_2(t)} = \sqrt{2}V_2 \begin{bmatrix} \cos(\omega_2 t + \gamma) \\ \cos(\omega_2 t + \gamma + \frac{2\pi}{3}) \\ \cos(\omega_2 t + \gamma - \frac{2\pi}{3}) \end{bmatrix} \tag{2.100}$$

Transforming into the RRF,

$$\mathbf{v_2'} = \begin{bmatrix} v_{q2} \\ v_{d2} \end{bmatrix} = \sqrt{3} \begin{bmatrix} \Re\left\{\bar{V}_2^* e^{j(P_2\omega_R+\omega_2)t}\right\} \\ \Re\left\{-j\bar{V}_2^* e^{j(P_2\omega_R+\omega_2)t}\right\} \end{bmatrix} \tag{2.101}$$

By inspection of (2.97) and (2.101), it is seen that negative sequence excitation introduces a sign change in ω_2. Otherwise, the two expressions are identical. The same results are obtained for the currents relating to the second winding, i.e. for $\mathbf{i_2'}$ and $\mathbf{i'_{R2_i}}$. This suggests, the following simplifying convention. Negative sequence excitation will be represented by a negative value, $\omega_2 = -2\pi f_2$, and positive sequence excitation by a positive value, $\omega_2 = 2\pi f_2$, so that the value of ω_2 holds its sign[3]. This results in a frequency $P_2\omega_R - \omega_2$ for both the positive and negative sequence voltages and currents. Hence, only one set of voltages and currents is needed to model steady-state performance.

To determine the steady-state voltage equations, the values of the currents and voltages are substituted into the matrix voltage equation, given by (2.74), and simplified. Further simplification is achieved by noting that the d axis quantities are just phase shifted q axis quantities, i.e. $v_{d1} = -jv_{q1}$. Thus, considering just the q axis voltage, the first winding voltage equation is given as

$$\begin{aligned} \Re\left\{V_1 e^{j(P_1\omega_R-\omega_1)t}\right\} = \Re\left\{(R_1 - j\omega_1 L_1)\bar{I}_1^* - j\omega_1 \mathbf{M_{1R}}\bar{\mathbf{I}}_{\mathbf{R1}} e^{j(P_1\omega_R-\omega_1)t}\right\} \\ + \Re\left\{-j\omega_1 \mathbf{M_{1R}}\bar{\mathbf{I}}^*_{\mathbf{R2}} + j(P_1+P_2)\omega_R \mathbf{M_{1R}}\bar{\mathbf{I}}^*_{\mathbf{R2}} e^{j(P_2\omega_R-\omega_2)t}\right\} \end{aligned} \tag{2.102}$$

where the factor $\sqrt{3}$ has been cancelled from both sides of the equation. Instead of using summations, a matrix equation was written by organising the equivalent mutual inductances into a row vector,

$$\mathbf{M_{1R}} = \begin{bmatrix} M'_{1R_1} & \cdots & M'_{1R_{N_l}} \end{bmatrix} \tag{2.103}$$

and the rotor currents into a column vector,

$$\bar{\mathbf{I}}_{\mathbf{R1}} = \begin{bmatrix} \bar{I}_{R1_1} \\ \vdots \\ \bar{I}_{R1_{N_l}} \end{bmatrix} \tag{2.104}$$

[3]This is purely a mathematical convenience and does not hold true physical significance, except to indicate a negative sequence excitation.

In order to represent the voltage equation in terms of phasors, each of the frequencies must have the same magnitude. This condition is the mathematical definition of synchronism, i.e. the frequency of the rotor currents induced by each stator winding must be equal. Thus, either

$$P_2\omega_R - \omega_2 = P_1\omega_R - \omega_1 \tag{2.105}$$

resulting in a rotor speed

$$\omega_R = \frac{\omega_1 - \omega_2}{P_1 - P_2} \tag{2.106}$$

or

$$P_2\omega_R - \omega_2 = \omega_1 - P_1\omega_R \tag{2.107}$$

resulting in a rotor speed

$$\omega_R = \frac{\omega_1 - \omega_2}{P_1 + P_2} \tag{2.108}$$

Clearly the speed equation in (2.106) does not match that given in (1.1), yet (2.108) does match it. Analysis and experiment has shown that when the rotor is constructed with $P_1 + P_2$ nests, the speed will be given by (2.108). However, when constructed with $P_1 - P_2$ nests, it will be dictated by (2.106)[4]. Using the frequency relationship in (2.107), and taking the conjugate as needed, results in the steady-state voltage equation,

$$V_1 = (R_1 + j\omega_1 L_1)\bar{I}_1 + j\omega_1 \mathbf{M_{1R}}(\bar{\mathbf{I}}_{\mathbf{R1}} + \bar{\mathbf{I}}^*_{\mathbf{2R}}) \tag{2.109}$$

By similar analysis, the voltage equations for the second winding and two rotor components are determined to be

$$\bar{V}_2^* = (R_2 - j\omega_2 L_2)\bar{I}_2^* - j\omega_2 \mathbf{M_{2R}}(\bar{\mathbf{I}}_{\mathbf{R1}} + \bar{\mathbf{I}}^*_{\mathbf{2R}}) \tag{2.110}$$

$$\mathbf{0} = j(\omega_1 - P_1\omega_R)\mathbf{M}^{\mathbf{T}}_{\mathbf{1R}}\bar{I}_1 + \bar{\mathbf{Z}}_{\mathbf{RR}}\bar{\mathbf{I}}_{\mathbf{R1}} \tag{2.111}$$

$$\mathbf{0} = j(P_2\omega_R - \omega_2)\mathbf{M}^{\mathbf{T}}_{\mathbf{2R}}\bar{I}_2^* + \bar{\mathbf{Z}}_{\mathbf{RR}}\bar{\mathbf{I}}^*_{\mathbf{R2}} \tag{2.112}$$

[4]Although shown theoretically to be the case in this analysis and by Ferreira [31], it has not been tested experimentally. This is probably due to investigators seeing no perceived benefit in using a rotor with a low number of bars.

where the mutual impedance matrix $\mathbf{M_{2R}}$ is arranged as a row vector,

$$\mathbf{M_{2R}} = \begin{bmatrix} M'_{2R_1} & \cdots & M'_{2R_{N_l}} \end{bmatrix} \tag{2.113}$$

and the rotor current $\bar{\mathbf{I}}_{\mathbf{R2}}$ is arranged as a column vector,

$$\bar{\mathbf{I}}_{\mathbf{R2}} = \begin{bmatrix} \bar{I}_{R2_1} \\ \vdots \\ \bar{I}_{R2_{N_l}} \end{bmatrix} \tag{2.114}$$

The rotor impedance matrix, $\bar{\mathbf{Z}}_{\mathbf{RR}}$, is the same for both cases by virtue of the relationship between the frequencies given in (2.107). Of dimension $N_l \times N_l$, it is expressed

$$\bar{\mathbf{Z}}_{\mathbf{RR}} = \begin{bmatrix} \bar{Z}_{R_i R_j} \\ i,j \in \{1,\ldots,N_l\} \end{bmatrix} \tag{2.115}$$

where

$$\bar{Z}_{R_i R_j} = R'_{ij} + j(\omega_1 - P_1\omega_R)L'_{ij} \tag{2.116}$$

The voltage equations can be further simplified by solving both (2.111) and (2.112) for the rotor currents yielding

$$\bar{\mathbf{I}}_{\mathbf{R1}} = -j(\omega_1 - P_1\omega_R)\bar{\mathbf{Z}}_{\mathbf{RR}}^{-1}\mathbf{M}_{\mathbf{1R}}^{\mathbf{T}}\bar{I}_1 \tag{2.117}$$

$$\bar{\mathbf{I}}_{\mathbf{R2}}^{*} = -j(P_2\omega_R - \omega_2)\bar{\mathbf{Z}}_{\mathbf{RR}}^{-1}\mathbf{M}_{\mathbf{2R}}^{\mathbf{T}}\bar{I}_2^{*} \tag{2.118}$$

and substituting the results into (2.109) and (2.110) to obtain, after simplification,

$$V_1 = \left(R_1 + j\omega_1 L_1 + \omega_1(\omega_1 - P_1\omega_R)\mathbf{M_{1R}}\bar{\mathbf{Z}}_{\mathbf{RR}}^{-1}\mathbf{M}_{\mathbf{1R}}^{\mathbf{T}}\right)\bar{I}_1 + \omega_1(P_2\omega_R - \omega_2)\mathbf{M_{1R}}\bar{\mathbf{Z}}_{\mathbf{RR}}^{-1}\mathbf{M}_{\mathbf{2R}}^{\mathbf{T}}\bar{I}_2^{*} \tag{2.119}$$

$$V_2^{*} = \left(R_2 - j\omega_2 L_2 - \omega_2(P_2\omega_R - \omega_2)\mathbf{M_{2R}}\bar{\mathbf{Z}}_{\mathbf{RR}}^{-1}\mathbf{M}_{\mathbf{2R}}^{\mathbf{T}}\right)\bar{I}_2^{*} - \omega_2(\omega_1 - P_1\omega_R)\mathbf{M_{2R}}\bar{\mathbf{Z}}_{\mathbf{RR}}^{-1}\mathbf{M}_{\mathbf{1R}}^{\mathbf{T}}\bar{I}_1 \tag{2.120}$$

These equations, although achieved by transformation into the RRF, represent a per-phase equivalent system capable of predicting the electrical performance of

the machine. The voltages and currents are rms phase quantities. The rotor currents, now implicit in the voltage equations of (2.119) and (2.120), can be determined using (2.117) and (2.118) to obtain a combined current[5], $\bar{\mathbf{I}}_{\mathbf{R}} = \bar{\mathbf{I}}_{\mathbf{R1}} + \bar{\mathbf{I}}^{*}_{\mathbf{R2}}$. This total current is a vector containing each of the loop currents in the first nest. The currents in the other nests are just phase shifted versions of these currents.

Throughout this analysis, the first winding axis was used as the reference. Under steady-state conditions this equates to the voltage phasor, V_1, becoming the reference with zero phase angle. All other phase angles in the steady-state voltage equations are measured with respect to this reference.

2.5.2 Torque Equation

Equations for the four components of torque given in (2.84)–(2.87) are used along with the definitions of the steady-state currents to arrive at an expression for the steady-state torque produced by the machine. When performing these calculations, the currents should be expressed in real form. Thus,

$$\mathbf{i}'_{\mathbf{1}} = \sqrt{3}\begin{bmatrix} I_1\cos((\omega_1 - P_1\omega_R)t + \phi_1) \\ -I_1\sin((\omega_1 - P_1\omega_R)t + \phi_1) \end{bmatrix} \tag{2.121}$$

where the conjugate of (2.93) was performed before subsequently converting to real form. The same can be done for the rotor currents in the i-th rotor loop system induced by the first winding,

$$\mathbf{i}'_{\mathbf{R1_i}} = \sqrt{3}\begin{bmatrix} I_{R1_i}\cos((\omega_1 - P_1\omega_R)t + \phi_{R1_i}) \\ -I_{R1_i}\sin((\omega_1 - P_1\omega_R)t + \phi_{R1_i}) \end{bmatrix} \tag{2.122}$$

For the second winding, using the frequency convention where ω_2 holds its sign,

$$\mathbf{i}'_{\mathbf{2}} = \sqrt{3}\begin{bmatrix} I_2\cos((P_2\omega_R - \omega_2)t - \phi_2) \\ I_2\sin((P_2\omega_R - \omega_2)t - \phi_2) \end{bmatrix} \tag{2.123}$$

The rotor currents in the i-th rotor loop system induced by the second winding are given as

$$\mathbf{i}'_{\mathbf{R2_i}} = \sqrt{3}\begin{bmatrix} I_{R2_i}\cos((P_2\omega_R - \omega_2)t - \phi_{R2_i}) \\ I_{R2_i}\sin((P_2\omega_R - \omega_2)t - \phi_{R2_i}) \end{bmatrix} \tag{2.124}$$

[5]The complex sum $\bar{\mathbf{I}}_{\mathbf{R}} = \bar{\mathbf{I}}_{\mathbf{R1}} + \bar{\mathbf{I}}^{*}_{\mathbf{R2}}$ is used in the steady-state analysis. However, dynamic analysis still uses the sum $\mathbf{I}_{\mathbf{R}} = \mathbf{I}_{\mathbf{R1}} + \mathbf{I}_{\mathbf{R2}}$

The electromagnetic torque produced by the BDFM is given by the summation of four components, indicated by (2.83). By inspection of the expressions for the torque components given in (2.84)–(2.87), it can be seen that each of these terms contains a product of two currents. Since each of the currents varies sinusoidally, each product will result in the sum and difference of the two trigonometric function arguments. Consequently, by using the definition of synchronism, $\omega_1 - P_1\omega_R = P_2\omega_R - \omega_2$, each product of currents in the torque equations will lead to one term which pulsates at twice the frequency of the currents and a second term that is constant. This constant term represents the steady-state torque produced. Therefore, by inspection

$$T_{11} = 3P_1 I_1 \sum_{i=1}^{N_l} M'_{R1_i} I_{R1_i} \sin(\phi_1 - \phi_{R1_i}) \tag{2.125}$$

$$T_{12} = 3P_1 I_1 \sum_{i=1}^{N_l} M'_{R1_i} I_{R2_i} \sin(\phi_1 + \phi_{R2_i}) \tag{2.126}$$

$$T_{21} = -3P_2 I_2 \sum_{i=1}^{N_l} M'_{R2_i} I_{R1_i} \sin(-\phi_2 - \phi_{R1_i}) \tag{2.127}$$

$$T_{22} = -3P_2 I_2 \sum_{i=1}^{N_l} M'_{R2_i} I_{R2_i} \sin(-\phi_2 + \phi_{R2_i}) \tag{2.128}$$

This set of equations can be expressed using complex notation as

$$T_{11} = 3P_1 \Im\left\{\bar{I}_1 \mathbf{M_{R1}} \bar{\mathbf{I}}^*_{\mathbf{R1}}\right\} \tag{2.129}$$

$$T_{12} = 3P_1 \Im\left\{\bar{I}_1 \mathbf{M_{R1}} \bar{\mathbf{I}}_{\mathbf{R2}}\right\} \tag{2.130}$$

$$T_{21} = -3P_2 \Im\left\{\bar{I}^*_2 \mathbf{M_{R2}} \bar{\mathbf{I}}^*_{\mathbf{R1}}\right\} \tag{2.131}$$

$$T_{22} = -3P_2 \Im\left\{\bar{I}^*_2 \mathbf{M_{R2}} \bar{\mathbf{I}}_{\mathbf{R2}}\right\} \tag{2.132}$$

where $\Im\{\cdot\}$ signifies the imaginary part of the function.

The equations for torque can be combined into one expression and simplified by substituting for the complete rotor current, $\bar{\mathbf{I}}_{\mathbf{R}} = \bar{\mathbf{I}}_{\mathbf{R1}} + \bar{\mathbf{I}}^*_{\mathbf{R2}}$, yielding

$$T_e = \Im\left\{3P_1 \bar{I}_1 \mathbf{M_{R1}} \bar{\mathbf{I}}^*_{\mathbf{R}} - 3P_2 \bar{I}^*_2 \mathbf{M_{R2}} \bar{\mathbf{I}}^*_{\mathbf{R}}\right\} \tag{2.133}$$

For analysis, it may be important to know what components make up the total electromagnetic torque on the machine. In this case, (2.129)–(2.132) are used. However, if the components are not important, then just the expression in (2.133) need be used.

2.5.3 Discussion

The torque equation and two voltage equations, (2.119) and (2.120), form the steady-state voltage model of the BDFM. By decomposing the rotor currents into two separate components, the effect of each stator winding can be determined which can potentially facilitate design of the BDFM. This model is an improvement over the model presented in [21] because of its ability to determine the rotor loop currents.

This model was first published as a conference paper in 1996 [22]. Subsequent to this, an alternative steady-state model for the BDFM was proposed by Ferreira in [23], which used harmonic analysis instead of dq analysis. The model incorporated the spatial harmonics generated by the actual non-sinusoidal distribution of the windings around the stator circumference. The harmonic model, like the dq model presented here, provides for the determination of the rotor loop currents. Moreover, it has the advantage of slightly improved accuracy because of the inclusion of the spatial harmonics. However, this is achieved at the expense of greater complexity.

The harmonic model divides the analysis into two different cases, one for positive sequence excitation and another for negative sequence excitation. Two different sets of voltage and torque equations result. Nevertheless, it can be shown that if only the fundamental harmonics are considered in the harmonic model, the resulting equations for both positive and negative sequence excitation are identical to the single set of equations presented in this section. The harmonic model has been verified extensively in [31, 23], and is verified in the presence of inter-bar currents in Chapter 4. However, results are presented which demonstrate the typical improvement achieved by the inclusion of the spatial harmonics.

The following tests were carried out on a BDFM that used a rotor where

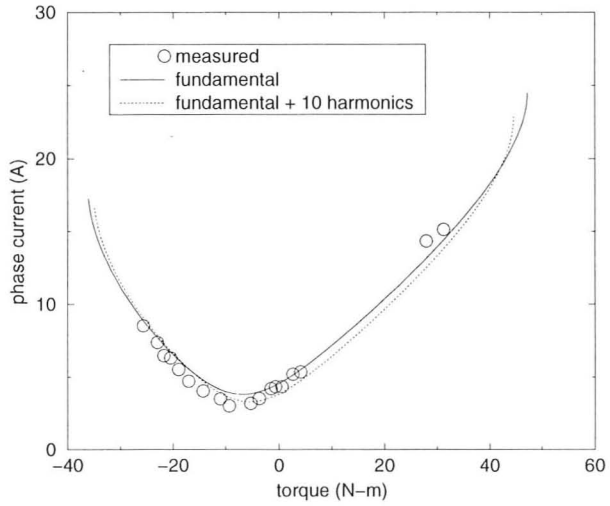

Figure 2.6: First winding phase current of the BDFM with an insulated rotor at 400 r/min with 50 V applied to the first winding and 20 V applied to the second winding.

the rotor bars and rotor iron were electrically insulated from each other[6]. The first winding was supplied via a mains connected auto-transformer at a phase voltage of 50 V and a frequency of 50 Hz. The second winding was supplied via a controlled synchronous machine which provided a phase voltage of 20 V at 10 Hz. This voltage was connected in opposite sequence to that of the first winding which resulted in a rotor speed of 400 r/min. The measured and predicted phase currents for the first winding are shown in Fig. 2.6 and in Fig. 2.7 for the second winding.

As can be seen, both models are reasonably accurate. However, the additional harmonics, ten beyond the fundamental in this case, help improve the accuracy. This amount of improvement is typical. Inclusion of more harmonics beyond ten does not appreciably change the predicted results. The accuracy of the results suggest that the model presented here is suitable for design purposes.

[6]The details of the stator of this BDFM are given in Chapter 4

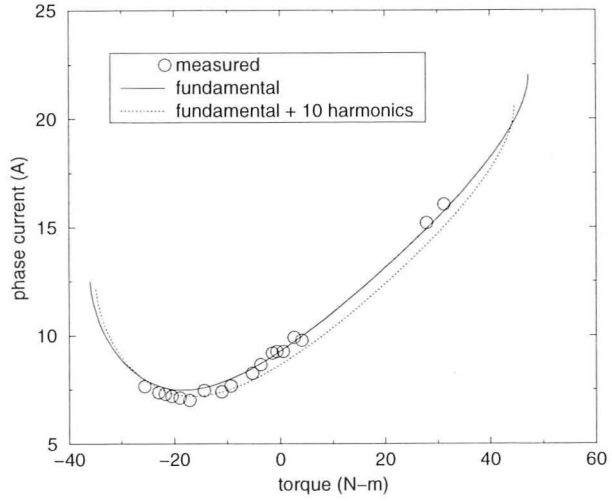

Figure 2.7: Second winding phase current of the BDFM with an insulated rotor at 400 r/min with 50 V applied to the first winding and 20 V applied to the second winding.

Chapter 3

Inter-bar Resistance Model

3.1 Preliminary

3.1.1 Overview

The research group at Oregon State University tested a BDFM using a die-cast rotor. They observed greatly reduced performance. So poor was the performance, the BDFM would not always synchronise. When it did, the stator winding currents were greatly increased. Through collaboration with staff at the University of Cambridge, inter-bar currents flowing between the rotor bars, through the rotor iron, were presumed to be cause of the problem.

The group did not have any capability to model this phenomenon because all previous models developed contained the implicit assumption that the rotor bars were insulated from the rotor iron, an assumption not previously identified. The observed poor performance made it obvious that if inter-bar currents were the cause of the problem and were always going to be present in die-cast rotors, then a die-cast rotor could not be used in the BDFM, which would make the BDFM commercially unattractive. This chapter presents a coupled-circuit model which attempts to describe the inter-bar current phenomenon in the BDFM and determine whether the observed performance degradation is indeed due to the flow of inter-bar currents in the rotor. The model is based on harmonic analysis and follows the same analysis procedure described by Ferreira in [31] and also by Williamson, Ferreira and Wallace in [23].

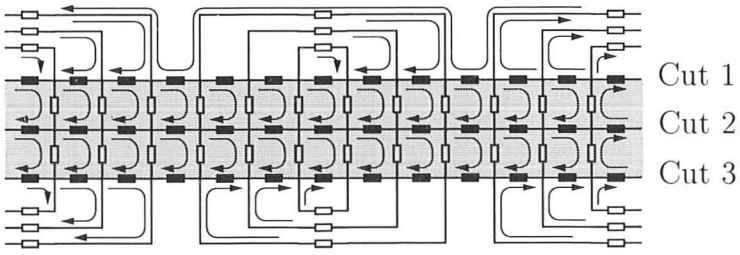

Figure 3.1: Rotor circuit configuration of a Type I rotor with three cuts where inter-bar resistance paths are shown in black.

Modelling of the inter-bar currents, a distributed and uneven phenomenon, can be accomplished by constraining the rotor currents to flow between adjacent bars only at specific axial locations, called *cuts*. Different levels of insulation can be simulated by adjusting the value of resistance between the bars. A high level of resistance in comparison to the rotor bar resistance results in, effectively, an insulated rotor. Conversely, a low level of resistance models an uninsulated rotor with characteristics similar to that of a poorly insulated squirrel cage, which, as will be shown, results in significantly degraded performance. It is believed that the effect of currents flowing through the iron between non-adjacent bars can be adequately modelled by modifying the resistances between adjacent bars. However, current paths between non-adjacent bars can be accommodated by modifying this analysis at the expense of greater complexity—a topic for further research.

Consider a rotor connected in a Type I (Creedy) configuration with three loops within each nest. Figure 3.1 shows the equivalent rotor circuit configuration for one of the rotor nests where three cuts have been made. The inter-bar currents are assumed to flow only between adjacent bars where the cuts are made. The combination of inter-bar resistances, rotor bar segments and end-connections forms a network of loops, each of which will have an associated mesh current flowing in it as indicated in Fig. 3.1. Each loop will contain bar segments or end-connections, and, at most, two inter-bar resistances. Williamson, Healey, and Lloyd used a similar electrical network to represent a squirrel cage rotor in their investigation of inter-bar currents in single-phase motors [27]. The machine can now be regarded as a set of circuits consisting of the windings of the stator and the above-defined loops of the rotor. A steady-state matrix voltage equation can be written of the

form,

$$\bar{\mathbf{V}} = \bar{\mathbf{Z}}\bar{\mathbf{I}} \tag{3.1}$$

where $\bar{\mathbf{V}}$ is the applied voltage vector (equal to zero for the rotor circuits), $\bar{\mathbf{Z}}$ is the impedance matrix containing the impedances between both stator systems and the rotor, and $\bar{\mathbf{I}}$ is the vector of currents in each of the circuits, of which some of the currents may be known. The problem therefore becomes one of defining coupling impedances which link all of these circuits together via the air-gap flux. In order to simplify the analysis, and bearing in mind that the primary objective of this work is to prove the existence of inter-bar currents as the cause of degraded performance, the following assumptions are made

- saturation may be ignored;
- both the stator and the rotor are smooth, un-slotted surfaces;
- the stator windings are excited by balanced, sinusoidal three phase supplies.

3.1.2 Coordinate Systems

In order to facilitate the analysis, three Cartesian coordinate systems are used. In all of them, there has been an implicit conversion between the natural cylindrical coordinates and the Cartesian system used in this analysis. The conversion is achieved by flattening the motor so that the stator and rotor air-gap surfaces appear as plates separated by the air-gap. Periodicity in the fields is achieved by using the harmonic wave number, explained later.

The first coordinate system is the stationary (stator) reference frame (SRF), designated by the coordinates (x, y, z), with direction vectors $\hat{a}_x$, $\hat{a}_y$, and $\hat{a}_z$. The $\hat{a}_x$ direction is along the axis of the motor, perpendicular to the plane of the laminations. The $\hat{a}_y$ direction is along the circumference of the motor and the $\hat{a}_z$ direction is radial from the rotor to the stator, perpendicular to the air-gap.

The second coordinate system is fixed on the rotor and uses coordinate triples (x', y', z). The corresponding direction vectors are $\hat{a}_{x'}$, $\hat{a}_{y'}$, and $\hat{a}_z$. This coordinate system forms the rotor reference frame (RRF). The RRF and SRF are related such that at time $t = 0$, the two systems are coincident and share a common origin.

When the rotor rotates at velocity, v, there will be relative motion between the $\hat{a}_y$ and $\hat{a}_{y'}$ directions. Figure 3.2 illustrates the relationship between a point on the stator and a point on the rotor, which can be written as

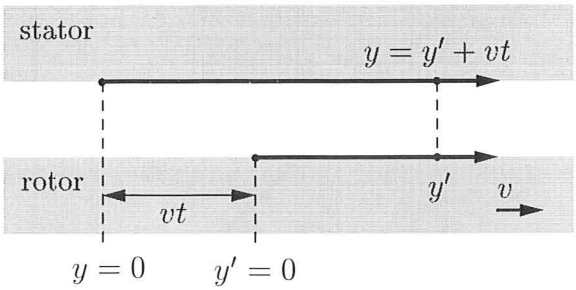

Figure 3.2: Diagram showing the relationship between the stator reference frame and the rotor reference frame assuming the systems are initially aligned at $t = 0$.

$$y = y' + vt = y' + \frac{d}{2}\omega_R t \tag{3.2}$$

where substitution of $v = \omega_R \frac{d}{2}$ has been made. ω_R is the angular velocity of the rotor and d the diameter to the air-gap. The x' and z coordinates are the same as those in the SRF[1].

If the rotor is skewed, a third system is used with coordinates (x'', y'', z) and corresponding direction vectors, $\hat{a}_{x''}$, $\hat{a}_{y''}$, and $\hat{a}_z$. The origin of this RRF system is assumed to be coincident with the origin of the previous RRF system, but rotated by a skew angle, γ, such that the $\hat{a}_{x''}$ direction vector is parallel to the rotor bars. Note that if there is no skew, $\gamma = 0$ and the two RRF systems are identical.

In the ensuing analysis it is necessary to convert between the two RRF coordinate systems. Equations relating coordinates in the skewed RRF to coordinates in the standard RRF are derived from the dot product between a vector to an arbitrary point in the standard RRF and the individual direction vectors in the skewed RRF (see Fig. 3.3). For example, let $\vec{R} = x\hat{a}_{x'} + y\hat{a}_{y'}$. Taking the dot product, first with $\hat{a}_{x''}$ and then with $\hat{a}_{y''}$, results in the transformation equations given in (3.3)–(3.4). Note that skew angles are measured in the conventional sense; increasing angles are in the counter-clockwise direction.

$$x'' = \vec{R} \cdot \hat{a}_{x''} = x' \cos\gamma + y' \sin\gamma \tag{3.3}$$

[1]The z coordinate has not been primed since it is common in all three coordinate systems.

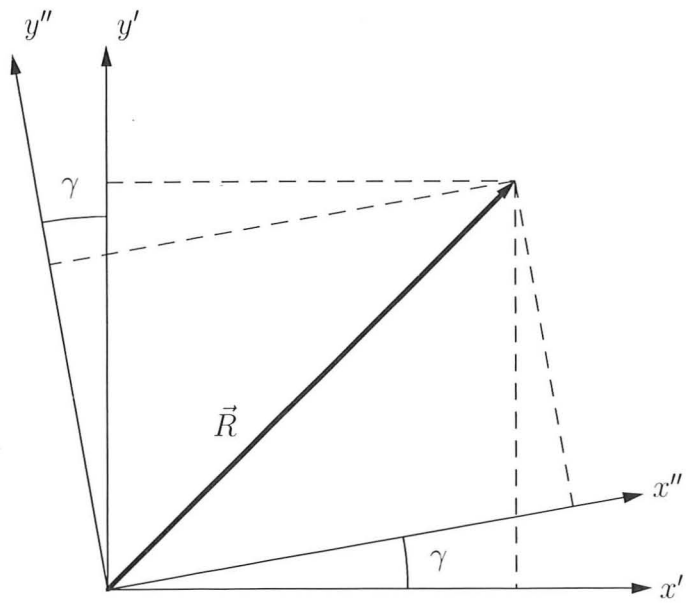

Figure 3.3: A vector $\vec{R}$ shown in the skewed and standard RRF.

$$y'' = \vec{R} \cdot \hat{a}_{y''} = -x' \sin\gamma + y' \cos\gamma \tag{3.4}$$

3.1.3 Rotor Configurations

In this work, three different rotor configurations are considered. Described in Chapter 2 during the development of the *dq* model, they are the Type I (Creedy), Type II (Broadway), and Type III (modified Broadway). For each configuration it is assumed,

- there are $N_n = P_1 + P_2$ nests;
- the bars may be of different diameters and sizes;
- all rotor slots have the same slot mouth opening;
- the bars are not necessarily equidistant about the rotor circumference;
- the general loop-within-nest configuration is maintained.

When specifying the locations of the imaginary cuts across the rotor bars, i.e. the location of the inter-bar resistances, a cut must be placed along the edge of the rotor iron whenever there is no common end-ring present. For example, since the Type I rotor configuration has no common end-rings, it requires at least two cuts, each placed along the edge of the rotor iron. The Type II and Type III configurations require at least one cut because they both have one common end-ring. Additional cuts beyond the minimum number need not be equidistant. Placing the initial cuts along the edge of the rotor iron, as advised, is necessary to properly account for the air-gap coupling between the rotor loops. Although necessary, the initial placement does not diminish the capabilities of the model.

Figure 3.4 shows a multi-nested Type I rotor (with three loops per nest) where two cuts have been specified. The lower half of the figure shows the associated impedance network formed by placing resistances between adjacent bars along the cuts. Bar resistances are shown in white and inter-bar resistances in black. This network, modelled using mesh currents, contains B branches and N nodes. By electrical network theory, there will be $B - N + 1$ independent loop currents. These are the currents that flow in the "windows" as well as an additional loop current that flows around the circuit formed by the outer end connections and inter-bar resistance links (see Fig. 3.1). Algebraically,

$$N_{eq} = 2N_c N_n N_l + 1 \tag{3.5}$$

where N_{eq} is the number of independent current-loops, N_c is the number of cuts made, N_n is the number of rotor nests, and N_l is the number of loops within each of the rotor nests. The configuration and equivalent circuit for the Type II and Type III rotor are shown in Figs. 3.5 and 3.6, respectively, where two cuts have been made. The number of independent loop currents in all three configurations is summarised in Table 3.1.

3.2 Conductor Density Functions

In harmonic analysis, the stator and rotor windings are mathematically described using conductor density functions [25], which are complex Fourier series used to describe the non-sinusoidal distribution of the conductors. These functions are

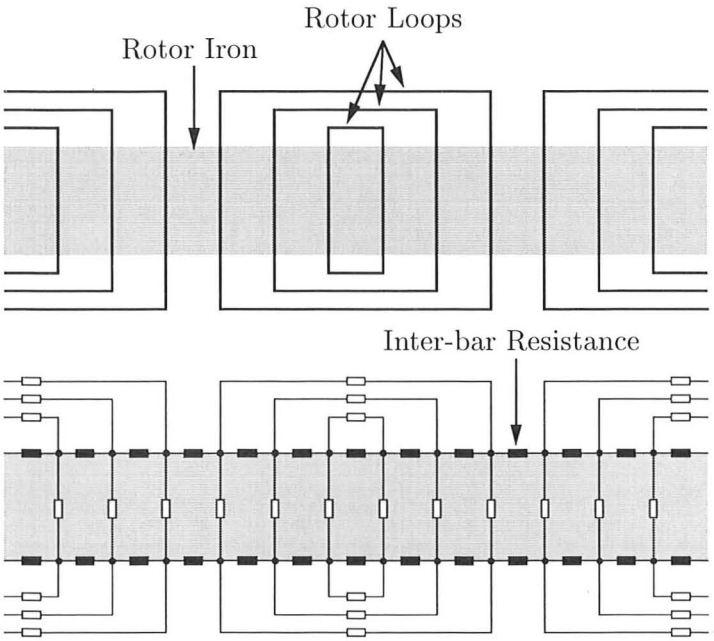

Figure 3.4: One nest of a multi-nested Type I rotor (three loops per nest) showing two cuts and the associated impedance network due to the cuts.

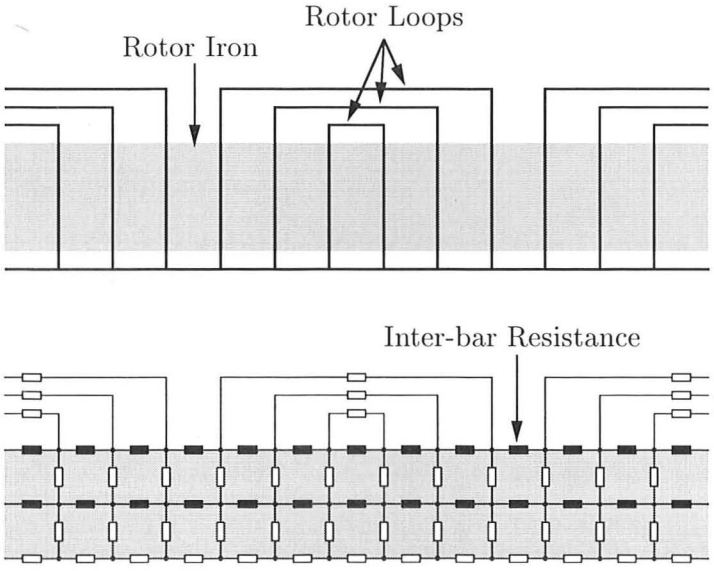

Figure 3.5: One nest of a multi-nested Type II rotor (three loops per nest) showing two cuts and the associated impedance network due to the cuts.

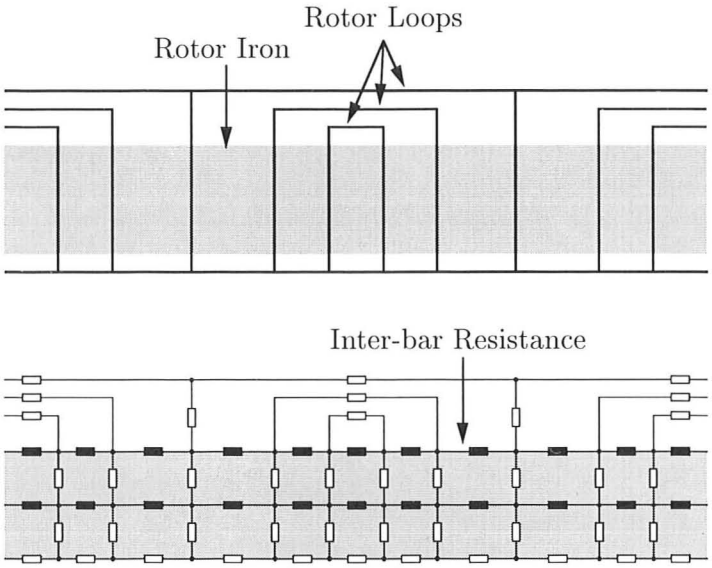

Figure 3.6: One nest of a multi-nested Type III rotor (three loops per nest) showing two cuts and the associated impedance network due to the cuts.

Table 3.1: Number of Independent Rotor Mesh Currents (N_{eq})

Rotor Configuration	N_{eq}
I	$2N_cN_nN_l + 1$
II	$2N_cN_nN_l + N_nN_l + 1$
III	$N_cN_n(2N_l - 1) + N_nN_l + 1$

used to develop expressions for the coupling impedances. The results presented in Appendix A, which pertain to the conductor density of a typical three-phase, balanced stator winding, act as a basis for the development of the conductor density functions for both stator windings and for the rotor current-loops.

3.2.1 Stator

Since each stator winding is balanced and three-phase, the results given in Appendix A can be applied directly. For the first winding, using equations (A.20)–(A.22) with the proper substitutions,

$$\vec{c}_{1A}(y) = \sum_{\kappa} \bar{C}_1^{\kappa} e^{-jky} \hat{a}_x \tag{3.6}$$

$$\vec{c}_{1B}(y) = \sum_{\kappa} \bar{C}_1^{\kappa} e^{-jk\left(y+\frac{2\pi d}{6P_1}\right)} \hat{a}_x \tag{3.7}$$

$$\vec{c}_{1C}(y) = \sum_{\kappa} \bar{C}_1^{\kappa} e^{-jk\left(y-\frac{2\pi d}{6P_1}\right)} \hat{a}_x \tag{3.8}$$

where κ is the spatial harmonic, $k = \frac{2\kappa}{d}$ is the wave number which accounts for the periodicity of the electromagnetic fields, P_1 is the number of pole-pairs of the winding,

$$\bar{C}_1^{\kappa} = -j\frac{N_{ph1}}{\pi d} K_{b1}^{\kappa} K_{p1}^{\kappa} K_{d1}^{\kappa} e^{j\left(\frac{\pi\kappa}{6P_1} - \frac{\pi\kappa}{N_s}\right)} e^{jky_{01}} \tag{3.9}$$

is the conductor density coefficient, N_{ph1} is the number of turns per phase of the winding, d is the diameter to the air-gap, y_{01} is the offset of the reference coil of the phase from the origin of the SRF,

$$K_{b1}^{\kappa} = \frac{\sin\left(\frac{kb_s}{2}\right)}{\left(\frac{kb_s}{2}\right)} \tag{3.10}$$

is the slot width factor of the winding, b_s is the slot mouth opening of the stator,

$$K_{p1}^{\kappa} = \sin\left(\frac{k\alpha_1}{2}\right) \tag{3.11}$$

is the pitch factor of a coil of the winding, α_1 is the span of a coil (in metres),

$$K_{d1}^{\kappa} = \frac{\sin\left(\frac{\pi\kappa}{6P_1}\right)}{\frac{N_s}{6P_1}\sin\left(\frac{\pi\kappa}{N_s}\right)} \tag{3.12}$$

is the distribution factor of the winding, and N_s is the number of stator slots. A similar set of equations holds for the second winding,

$$\vec{c}_{2A}(y) = \sum_{\lambda} \bar{C}_2^{\lambda} e^{-jly} \hat{a}_x \tag{3.13}$$

$$\vec{c}_{2B}(y) = \sum_{\lambda} \bar{C}_2^{\lambda} e^{-jl\left(y+\frac{2\pi d}{6P_2}\right)} \hat{a}_x \tag{3.14}$$

$$\vec{c}_{2C}(y) = \sum_{\lambda} \bar{C}_2^{\lambda} e^{-jl\left(y-\frac{2\pi d}{6P_2}\right)} \hat{a}_x \tag{3.15}$$

where the conductor density coefficient for the second winding is

$$\bar{C}_2^{\lambda} = -j\frac{N_{ph2}}{\pi d} K_{b2}^{\lambda} K_{p2}^{\lambda} K_{d2}^{\lambda} e^{j\left(\frac{\pi\lambda}{6P_2}-\frac{\pi\lambda}{N_s}\right)} e^{jly_{02}} \tag{3.16}$$

The slot width, pitch, and distribution factors are similar to those for the first winding and are made specific to the second winding by proper substitution. Detailed explanations of the various factors and coefficients are contained in Appendix A.

3.2.2 Rotor

Consider the n-th rotor current-loop of the impedance network shown in Fig. 3.7. It has a span σ_n in the $\hat{a}_{y'}$ direction and axial depth w' in the $\hat{a}_{x'}$ direction. The loop is assumed centred at (x''_{0n}, y''_{0n}) (not shown). Multiplying the dimensions in the $\hat{a}_{y'}$ direction by $\cos\gamma$ yields the projections of these lengths in the $\hat{a}_{y''}$ direction.

Loop n will have a conductor density as shown in Fig. 3.8 when looking in the $\hat{a}_{x''}$ direction in the skewed RRF—it has a positive conductor density along one bar and a negative density along the other. The slot mouth opening has width b_R in the $\hat{a}_{y'}$ direction and width $b_R \cos\gamma$ in the $\hat{a}_{y''}$ direction, as shown. The conductor density of loop $(n+1)$ is also shown to demonstrate the way in which the rotor conductors are modelled.

The spatial harmonics of the rotor current-loop are represented by the harmonic number μ with a corresponding wave number, m, where μ is any signed integer value. In addition to the previously mentioned dimensions, the effective wave number, m'', is introduced to account for the skew of the rotor. It can be

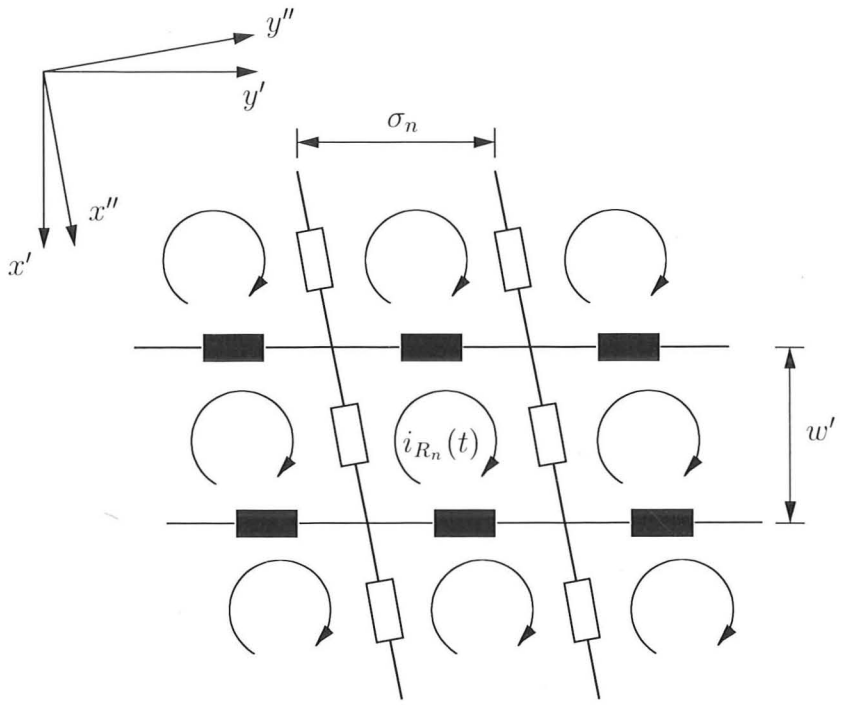

Figure 3.7: A portion of a rotor current mesh showing loop n, assumed current directions and important dimensions.

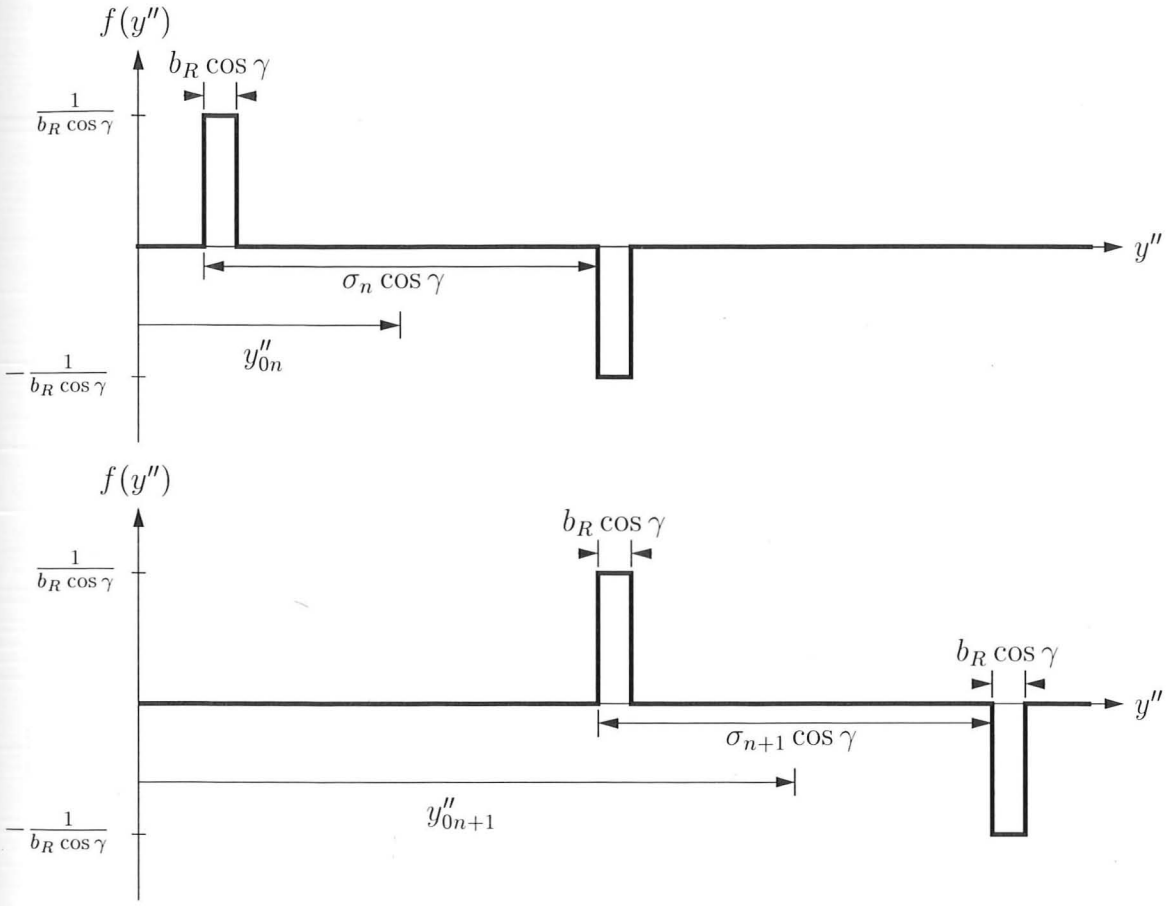

Figure 3.8: Rotor turns density viewed in the $\hat{a}_{x''}$ direction for loop n and loop $(n+1)$.

derived by equating the electrical distance to the actual distance travelled by one full period of a harmonic field to the circumference of the rotor, i.e.

$$m''(\pi d \cos\gamma) = 2\pi\mu$$
$$m'' = \frac{2\mu}{d\cos\gamma} = \frac{m}{\cos\gamma}$$

Using the effective wave number and the results in Appendix A, the conductor density function for loop n is (using the subscript R_n to signify rotor current-loop n)

$$\vec{c}_{R_n}(y'') = \sum_{\mu} \bar{C}^{\mu}_{R_n} e^{-jm''y''} \hat{a}_{x''} \tag{3.17}$$

where the conductor density coefficient can be expressed as

$$\bar{C}^{\mu}_{R_n} = -j\frac{2}{\pi d\cos\gamma} K^{\mu}_{bR} K^{\mu}_{pR_n} e^{jm''y''_{0n}} \tag{3.18}$$

where

$$K^{\mu}_{bR} = \frac{\sin\left(\frac{mb_R}{2}\right)}{\frac{mb_R}{2}} \tag{3.19}$$

is the slot width factor for the μ-th harmonic and

$$K^{\mu}_{pR_n} = \sin\left(\frac{m\sigma_n}{2}\right) \tag{3.20}$$

is the pitch factor of loop n for the μ-th harmonic. Both equations (3.17) and (3.18) can be transformed to the standard RRF using the relationship in (3.4) yielding,

$$\vec{c}_{r_n}(x', y') = \sum_{\mu} \bar{C}^{\mu}_{R_n} e^{jmx'\tan\gamma} e^{-jmy'} \hat{a}_{x''} \tag{3.21}$$

$$\bar{C}^{\mu}_{R_n} = -j\frac{2}{\pi d\cos\gamma} K^{\mu}_{bR} K^{\mu}_{pR_n} e^{-jmx'_{0n}\tan\gamma} e^{jmy'_{0n}} \tag{3.22}$$

Equations (3.21) and (3.22) specify the conductor density function for a particular rotor loop in the standard RRF, which will be useful in the development of the coupling impedance expressions.

3.3 Impedance Relationships

The expressions for the coupling impedances between the electrical circuits are derived using the conductor density functions of the rotor and stator windings as well as the geometry of the machine. This is a two step process. The first step is to examine the stator produced fields. This will lead to expressions for the self impedances of the two stator windings. It will also lead to expressions for the voltages induced in the rotor current-loops. This expression contains the mutual impedance between the stator and the rotor. The second step examines the rotor produced fields. Currents that flow in the rotor current-loops produce fields which couple with the rotor loops themselves as well as with the stator. Analysis of this coupling yields expressions for the rotor self-impedance as well as the rotor-stator coupling impedance.

3.3.1 Stator Fields

The analysis relies on the assumption that balanced currents flow in a particular stator winding. These currents set up a travelling wave of current density which produces a magnetic field. This magnetic field is associated with
an electric field which, in conjunction with the conductor density function, can then be used to determine the air-gap inductance of the stator winding as well as the coupling impedance relating stator currents to induced rotor voltages. For the moment, only air-gap fields are considered. Leakage components and resistance are added after the main air-gap produced inductances are calculated.

For a general stator winding, assume positive sequence balanced currents with frequency ω_S of the form,

$$i_A(t) = \Re\left\{\sqrt{2}\bar{I}_S e^{j\omega_S t}\right\} \tag{3.23}$$

$$i_B(t) = \Re\left\{\sqrt{2}\bar{I}_S e^{j\left(\omega_S t - \frac{2\pi}{3}\right)}\right\} \tag{3.24}$$

$$i_C(t) = \Re\left\{\sqrt{2}\bar{I}_S e^{j\left(\omega_S t + \frac{2\pi}{3}\right)}\right\} \tag{3.25}$$

Multiplication of these currents by the conductor density functions for each of the phases yields the current density produced by the stator winding,

$$\vec{j}_S(y,t) = \vec{c}_A(y)i_A(t) + \vec{c}_B(y)i_B(t) + \vec{c}_C(y)i_C(t) \tag{3.26}$$

Simplifying and assuming the spatial harmonics are represented by κ and the wave number by k,

$$\vec{j}_S(y,t) = \Re\left\{\sqrt{2}\sum_{\kappa} 3\bar{C}_S^{\kappa}\bar{I}_S e^{j(\omega_S t - ky)}\right\}\hat{a}_x \tag{3.27}$$

in which the harmonics are constrained by the relationship

$$\kappa = (6q+1)\kappa_1 \tag{3.28}$$

where q is any integer and κ_1 is the fundamental harmonic, which is also the pole-pair number of the winding.

If a negative sequence current set is impressed on the windings instead, the same current density expression in (3.27) results except with the constraint on the harmonics being

$$\kappa = (6q-1)\kappa_1 \tag{3.29}$$

For both types of excitation, the current density calculation confirms that a balanced three phase winding produces the expected harmonics associated with a three phase machine, $1, -5, 7, -11, 13\ldots$ However, in order to use just one expression for the constraint on the stator harmonics, that given in (3.28), the fundamental harmonic for negative sequence excitation is assigned a negative value, $\kappa_1 = -P$. This attaches some physical significance to the fundamental harmonic since, in actuality, the negative sequence fields travel in an opposite direction to positive sequence fields.

The magnetic flux density due to the current flowing in the different windings can be determined from the application of Ampère's Law. It is assumed that the rotor and stator iron are infinitely permeable and that the permeability of the air-gap is that of free space (μ_0). Integrating counter-clockwise along the path shown in Fig. 3.9 yields a relationship between the flux density and the current density,

$$\begin{aligned} \frac{1}{\mu_0}\left(\vec{b}_S(y,t) + \frac{\partial \vec{b}_S(y,t)}{\partial y}\Delta y\right) g - \frac{\vec{b}_S(y,t)}{\mu_0} g &= \vec{j}_S(y,t)\Delta y \\ \frac{\partial \vec{b}_S(y,t)}{\partial y} &= \frac{\mu_0}{g}\,\vec{j}_S(y,t) \end{aligned} \tag{3.30}$$

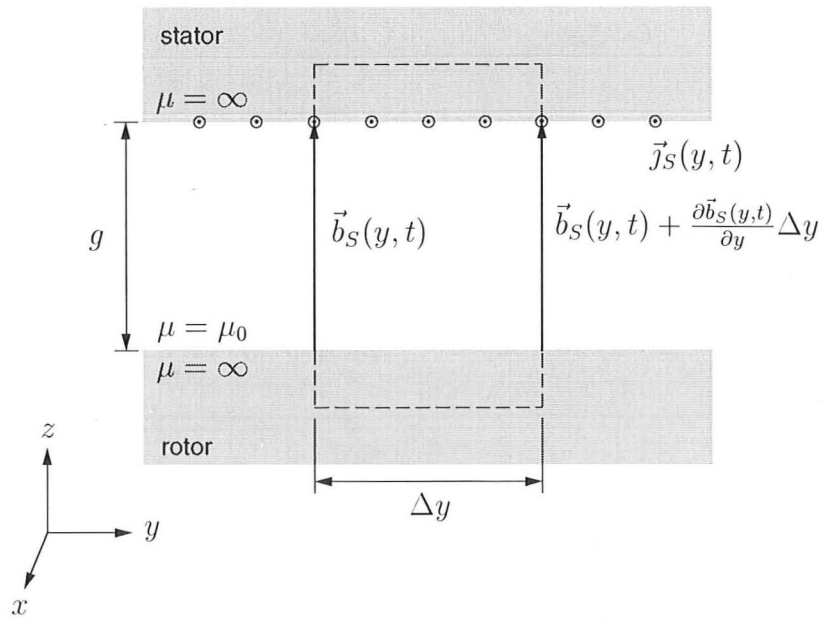

Figure 3.9: Representation of the magnetic field in the air-gap.

The expression for the magnetic flux density will have a form similar to that of the current density,

$$\vec{b}_S(y,t) = \Re\left\{\sum_{\kappa} \sqrt{2}\bar{B}_S^{\kappa} e^{j(\omega_S t - ky)}\right\}\hat{a}_z \tag{3.31}$$

Therefore, by differentiating and comparing terms,

$$\bar{B}_S^{\kappa} = j\frac{3\mu_0}{gk}\bar{C}_S^{\kappa}\bar{I} \tag{3.32}$$

The electric field in the stator reference frame can be calculated using Faraday's Law,

$$\nabla \times \vec{e} = -\frac{\partial \vec{b}}{\partial t} \tag{3.33}$$

and realising that the electric field and magnetic flux density are orthogonal to each other in this system. The expression for the electric field can be assumed to

have a form similar to the magnetic field,

$$\vec{e}_S(y,t) = \Re\left\{\sum_{\kappa} \sqrt{2}\bar{E}_S^{\kappa} e^{j(\omega_S t - ky)}\right\}\hat{a}_x \tag{3.34}$$

Differentiating and equating terms yields the expression

$$\bar{E}_S^{\kappa} = -\frac{\omega_S}{k}\bar{B}_S^{\kappa} \tag{3.35}$$

As indicated in (3.34), the electric field points in the same direction as the conductor density function.

Thus far the analysis has derived an expression for the electric field produced by an arbitrary stator winding. This general expression can be made specific by proper substitution. Explicitly, the electric field produced by the first winding is

$$\vec{e}_1(y,t) = \Re\left\{\sum_{\kappa} \sqrt{2}\bar{E}_1^{\kappa} e^{j(\omega_1 t - ky)}\right\}\hat{a}_x \tag{3.36}$$

where

$$\bar{E}_1^{\kappa} = -\frac{\omega_1}{k}\bar{B}_1^{\kappa} \tag{3.37}$$

in which the harmonics included in the summation, which comes directly from (3.28), are given by

$$\kappa = (6q_1 + 1)\kappa_1 \tag{3.38}$$

For the second winding,

$$\vec{e}_2(y,t) = \Re\left\{\sum_{\lambda} \sqrt{2}\bar{E}_2^{\lambda} e^{j(\omega_2 t - ly)}\right\}\hat{a}_x \tag{3.39}$$

where

$$\bar{E}_2^{\lambda} = -\frac{\omega_2}{l}\bar{B}_2^{\lambda} \tag{3.40}$$

For the second winding, the spatial harmonics are denoted by λ and the associated wave number is l in order to distinguish the spatial harmonics produced by the

second winding from those produced by the first winding. The harmonics present in the electric field are given by

$$\lambda = (6q_2 + 1)\lambda_1 \tag{3.41}$$

where the value of the fundamental (λ_1) can be either positive or negative depending on whether the winding is excited with either positive or negative sequence currents, respectively, and q_2 is any signed integer.

The expressions for the electric fields produced by both windings are used to determine the stator induced voltages in both stator windings as well as in the rotor.

3.3.2 Stator-Stator Coupling

Self Induced Back EMF

The electric field produced by an arbitrary stator winding couples with itself, producing a back emf. In order to determine the back emf, the product of the electric field and the conductor density for that winding is integrated over the surface area spanned by the coils considered in the conductor density function. For the stator conductor density function used in this analysis, the area considered is the stator bore. Hence, the back emf, $u_{SS}(t)$, is determined by the integral expression

$$u_{SS}(t) = \int_0^W \int_0^{\pi d} \vec{e}_S(y,t) \cdot \vec{c}_S(y)\, dy\, dx \tag{3.42}$$

where the double subscript denotes the voltage induced in one winding due to currents in the other. For this situation, the same subscript is used.

By direct substitution of the expressions for the electric field and conductor density function for the first phase of an arbitrary three-phase stator winding given in (A.20),

$$\begin{aligned} u_{SS}(t) &= \int_0^W \int_0^{\pi d} \Re\left\{\sum_\kappa \sqrt{2}\bar{E}_S^\kappa e^{j(\omega_S t - ky)}\right\} \hat{a}_x \cdot \sum_{\kappa'} \bar{C}_S^{\kappa'} e^{-jk'y} \hat{a}_x\, dy\, dx \\ &= \Re\left\{\sum_\kappa \sum_{\kappa'} \sqrt{2} W \bar{E}_S^\kappa \bar{C}_S^{\kappa'} e^{j\omega_S t} \int_0^{\pi d} e^{-j(k+k')y}\, dy\right\} \end{aligned} \tag{3.43}$$

Only the first phase quantity needs to be considered because the windings are balanced. To simplify the expression in (3.43), the conductor density function, because it is wholly real, was moved to within the influence of the real operator. In order to distinguish between harmonics, the spatial harmonics considered in the conductor density function were denoted with a prime.

The integral reduces to a non-zero result *only* when $k + k' = 0$, in which case the integral reduces to the value πd. Substituting $k' = -k$, and recognising that $\bar{C}_S^{-\kappa} = \bar{C}_S^{\kappa *}$, yields a general expression for the self induced back emf,

$$u_{SS}(t) = -\Re\left\{\sum_{\kappa} \sqrt{2}\bar{Z}_{SS}^{\kappa}\bar{I}_S e^{j\omega_S t}\right\} \tag{3.44}$$

which contains the air-gap impedance, $\bar{Z}_{SS}^{\kappa}$, given by

$$\bar{Z}_{SS}^{\kappa} = j\frac{3\mu_0\pi dW\omega_S}{gk^2}\left|\bar{C}_S^{\kappa}\right|^2 \tag{3.45}$$

It should be noted that the emf calculated acts in the same sense as positive current flow. Algebraically, this is represented by a voltage equation of the form $v + u = 0$ where v is the applied voltage and u the induced voltage. Thus, a negative induced voltage is a back emf and the impedance shown is that which is usually used in coupled-circuit analysis. The expression for the induced voltage can be made specific to each of the two stator windings. For the first stator winding,

$$u_{11}(t) = -\Re\left\{\sum_{\kappa} \sqrt{2}\bar{I}_1\bar{Z}_{11}^{\kappa}e^{j\omega_1 t}\right\} \tag{3.46}$$

where

$$\bar{Z}_{11}^{\kappa} = j\frac{3\mu_0\pi dW\omega_1}{gk^2}\left|\bar{C}_1^{\kappa}\right|^2 \tag{3.47}$$

For the second winding,

$$u_{22}(t) = -\Re\left\{\sum_{\lambda} \sqrt{2}\bar{I}_2\bar{Z}_{22}^{\kappa}e^{j\omega_2 t}\right\} \tag{3.48}$$

where

$$\bar{Z}_{22}^{\kappa} = j\frac{3\mu_0\pi dW\omega_2}{gl^2}\left|\bar{C}_2^{\lambda}\right|^2 \tag{3.49}$$

The expressions in (3.47) and (3.49) are the self impedances of the windings due only to air-gap flux. They must be supplemented with the resistance of the winding and the leakage inductance, calculated by classical means, to make them complete.

Coupling Between the Two Stator Windings

For proper operation of the BDFM, there should be no coupling between the fields produced by the two stator windings. This is achieved by proper selection of the pole-numbers of the windings. For example, a four pole winding produces a field with $4, -20, +28, 44, \ldots$ etc. poles and an eight pole winding produces a field with $8, -40, +56, -88, \ldots$ etc. poles. Investigation of the voltage induced in one winding by the other will yield a condition under which coupling occurs. This is determined by integrating the product of the electric field produced by the first winding and the conductor density function of the second winding yielding

$$\begin{aligned} u_{21}(t) &= \int_0^W \int_0^{\pi d} \vec{e}_1(y,t)\vec{c}_2(y)\, dy\, dx \\ &= \Re\left\{ \sum_{\kappa} \sum_{\lambda} \sqrt{2} W \bar{E}_1^{\kappa} \bar{C}_2^{\lambda} \int_0^{\pi d} e^{-j(k+l)y}\, dy \right\} \end{aligned} \tag{3.50}$$

By inspection, the integral reduces to zero unless $k + l = 0$. In this case, coupling occurs. Therefore the condition $k + l = 0$ must be avoided. This is equivalent to the condition $\kappa + \lambda = 0$. By substitution for the harmonics contained in the fields produced by the windings, the following condition on the fundamental harmonics must be avoided,

$$\frac{\kappa_1}{\lambda_1} = \mp\left(\frac{6q_2 + 1}{6q_1 + 1}\right) \tag{3.51}$$

where $\kappa_1 = P_1$ and $\lambda_1 = P_2$ for positive sequence excitation and $\lambda_1 = -P_2$ for negative sequence excitation. The values of pole-pair combinations that should not be used for both sequence cases are summarised in Table 3.2 for $P_1 \leq 10$ and $P_2 \leq 10$. This table also identifies those combinations where the pole-pairs must differ by more than one in order to avoid unbalanced magnetic pull (UMP) [10].

Table 3.2: Discouraged Stator Pole-Pair Combinations of the BDFM

Pole-Pairs	1	2	3	4	5	6	7	8	9	10
1	×	×			×		×			
2	×	×	×							×
3		×	×	×						
4			×	×	×					
5	×			×	×	×	×			
6					×	×	×			
7	×				×	×	×	×		
8							×	×	×	
9								×	×	×
10		×							×	×

3.3.3 Stator-Rotor Coupling

In order to determine the voltage induced in a rotor loop due to currents flowing in an arbitrary stator winding, a change of variables is performed on the stator current density using the relationship in (3.2) in order to transform the current density into the RRF. The same analysis procedure used to determine the electric field in the SRF is followed to determine the expression for the stator produced electric field in the RRF,

$$\vec{e}_S(y',t) = \Re\left\{\sum_{\kappa} \sqrt{2}\bar{E}_S^{\kappa} e^{j(\omega_S' t - ky')}\right\}\hat{a}_x \tag{3.52}$$

where

$$\bar{E}_S^{\kappa} = -j\frac{3\mu_0\omega_S'}{gk^2}\bar{C}_S^{\kappa}\bar{I} \tag{3.53}$$

and the frequency of the currents produced in the rotor circuits, ω_S', is given as

$$\omega_S' = \omega_S - \kappa\omega_R \tag{3.54}$$

where ω_R is the rotor speed.

Equation (3.52) is the electric field, produced by a stator winding, seen by a rotor circuit. The frequency of the field, as shown in (3.54), depends on rotor speed. In order to calculate the induced emf in a rotor circuit, the product of the stator produced electric field and the conductor density of the rotor current-loop is integrated over the area where that rotor current-loop conductor density function is defined. For the n-th rotor current-loop,

$$u_{R_n S}(t) = \int_{x'_{0n}-w'/2}^{x'_{0n}+w'/2} \int_0^{\pi d} \vec{e}_S(y',t)\vec{c}_{R_n}(x',y')\, dy\, dx \tag{3.55}$$

Note that the limits of integration are taken over the depth of the rotor loop in the $\hat{a}_{x'}$ direction and are over the entire circumference. For convenience, the limits are given in reference to the coordinates of the centre of the loop. Both (3.53) and (3.21) are substituted into (3.55), and making use of the fact that $\vec{c}_{R_n}(x',y')$ is wholly real, to yield

$$u_{R_n S}(t) = \Re\left\{\sum_\kappa \sum_\mu \sqrt{2}\bar{E}_S^\kappa \bar{C}_{R_n}^\mu \cos\gamma e^{j\omega'_S t}\cdot \right. \\ \left. \int_{x'_{0n}-w'/2}^{x'_{0n}+w'/2} \int_0^{\pi d} e^{-j(k+m)y'} e^{jmx'\tan\gamma}\, dy'\, dx' \right\} \tag{3.56}$$

The integral with respect to y' reduces to πd when $k+m=0$. However, the integral with respect to x' requires a further simplification,

$$\int_{x'_{0n}-w'/2}^{x'_{0n}+w'/2} e^{(jmx'\tan\gamma)}\, dx' = w' e^{jmx'_{0n}\tan\gamma} K_{sk}^\mu \tag{3.57}$$

which introduces the harmonic skew factor, K_{sk}^μ, given by

$$K_{sk}^\mu = \frac{\sin\left(\frac{mw'\tan\gamma}{2}\right)}{\frac{mw'\tan\gamma}{2}} \tag{3.58}$$

Using this result to simplify (3.56) yields the induced emf in n-th rotor current-loop due to currents flowing in a stator system. This emf, $u_{R_n S}(t)$, given in terms of the stator harmonics, is expressed

$$u_{R_n S}(t) = -\Re\left\{\sqrt{2}\sum_\kappa \bar{Z}_{R_n S}^\kappa \bar{I}_S e^{j\omega'_S t}\right\} \tag{3.59}$$

where the coupling impedance, $\bar{Z}^{\kappa}_{R_n S}$, is given by

$$\bar{Z}^{\kappa}_{R_n S} = -\frac{6\mu_0 w' \omega'_S}{gk^2} K^{\kappa}_{sk} K^{\kappa}_{bR} K^{\kappa}_{pR_n} e^{-jky'_{0n}} \bar{C}^{\kappa}_{S} \tag{3.60}$$

Proper substitution yields the expression for the induced emf due to the first winding,

$$u_{R_n 1}(t) = -\Re\left\{\sqrt{2}\sum_{\kappa} \bar{Z}^{\kappa}_{R_n 1} \bar{I}_1 e^{j\omega'_1 t}\right\} \tag{3.61}$$

where

$$\bar{Z}^{\kappa}_{R_n 1} = -\frac{6\mu_0 w' \omega'_1}{gk^2} K^{\kappa}_{sk} K^{\kappa}_{bR} K^{\kappa}_{pR_n} e^{-jky'_{0n}} \bar{C}^{\kappa}_{1} \tag{3.62}$$

and

$$\omega'_1 = \omega_1 - \kappa\omega_R \tag{3.63}$$

Similarly for the rotor loop voltages induced by the second winding,

$$u_{R_n 2}(t) = -\Re\left\{\sqrt{2}\sum_{\lambda} \bar{Z}^{\lambda}_{R_n 2} \bar{I}_2 e^{j\omega'_2 t}\right\} \tag{3.64}$$

where

$$\bar{Z}^{\lambda}_{R_n 2} = -\frac{6\mu_0 w' \omega'_2}{gl^2} K^{\lambda}_{sk} K^{\lambda}_{bR} K^{\lambda}_{pR_n} e^{-jly'_{0n}} \bar{C}^{\lambda}_{2} \tag{3.65}$$

and

$$\omega'_2 = \omega_2 - \lambda\omega_R \tag{3.66}$$

The resulting expressions show that each stator winding induces a separate rotor voltage component. Each component will consist of a harmonic series of voltages at frequencies determined by the spatial harmonics of the particular stator winding distribution, the rotor speed, and the frequency of the stator currents. For certain harmonics the two components of rotor voltage will be at the same frequency. In this case, cross coupling from one stator winding to the other occurs. This concept is discussed later.

3.3.4 Rotor Fields

Each component of induced rotor voltage gives rise to a component of rotor current. Determination of the fields produced by the currents flowing in a rotor loop proceeds in a manner similar to that used in the determination of the stator fields. Expressions for the rotor fields are needed to determine the voltage induced in a stator winding. Equation (3.59) shows that an arbitrary stator winding induces rotor voltages with a frequency ω'_S. The rotor currents will vary with the same frequency. Therefore, the component of current which flows in the n-th rotor loop can be written

$$i_{R_n}(t) = \Re\left\{\sum_{\kappa} \sqrt{2}\bar{I}^{\kappa}_{R_n} e^{j\omega'_S t}\right\} \tag{3.67}$$

The κ-th component of rotor current density is given by the product of the conductor density function of the rotor loops and the rotor current,

$$\vec{j}^{\kappa}_{R_n}(x', y', t) = \vec{c}_{R_n}(x', y') i^{\kappa}_{R_n} \tag{3.68}$$

Substituting (3.21) and (3.67) yields,

$$\vec{j}^{\kappa}_{R_n}(x', y', t) = \Re\left\{\sum_{\mu} \sqrt{2}\bar{C}^{\mu}_{R_n} \bar{I}^{\kappa}_{R_n} e^{j\left(\omega'_S t - m y'\right)}\right\} \hat{a}_{x''} \tag{3.69}$$

The rotor current density points in the direction of the rotor bars. However, because of the laminations, only the $\hat{a}_{x'}$ component produces useful flux. Other components will be ignored. The $\hat{a}_{x'}$ component of current density is given as

$$\vec{j}^{\kappa}_{R_n}(x', y', t) = \Re\left\{\sum_{\mu} \sqrt{2}\bar{C}^{\mu}_{R_n} \cos\gamma \bar{I}^{\kappa}_{R_n} e^{j\left(\omega'_S t - m y'\right)}\right\} \hat{a}_{x'} \tag{3.70}$$

By analysing the rotor fields in the SRF, an expression for the induced emf is more easily derived. The current density is transformed into the SRF by the change of variables specified in (3.2). Performing the transformation and simplifying yields

$$\vec{j}^{\kappa}_{R_n}(x, y, t) = \Re\left\{\sum_{\mu} \sqrt{2}\bar{J}^{\kappa}_{R_n}(x) e^{j\left(\omega''_S t - m y\right)}\right\} \hat{a}_x \tag{3.71}$$

where

$$\bar{J}^{\kappa}_{R_n}(x) = \bar{C}^{\mu}_{R_n} \cos\gamma \bar{I}^{\kappa}_{R_n(p)} e^{jmx\tan\gamma} \tag{3.72}$$

The transformation produces a change of frequency to ω''_S, such that

$$\omega''_S = \omega_S + (\mu - \kappa)\omega_R \tag{3.73}$$

This expression shows that the frequency of the rotor current density, as viewed from the stator, consists of a stator supply component with an additional speed and harmonic dependent component superimposed.

The rotor current density is used to calculate the magnetic flux density. Using Ampère's Law, as was done to determine an expression for the magnetic flux density produced by the stator winding, yields the following relationship between the harmonic components of rotor magnetic flux density and current density,

$$\frac{\partial \vec{b}^{\kappa}_{R_n}(x,y,t)}{\partial y} = \frac{\mu_0}{g} \vec{j}^{\kappa}_{R_n}(x,y,t) \tag{3.74}$$

The κ-th component of magnetic flux density can be expressed

$$\vec{b}^{\kappa}_{R_n}(x,y,t) = \Re\left\{ \sum_{\mu} \sqrt{2} \bar{B}^{\kappa}_{R_n}(x) e^{j\left(\omega''_S t - my\right)} \right\} \hat{a}_z \tag{3.75}$$

Differentiating and equating terms yields an expression for the rms vale of the magnetic flux density,

$$\bar{B}^{\kappa}_{R_n}(x) = j\frac{\mu_0}{gm} \bar{J}^{\mu}_{R_n}(x) \tag{3.76}$$

The κ-th component of rotor electric field is determined using Faraday's flux cutting rule,

$$\frac{\partial \vec{e}^{\kappa}_{R_n}(x,y,t)}{\partial y} = \frac{\partial \vec{b}^{\kappa}_{R_n}(x,y,t)}{\partial t} \tag{3.77}$$

The expression for the electric field can be expressed as

$$\vec{e}^{\kappa}_{R_n}(x,y,t) = \Re\left\{ \sum_{\mu} \sqrt{2} \bar{E}^{\kappa}_{R_n}(x) e^{j\left(\omega''_S t - my\right)} \right\} \hat{a}_x \tag{3.78}$$

where by differentiation and equating of terms,

$$\bar{E}^{\kappa}_{R_n}(x) = -\frac{\omega''_S}{m}\bar{B}^{\mu}_{R_n}(x) \tag{3.79}$$

Each κ-th component of rotor electric field will induces voltages in the stator windings containing a range of harmonics, evidenced by the summation over μ in (3.78). Even though there is no constraint on the value that μ can hold—any signed integer—κ is constrained by the relationship expressed in (3.28), i.e. $\kappa = (6q + 1)\kappa_1$.

The BDFM contains two stator windings, each of which causes a set of rotor currents to flow. One set of rotor currents is due to the first stator winding and the other due to the second stator winding. The rotor field analysis just presented for an arbitrary stator winding can be made specific to a particular stator winding by proper substitution. Hence,

$$\vec{e}^{\,\kappa}_{R_n 1}(x, y, t) = \Re\left\{\sum_{\mu} \sqrt{2}\bar{E}^{\kappa}_{R_n 1}(x)e^{j\left(\omega''_1 t - my\right)}\right\}\hat{a}_x \tag{3.80}$$

where

$$\bar{E}^{\kappa}_{R_n 1}(x) = -\frac{\omega''_1}{m}\bar{B}^{\mu}_{R_n 1}(x) \tag{3.81}$$

$$\bar{B}^{\kappa}_{R_n 1} = j\frac{\mu_0}{gm}\bar{J}^{\mu}_{R_n 1}(x) \tag{3.82}$$

$$\bar{J}^{\kappa}_{R_n 1}(x) = \bar{C}^{\mu}_{R_n}\cos\gamma\bar{I}^{\kappa}_{R_n 1}e^{jmx\tan\gamma} \tag{3.83}$$

for a rotor current induced by the first winding. The second subscript, 1, emphasises that the rotor quantity is due to the first stator winding. The harmonic number κ is given by (3.38), i.e. $\kappa = (6q_1 + 1)\kappa_1$. The frequency of the rotor fields in the SRF, by making the proper substitutions into (3.73), is given as

$$\omega''_1 = \omega_1 + (\mu - \kappa)\omega_R \tag{3.84}$$

Similar substitutions for the second winding show that

$$\vec{e}^{\,\lambda}_{R_n 2}(x, y, t) = \Re\left\{\sum_{\mu} \sqrt{2}\bar{E}^{\lambda}_{R_n 2}(x)e^{j\left(\omega''_2 t - my\right)}\right\}\hat{a}_x \tag{3.85}$$

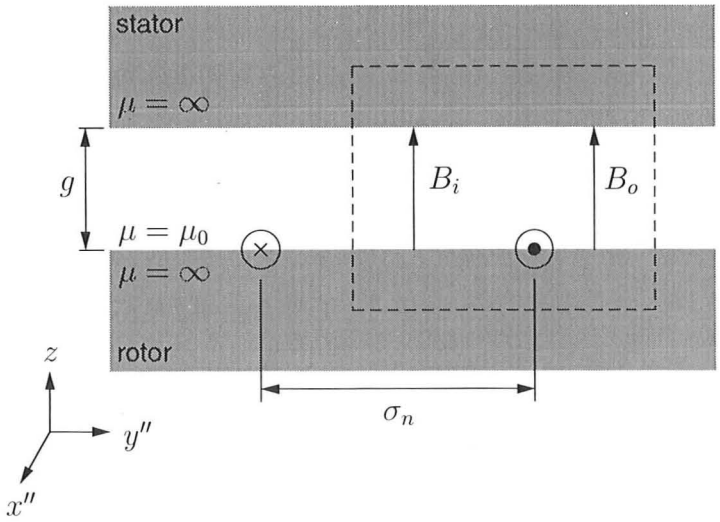

Figure 3.10: Magnetic flux density produced by a single rotor loop.

where

$$\bar{E}^{\lambda}_{R_n 2}(x) = -\frac{\omega_2''}{m}\bar{B}^{\mu}_{R_n 2}(x) \tag{3.86}$$

$$\bar{B}^{\lambda}_{R_n 2} = j\frac{\mu_0}{gm}\bar{J}^{\mu}_{R_n 2}(x) \tag{3.87}$$

$$\bar{J}^{\lambda}_{R_n 2}(x) = \bar{C}^{\mu}_{R_n}\cos\gamma\bar{I}^{\lambda}_{R_n 2}e^{jmx\tan\gamma} \tag{3.88}$$

The harmonic number λ is given by (3.41), i.e. $\lambda = (6q_2 + 1)\lambda_1$. The frequency of these fields in the SRF, ω_2'', is expressed

$$\omega_2'' = \omega_2 + (\mu - \lambda)\omega_R \tag{3.89}$$

The expressions for the rotor electric fields are used to determine the voltages induced in the stator windings. Before doing so, it is more convenient to calculate the rotor self-impedances.

3.3.5 Rotor-Rotor Coupling

The self impedance of a rotor loop is determined by exciting the n-th loop with a current I_{R_n} and assuming all other rotor currents to be zero. Figure 3.10 shows the magnetic flux density produced by a current flowing in a single rotor loop of

span σ_n. Ampère's Law is used around the integration path shown in Fig. 3.10 to relate the flux density produced within the span of the rotor loop, B_i, to the returning flux outside the span of the rotor loop, B_o. This relationship can be expressed

$$\frac{B_o g}{\mu_0} - \frac{B_i g}{\mu_0} = I_{R_n} \tag{3.90}$$

where it assumed that the flux crosses perpendicularly to the rotor surface and that the iron has infinite permeability. By Gauss' Law, the flux produced by the loop returns via the remainder of the circumference of the rotor. Thus, a further relationship between B_i and B_o is obtained,

$$B_i \sigma_n + B_o(\pi d - \sigma_n) = 0 \tag{3.91}$$

Combining (3.90) and (3.91), and isolating the variables, yields expressions for the flux densities,

$$B_o = -\frac{\mu_0 \sigma_n}{\pi d g} I_{R_n} \tag{3.92}$$

$$B_i = \frac{\mu_0}{g}\left(1 - \frac{\sigma_n}{\pi d}\right) I_{R_n} \tag{3.93}$$

The n-th rotor current-loop has a span σ_n and a depth w'. The product of loop area and inner flux density yields the flux produced by a rotor loop. Inductance, by definition, is flux per unit current. Therefore, the self inductance of a rotor loop can be expressed

$$L_{R_n R_n} = \frac{\mu_0}{g}\left(1 - \frac{\sigma_n}{\pi d}\right) w' \sigma_n \tag{3.94}$$

However, by making cuts along the rotor in order to represent the inter-bar resistance paths, the rotor is divided into axial segments designated as bands, that is the portion of the rotor between two adjacent cuts. Rotor loops in the same band couple with each other. However, flux produced by a loop in one band does not couple with rotor loops in other bands. Therefore, for loops that couple, the mutual inductance between the n-th and m-th rotor current-loops can be expressed

$$L_{R_n R_m} = L_{R_m R_n} = -\frac{\mu_0 \sigma_n \sigma_m w'}{\pi d g} \tag{3.95}$$

The κ-th component of rotor current, assumed to be due to the flux produced by an arbitrary stator winding, has a frequency ω'_S, given by (3.54). Expressions for the values of the rotor self-impedances and mutual impedances are determined by multiplying the rotor inductance by the frequency of the κ-th harmonic rotor current, ω'_S, thus

$$\bar{Z}^{\kappa}_{R_n R_n} = j\frac{\mu_0 w' \sigma_n}{g}\left(1 - \frac{\sigma_n}{\pi d}\right)\omega'_S \tag{3.96}$$

$$\bar{Z}^{k}_{R_n R_m} = \bar{Z}_{R_m R_n} = -j\frac{\mu_0 \sigma_n \sigma_m w'}{\pi d g}\omega'_S \tag{3.97}$$

The induced emf in loop n due to the κ-th component of rotor current in loop m can be expressed

$$u^{\kappa}_{R_n R_m}(t) = -\Re\left\{\bar{Z}^{\kappa}_{R_n R_m}\bar{I}^{\kappa}_{R_m}e^{j\omega'_S t}\right\} \tag{3.98}$$

In addition to the impedance due to air-gap coupling, the self impedance of a loop must be supplemented with the resistance of the segments that make up the loop as well as any leakage reactance (which may be frequency dependent) of the loop.

3.3.6 Rotor-Stator Coupling

A single rotor loop current couples with both stator windings. It will have been induced by a particular stator winding. When that rotor current couples with the stator winding which induced it, the coupling is called *direct coupling*. When it couples with the other stator winding, it is called *cross coupling*. It is cross coupling which allows the two stator windings to interact in a constructive manner. This process is shown diagrammatically in Fig. 1.5.

For example, the rotor loop current $i^{\kappa}_{R_n 1}$ is induced by the first winding. This rotor loop current directly couples with the first stator winding and cross couples with the second stator winding. Similarly, rotor loop current $i^{\lambda}_{R_n 2}$ is induced by the second winding. It cross couples with the first winding and directly couples with the second winding.

Direct Coupling

In order to determine the voltages induced in a stator winding due to directly coupled rotor currents, the product of the rotor electric field and the conductor density of the stator winding is integrated over the diameter of the machine and the depth of the rotor loop. For coupling between the κ-th component of rotor electric field, $\vec{e}^{\,\kappa}_{R_n 1}(x, y, t)$, and the first stator winding,

$$u^{\kappa}_{1R_n 1}(t) = \int_{x_{0n}-w'/2}^{x_{0n}+w'/2} \int_{0}^{\pi d} \vec{e}^{\,\kappa}_{R_n 1}(x, y, t) \cdot \vec{c}_1(y)\, dy\, dx \tag{3.99}$$

After considerable simplification,

$$u^{\kappa}_{1R_n 1}(t) = -\Re\left\{ \sqrt{2} \sum_{\mu} \bar{Z}^{\mu}_{1R_n 1} \bar{I}^{\kappa}_{R_n 1} e^{j\omega''_1 t} \right\} \tag{3.100}$$

where the frequency of voltages is given in (3.84) and

$$\bar{Z}^{\mu}_{1R_n 1} = \frac{2\mu_0 \omega''_1 w'}{gm^2} K^{\mu}_{bR} K^{\mu}_{pR_n} K^{\mu}_{sk} e^{jmy'_{0n}} \bar{C}^{\mu *}_1 \tag{3.101}$$

is the direct-coupling impedance. Similarly, coupling between the λ-th component of rotor electric field, $\vec{e}^{\,\lambda}_{R_n 2}(x, y, t)$, and the second stator winding is expressed

$$u^{\lambda}_{2R_n 2}(t) = -\Re\left\{ \sqrt{2} \sum_{\mu} \bar{Z}^{\mu}_{2R_n 2} \bar{I}^{\lambda}_{R_n 2} e^{j\omega''_2 t} \right\} \tag{3.102}$$

where the frequency of voltages is given in (3.89) and

$$\bar{Z}^{\mu}_{2R_n 2} = \frac{2\mu_0 \omega''_2 w'}{gm^2} K^{\mu}_{bR} K^{\mu}_{pR_n} K^{\mu}_{sk} e^{jmy'_{0n}} \bar{C}^{\mu *}_2 \tag{3.103}$$

is the direct-coupling impedance.

Even though the same superscript μ is used in both (3.101) and (3.103), the values are independent of each other. The coupling impedances are given superscripts, κ or λ, which refer to the harmonic of the rotor current that induces the particular stator emf.

Cross Coupling

The induced stator voltages due to cross coupling are determined in the same manner as the voltages due to direct coupling with the exception that the conductor density function for the other stator winding is used.

The coupling between the κ-th component of rotor current and the second stator winding can be written directly as

$$u^{\kappa}_{2R_n1}(t) = -\Re\left\{\sqrt{2}\sum_{\mu}\bar{Z}^{\mu}_{2R_n1}\bar{I}^{\kappa}_{R_n1}e^{j\omega''_1 t}\right\} \tag{3.104}$$

where the frequency of voltages is given in (3.84) and

$$\bar{Z}^{\mu}_{2R_n1} = \frac{2\mu_0\omega''_1 w'}{gm^2}K^{\mu}_{bR}K^{\mu}_{pR_n}K^{\mu}_{sk}e^{jmy'_{0n}}\bar{C}^{\mu *}_{2} \tag{3.105}$$

is the cross-coupling impedance. Similarly for cross coupling between the λ-th component of rotor current and the first stator winding,

$$u^{\lambda}_{1R_n2}(t) = -\Re\left\{\sqrt{2}\sum_{\mu}\bar{Z}^{\mu}_{1R_n2}\bar{I}^{\lambda}_{R_n2}e^{j\omega''_2 t}\right\} \tag{3.106}$$

where the frequency of voltages is given in (3.89) and

$$\bar{Z}^{\mu}_{1R_n2} = \frac{2\mu_0\omega''_2 w'}{gm^2}K^{\mu}_{bR}K^{\mu}_{pR_n}K^{\mu}_{sk}e^{jmy'_{0n}}\bar{C}^{\mu *}_{1} \tag{3.107}$$

is the cross-coupling impedance.

Once again, the superscript μ in both sets of equations is independent. Following the convention used in writing the expressions for the direct-coupling impedances, the superscript of the impedance denotes the harmonic number of the rotor current which induces the stator voltages. A triple subscript is used to denote the winding where the voltage is induced, the rotor loop current which is responsible, and the stator winding which induced the rotor current, respectively.

3.4 Voltage Equations

Expressions for all of the coupling impedances have been determined. The next stage in the analysis is to assemble the voltage equations using these expressions.

Before assembling the voltage equations, the condition under which the BDFM synchronises is considered. As mentioned in Chapter 1, only synchronous operation is desirable when doubly-fed. Hence, this analysis will only consider that mode of operation.

When the currents induced in the rotor by both stator windings are at the same frequency, the components are indistinguishable. This relationship prescribes the condition for synchronous operation. Equating the two separately induced rotor current frequencies, ω_1 and ω_2,

$$\begin{aligned} \omega_1' &= \omega_2' \\ \omega_1 - \kappa\omega_R &= \omega_2 - \lambda\omega_R \\ \omega_R &= \frac{\omega_1 - \omega_2}{\kappa - \lambda} \end{aligned} \tag{3.108}$$

gives an expression for the rotor speed. It is known that the BDFM will synchronise at a speed dictated by the fundamental components of the stator fields. Thus,

$$\omega_R = \frac{\omega_1 - \omega_2}{\kappa_1 - \lambda_1} \tag{3.109}$$

Alternatively, allowing $\omega_1' = -\omega_2'$,

$$\omega_R = \frac{\omega_1 + \omega_2}{\kappa + \lambda} \tag{3.110}$$

For the fundamentals,

$$\omega_R = \frac{\omega_1 + \omega_2}{\kappa_1 + \lambda_1} \tag{3.111}$$

Two different speed equations exist that dictate the speed at which the BDFM will run synchronously, (3.109) and (3.111). It can be shown that when the rotor is constructed with $P_1 + P_2$ nests, the rotor will rotate at a speed given by (3.109) for negative sequence excitation applied to the second winding ($\lambda_1 < 0$) and at a speed governed by (3.111) for positive sequence excitation ($\lambda_1 > 0$)[31]. The opposite is true if the rotor is constructed with $|P_1 - P_2|$ nests[2]. This analysis is concerned with a rotor of $P_1 + P_2$ nests, which is the usual construction.

[2]Although theoretically possible, the author is unaware of a BDFM with $|P_1 - P_2|$ nests having been built.

Equations (3.108)–(3.111) can be used to determine which harmonics of the fields produced by one stator winding will produce voltages on the other stator winding at the supply frequency of the other stator winding. By equating the denominators of (3.108) and (3.109), $(\kappa - \lambda) = (\kappa_1 - \lambda_1)$, a constraint for cross coupling between λ and κ is obtained for negative sequence excitation applied to the second winding. Using (3.38) and (3.41) results in

$$\frac{\kappa_1}{\lambda_1} = \frac{q_2}{q_1} \tag{3.112}$$

Similarly for positive sequence excitation,

$$\frac{\kappa_1}{\lambda_1} = -\frac{q_2}{q_1} \tag{3.113}$$

Only those harmonics produced by a stator winding which satisfy either (3.112) or (3.113), depending on the excitation sequence applied to the second winding, will induce supply frequency voltages in the other stator winding, thus enabling cross coupling from one stator winding to the other via the rotor.

Because two separate expressions for speed exist depending on the sequence of excitation applied to the second winding, there are two possible cases to consider when developing the voltage equations. The first case will be concerned with negative sequence excitation, which results in the rotor speed given by (3.109). The second case is for positive sequence excitation with a rotor speed given by (3.111).

In both cases, the stator voltage equations have the general form,

$$v_1 + u_{11} + \sum_{n=1}^{N_{eq}} (u_{1R_n1} + u_{1R_n2}) = 0 \tag{3.114}$$

$$v_2 + u_{22} + \sum_{n=1}^{N_{eq}} (u_{2R_n1} + u_{2R_n2}) = 0 \tag{3.115}$$

where v_1 and v_2 are the applied stator voltages with form $v_S(t) = \Re\left\{\sqrt{2}\bar{V}_S e^{j\omega_S t}\right\}$. The remaining voltages, u, are the voltages derived in Section 3.3. The effects of the rotor are incorporated by the summation over all N_{eq} rotor loops. If a rotor loop does not couple via the air-gap flux, then the appropriate term is set to zero. Implicit in both equations is a summation over the relevant harmonics.

On a harmonic basis, the voltage equations for the n-th rotor loop can be written,

$$0 = u^{\kappa}_{R_n 1} + \sum_{m=1}^{N_{eq}} u^{\kappa}_{R_n R_m} \tag{3.116}$$

$$0 = u^{\lambda}_{R_n 2} + \sum_{m=1}^{N_{eq}} u^{\lambda}_{R_n R_m} \tag{3.117}$$

where the effect of the other rotor loops on the n-th loop is accounted for in the summation on m.

The equations in (3.114)–(3.117) can be solved by representing the quantities as phasors. However, all of the complex quantities must be at the same frequency. Determination of the correct frequencies, and hence the form of the equations, is dependent on the sequence of excitation applied to the second stator winding.

3.4.1 Negative Sequence Excitation

Consider the stator voltage equations given in (3.114) and (3.115). The self induced voltage (back emf) of each stator winding is already at the supply frequency, either ω_1 or ω_2 respectively. Thus, it is straightforward to express the self-induced voltages given by equations (3.46) and (3.48) in phasor form. Supplementing them with the phase resistance, R_1 or R_2, and leakage inductance, L_{l1} or L_{l2}, yields the phasor relationships

$$\bar{U}_{11} = -\left(R_1 + j\omega_1 L_{l1} + \sum_{\kappa} \bar{Z}^{\kappa}_{11}\right) \bar{I}_1 \tag{3.118}$$

$$\bar{U}_{22} = -\left(R_2 + j\omega_2 L_{l2} + \sum_{\lambda} \bar{Z}^{\lambda}_{22}\right) \bar{I}_2 \tag{3.119}$$

Considering the general voltage equation for the first winding, given by (3.114), the voltage induced due to the direct-coupled rotor current ($u_{1R_n 1}$) is at a frequency $\omega_1'' = \omega_1 + (\mu - \kappa)\omega_R$. In order for the voltage equation to be consistent, the frequency should be at the supply frequency, ω_1. By setting $\mu = \kappa$, $\omega_1'' = \omega_1$ and the induced voltage, simplifying (3.100), becomes

$$\bar{U}_{1R_n 1} = -\sum_{\kappa} \sqrt{2}\bar{Z}^{\kappa}_{1R_n 1}\bar{I}^{\kappa}_{R_n 1} \tag{3.120}$$

where

$$\bar{Z}^{\kappa}_{1R_n1} = \frac{2\mu_0\omega_1 w'}{gk^2} K^{\kappa}_{bR} K^{\kappa}_{pR_n} K^{\kappa}_{sk} e^{jky'_{0n}} \bar{C}^{\kappa *}_{1} \tag{3.121}$$

By a similar argument, setting $\mu = \lambda$ in the expression for ω''_2 results in

$$\bar{U}_{2R_n2} = -\sum_{\lambda} \sqrt{2}\bar{Z}^{\lambda}_{2R_n2}\bar{I}^{\lambda}_{R_n2} \tag{3.122}$$

where

$$\bar{Z}^{\lambda}_{2R_n2} = \frac{2\mu_0\omega_2 w'}{gl^2} K^{\lambda}_{bR} K^{\lambda}_{pR_n} K^{\lambda}_{sk} e^{jly'_{0n}} \bar{C}^{\lambda *}_{2} \tag{3.123}$$

By specifying μ, many harmonics, which generate ripple on the supply voltage, are ignored. Remembering the goal of this analysis, which was to show that inter-bar currents result in poor performance during operation of the BDFM, ignoring them does not adversely affect the accuracy of the solution desired. If their effect must be included, then a series of voltage equations, one for each stator time harmonic of interest, must be formulated with any source impedances seen by that harmonic included in the equation.

The voltage due to the cross-coupled rotor current, u_{1R_n2}, is at a frequency ω''_2. However, in order to achieve consistency in the voltage equation, this voltage should be a phasor at a frequency ω_1. Setting $\omega''_2 = \omega_1$ and solving for the rotor speed,

$$\omega_R = \frac{\omega_1 - \omega_2}{\mu - \lambda} \tag{3.124}$$

In order for this equation to match that in (3.108), μ must be set to $\mu = \kappa$. Substituting $\mu = \kappa$ into (3.106) and simplifying,

$$\bar{U}_{1R_n2} = -\sum_{\chi} \sqrt{2}\bar{Z}^{\kappa}_{1R_n2}\bar{I}^{\lambda}_{R_n2} \tag{3.125}$$

where

$$\bar{Z}^{\kappa}_{1R_n2} = \frac{2\mu_0\omega_1 w'}{gk^2} K^{\kappa}_{bR} K^{\kappa}_{pR_n} K^{\kappa}_{sk} e^{jky'_{0n}} \bar{C}^{\kappa *}_{1} \tag{3.126}$$

and the summation index has been changed to χ in order to designate that only those harmonics which satisfy the condition for cross coupling, (3.112), are included.

By a similar analysis for the other cross-coupled voltage, u_{2R_n1}, consistency in the voltage equations is obtained by setting $\omega_1'' = \omega_2$. This results in the condition, $\mu = \lambda$. Substituting into (3.104) and simplifying,

$$\bar{U}_{2R_n1} = -\sum_{\chi} \sqrt{2}\bar{Z}^{\lambda}_{2R_n1}\bar{I}^{\kappa}_{R_n1} \tag{3.127}$$

where

$$\bar{Z}^{\lambda}_{2R_n1} = \frac{2\mu_0\omega_2 w'}{gl^2} K^{\lambda}_{bR} K^{\lambda}_{pR_n} K^{\lambda}_{sk} e^{jly'_{0n}} \bar{C}^{\lambda *}_{2} \tag{3.128}$$

Once again the summation index χ is used to signify that the harmonics are constrained and only include the harmonics which cross couple.

Further simplification is achieved by expressing the rotor voltages as phasors and assembling into the matrix equations,

$$\bar{\mathbf{I}}^{\kappa}_{\mathbf{R}} = \begin{bmatrix} \bar{I}^{\kappa}_{R_1} & \bar{I}^{\kappa}_{R_2} & \cdots & \bar{I}^{\kappa}_{R_{N_{eq}}} \end{bmatrix}^T \tag{3.129}$$

$$\bar{\mathbf{I}}^{\lambda}_{\mathbf{R}} = \begin{bmatrix} \bar{I}^{\lambda}_{R_1} & \bar{I}^{\lambda}_{R_2} & \cdots & \bar{I}^{\lambda}_{R_{N_{eq}}} \end{bmatrix}^T \tag{3.130}$$

Consequently, the mutual impedances become vectors of dimension $1 \times N_{eq}$. The stator voltage equations can now be expressed

$$\bar{V}_1 = (R_1 + j\omega_1 L_{l1})\,\bar{I}_1 + \sum_{\kappa} \left(\bar{Z}^{\kappa}_{11} + \bar{\mathbf{Z}}^{\kappa}_{\mathbf{1R1}}\bar{\mathbf{I}}^{\kappa}_{\mathbf{R1}}\right)\bar{I}_1 + \sum_{\chi} \bar{\mathbf{Z}}^{\kappa}_{\mathbf{1R2}}\bar{\mathbf{I}}^{\lambda}_{\mathbf{R2}} \tag{3.131}$$

$$\bar{V}_2 = (R_2 + j\omega_1 L_{l2})\,\bar{I}_2 + \sum_{\lambda} \left(\bar{Z}^{\lambda}_{22} + \bar{\mathbf{Z}}^{\lambda}_{\mathbf{2R2}}\bar{\mathbf{I}}^{\lambda}_{\mathbf{R2}}\right)\bar{I}_2 + \sum_{\chi} \bar{\mathbf{Z}}^{\lambda}_{\mathbf{2R1}}\bar{\mathbf{I}}^{\kappa}_{\mathbf{R1}} \tag{3.132}$$

In order to simplify the voltage equations further, expressions for the rotor voltages need to be developed in phasor form. In matrix form the rotor equations can be expressed as

$$\mathbf{0} = \bar{\mathbf{Z}}^{\kappa}_{\mathbf{R1}}\bar{I}_1 + \bar{\mathbf{Z}}^{\kappa}_{\mathbf{RR}}\bar{\mathbf{I}}^{\kappa}_{\mathbf{R1}} \tag{3.133}$$

$$\mathbf{0} = \bar{\mathbf{Z}}^{\lambda}_{\mathbf{R2}}\bar{I}_2 + \bar{\mathbf{Z}}^{\lambda}_{\mathbf{RR}}\bar{\mathbf{I}}^{\lambda}_{\mathbf{R2}} \tag{3.134}$$

where the mutual impedances are expressed as vectors of dimension $N_{eq} \times 1$. For the n-th rotor loop that couples via the air gap flux,

$$\bar{Z}^{\kappa}_{R_n1} = -\frac{6\mu_0 w'\omega'_1}{gk^2} K^{\kappa}_{sk} K^{\kappa}_{bR} K^{\kappa}_{pR_n} e^{-jky'_{0n}} \bar{C}^{\kappa}_{1} \tag{3.135}$$

$$\bar{Z}^{\lambda}_{R_n2} = -\frac{6\mu_0 w'\omega'_2}{gl^2} K^{\lambda}_{sk} K^{\lambda}_{bR} K^{\lambda}_{pR_n} e^{-jly'_{0n}} \bar{C}^{\lambda}_{2} \tag{3.136}$$

which are the same expressions as (3.62) and (3.65), given here for the sake of completeness, and where $\omega_1' = (\omega_1 - \kappa\omega_R)$ and $\omega_2' = (\omega_2 - \lambda\omega_R)$. The rotor impedance matrices, $\bar{\mathbf{Z}}^{\kappa}_{\mathbf{RR}}$ and $\bar{\mathbf{Z}}^{\lambda}_{\mathbf{RR}}$, incorporate the effects each of the loops has on each other. The matrix is a simplified way to represent the impedances seen by each of the mesh currents (see Fig. 3.1). The diagonal elements include the air-gap self-impedance supplemented with the resistance of each of the branches of the rotor lop circuit and the leakage inductance of the rotor bar segments which form the loop. Off-diagonal elements will be non-zero for loops that are either adjacent or couple via the air-gap.

The harmonic rotor current in each equation can be isolated,

$$\bar{\mathbf{I}}^{\kappa}_{\mathbf{R1}} = -\bar{\mathbf{Z}}^{\kappa\,-1}_{\mathbf{RR}}\bar{\mathbf{Z}}^{\kappa}_{\mathbf{R1}}\bar{I}_1 \tag{3.137}$$

$$\bar{\mathbf{I}}^{\lambda}_{\mathbf{R2}} = -\bar{\mathbf{Z}}^{\lambda\,-1}_{\mathbf{RR}}\bar{\mathbf{Z}}^{\lambda}_{\mathbf{R2}}\bar{I}_2 \tag{3.138}$$

and substituted into the voltage equations, (3.133) and (3.134), to obtain

$$\bar{V}_1 = \left(R_1 + j\omega_1 L_{l1} + \sum_{\kappa}\bar{Z}^{\kappa}_{11} - \bar{\mathbf{Z}}^{\kappa}_{\mathbf{1R1}}\bar{\mathbf{Z}}^{\kappa\,-1}_{\mathbf{RR}}\bar{\mathbf{Z}}^{\kappa}_{\mathbf{R1}}\right)\bar{I}_1 + \sum_{\chi}\bar{\mathbf{Z}}^{\kappa}_{\mathbf{1R2}}\bar{\mathbf{Z}}^{\lambda\,-1}_{\mathbf{RR}}\bar{\mathbf{Z}}^{\lambda}_{\mathbf{R2}}\bar{I}_2 \tag{3.139}$$

$$\bar{V}_2 = \left(R_2 + j\omega_1 L_{l2} + \sum_{\lambda}\bar{Z}^{\lambda}_{22} - \bar{\mathbf{Z}}^{\lambda}_{\mathbf{2R2}}\bar{\mathbf{Z}}^{\lambda\,-1}_{\mathbf{RR}}\bar{\mathbf{Z}}^{\lambda}_{\mathbf{R2}}\right)\bar{I}_2 + \sum_{\chi}\bar{\mathbf{Z}}^{\lambda}_{\mathbf{2R1}}\bar{\mathbf{Z}}^{\kappa\,-1}_{\mathbf{RR}}\bar{\mathbf{Z}}^{\kappa}_{\mathbf{R1}}\bar{I}_1 \tag{3.140}$$

This set of equations, which may be cast into a matrix voltage equation of the form $\mathbf{V} = \mathbf{ZI}$, describes the electrical performance of the BDFM when negative sequence excitation is applied to the second winding. The speed of the machine will be governed by (3.109), where a negative fundamental is used to signify the negative sequence excitation. The harmonics that cross couple can be determined using (3.112) and are represented by the summation index χ. The stator currents are solved using (3.139) and (3.140). The rotor currents, if desired, can be solved on a harmonic basis using (3.137) and (3.146).

3.4.2 Positive Sequence Excitation

In the general voltage equations given in (3.114)–(3.117), each of the induced voltages must be at the same frequency. For positive sequence excitation applied

to the second winding the phasor relationships expressed in (3.118)–(3.123) are still valid and represent voltages at the corresponding stator supply frequencies. However, the situation changes when dealing with the voltages induced due to cross coupling.

Consider the first stator winding. The voltage due to cross coupling with the second winding, u_{1R_n2}, is at a frequency ω_2''. When set to the negative of the supply frequency, $\omega_2'' = -\omega_1$, the following expression for rotor speed is obtained,[3]

$$\omega_R = \frac{\omega_1 + \omega_2}{-\mu + \lambda} \tag{3.141}$$

This implies that in order to match the expression for rotor speed given in (3.110), μ should be set to $\mu = -\kappa$. Recognising that $\bar{Z}^{-\kappa} = \bar{Z}^{\kappa *}$, the conjugate relationship, the voltage in (3.125) can be written

$$\bar{U}_{1R_n2} = -\sum_{\chi} \sqrt{2}\bar{Z}^{\kappa *}_{1R_n2}\bar{I}^{\lambda}_{R_n2} \tag{3.142}$$

However, this voltage phasor is at a frequency $-\omega_1$. In order for the voltage to be at the positive frequency ω_1, the conjugate relationship is used,

$$\bar{U}^{*}_{1R_n2} = -\sum_{\chi} \sqrt{2}\bar{Z}^{\kappa}_{1R_n2}\bar{I}^{\lambda *}_{R_n2} \tag{3.143}$$

where the expression for the impedance is unchanged from that given in (3.126),

$$\bar{Z}^{\kappa}_{1R_n2} = \frac{2\mu_0\omega_1 w'}{gk^2} K^{\kappa}_{bR} K^{\kappa}_{pR_n} K^{\kappa}_{sk} e^{jky'_{0n}} \bar{C}^{\kappa *}_{1} \tag{3.144}$$

Hence, for the first stator winding,

$$\bar{V}_1 = (R_1 + j\omega_1 L_{l1})\,\bar{I}_1 + \sum_{\kappa} \left(\bar{Z}^{\kappa}_{11} + \bar{\mathbf{Z}}^{\kappa}_{\mathbf{1R1}}\bar{\mathbf{I}}^{\kappa}_{\mathbf{R1}}\right)\bar{I}_1 + \sum_{\chi} \bar{\mathbf{Z}}^{\kappa}_{\mathbf{1R2}}\bar{\mathbf{I}}^{\lambda *}_{\mathbf{R2}} \tag{3.145}$$

All of the current and voltage phasors in (3.145) are at the positive frequency ω_1, thus forming a consistent set of equations. As in (3.131), the summation index χ signifies that only those harmonics which cross couple (satisfy (3.113)) are included.

[3]It should be noted that setting $\omega_2'' = \omega_1$, as was done for negative sequence excitation, would not have resulted in an applicable expression for rotor speed. Consult [31] for more information.

An expression for the rotor current, $\bar{\mathbf{I}}_{\mathbf{R2}}^{\lambda *}$, is obtained by taking the conjugate of (3.138),

$$\bar{\mathbf{I}}_{\mathbf{R2}}^{\lambda *} = -\bar{\mathbf{Z}}_{\mathbf{RR}}^{\lambda * -1} \bar{\mathbf{Z}}_{\mathbf{R2}}^{\lambda *} \bar{I}_2^* \tag{3.146}$$

Substituting this expression along with the expression for rotor current given in (3.137) into (3.145) yields

$$\bar{V}_1 = \left(R_1 + j\omega_1 L_{l1} + \sum_{\kappa} \bar{Z}_{11}^{\kappa} - \bar{\mathbf{Z}}_{\mathbf{1R1}}^{\kappa} \bar{\mathbf{Z}}_{\mathbf{RR}}^{\kappa -1} \bar{\mathbf{Z}}_{\mathbf{R1}}^{\kappa} \right) \bar{I}_1 + \sum_{\chi} \bar{\mathbf{Z}}_{\mathbf{1R2}}^{\kappa} \bar{\mathbf{Z}}_{\mathbf{RR}}^{\lambda * -1} \bar{\mathbf{Z}}_{\mathbf{R2}}^{\lambda *} \bar{I}_2^* \tag{3.147}$$

For the second stator winding, the voltage $u_{2R_n 1}$ is at a frequency $-\omega_1''$. Setting $\omega_1'' = -\omega_2$ and solving for the rotor speed,

$$\omega_R = \frac{\omega_1 + \omega_2}{\kappa - \mu} \tag{3.148}$$

Setting $\mu = -\lambda$ in order to match the speed equation given in (3.110) and substituting into (3.104) results in the voltage phasor relationship

$$\bar{U}_{2R_n 1} = -\sum_{\chi} \sqrt{2} \bar{Z}_{2R_n 1}^{\lambda *} \bar{I}_{R_n 1}^{\kappa} \tag{3.149}$$

where

$$\bar{Z}_{2R_n 1}^{\lambda *} = \frac{2\mu_0 \omega_2 w'}{gl^2} K_{bR}^{\lambda} K_{pR_n}^{\lambda} K_{sk}^{\lambda} e^{-jly'_{0n}} \bar{C}_2^{\lambda} \tag{3.150}$$

which is simply the conjugate of the expression given in (3.128).

The voltage phasor in (3.149) is at a frequency $-\omega_2$. For consistency of frequency, use is made of the conjugate relationships of (3.119), (3.122), and (3.134) to obtain the voltage equation, in matrix form, for the second winding,

$$\bar{V}_2^* = \left(R_2 - j\omega_1 L_{l2} + \sum_{\lambda} \bar{Z}_{22}^{\lambda *} - \bar{\mathbf{Z}}_{\mathbf{2R2}}^{\lambda *} \bar{\mathbf{Z}}_{\mathbf{RR}}^{\lambda * -1} \bar{\mathbf{Z}}_{\mathbf{R2}}^{\lambda *} \right) \bar{I}_2^* + \sum_{\chi} \bar{\mathbf{Z}}_{\mathbf{2R1}}^{\lambda *} \bar{\mathbf{Z}}_{\mathbf{RR}}^{\kappa -1} \bar{\mathbf{Z}}_{\mathbf{R1}}^{\kappa} \bar{I}_1 \tag{3.151}$$

Equations (3.147) and (3.151) describe the electrical performance of the BDFM when the second winding is subjected to positive sequence excitation. In this case,

the speed equation in (3.111) holds. If required, the harmonic rotor currents can be solved for by using (3.137) and (3.146).

It should be noted that depending on the speed of operation desired, the BDFM will operate with either positive sequence or negative sequence operation. The appropriate set of equations for each sequence must be used to determine the performance of the machine.

3.5 Torque Equations

The electromagnetic torque equation is developed by considering the elemental force on a rotor bar segment that forms a rotor loop given by

$$d\vec{f} = -i_{R_n}(t)\, d\vec{r} \times \vec{b}(y', t) \tag{3.152}$$

where $i_{R_n}(t)$is the rotor current of the n-th loop, $d\vec{r}$ is the elemental position vector of the rotor segment through which the current flows, and $\vec{b}(y', t)$ is the flux density which passes through the current-loop as a function of time and rotor position (y').

The flux density is obtained directly from the currents using the equations in the previous section. After considerable simplification of the resulting expressions, the steady-state torque may be shown to be the sum of four components

$$T = T_{11} + T_{12} + T_{21} + T_{22} \tag{3.153}$$

where T_{11} and T_{22} are the components due to direct coupling and T_{12} and T_{21} are the components due to cross coupling. Expressions for each of the four elements are derived in detail in Appendix B. Repeating (B.39) and (B.40),

$$T_{11} = -dw'\Re\left\{\sum_{\kappa} \frac{3\mu_0}{gk} K_{pR_n}^{\kappa} K_{sk}^{\kappa} e^{jky_{0n}} \bar{C}_1^{\kappa *} \bar{I}_{R_n 1}^{\kappa} \bar{I}_1^{*}\right\} \tag{3.154}$$

$$T_{22} = -dw'\Re\left\{\sum_{\lambda} \frac{3\mu_0}{gl} K_{pR_n}^{\lambda} K_{sk}^{\lambda} e^{jly_{0n}} \bar{C}_2^{\lambda *} \bar{I}_{R_n 2}^{\lambda} \bar{I}_2^{*}\right\} \tag{3.155}$$

For negative sequence excitation applied to the second winding (from (B.47) and

(B.48)),

$$T_{12} = -dw'\Re\left\{\sum_{\chi}\frac{3\mu_0}{gk}K^{\kappa}_{pR_n}K^{\kappa}_{sk}e^{jky'_{0n}}\bar{C}^{\kappa *}_{1}\bar{I}^{\lambda}_{R_n 2}\bar{I}^{*}_{1}\right\} \tag{3.156}$$

$$T_{21} = -dw'\Re\left\{\sum_{\chi}\frac{3\mu_0}{gl}K^{\lambda}_{pR_n}K^{\lambda}_{sk}e^{jly'_{0n}}\bar{C}^{\lambda *}_{2}\bar{I}^{\kappa}_{R_n 1}\bar{I}^{*}_{2}\right\} \tag{3.157}$$

while for positive sequence excitation (from (B.45) and (B.46))

$$T_{12} = -dw'\Re\left\{\sum_{\chi}\frac{3\mu_0}{gk}K^{\kappa}_{pR_n}K^{\kappa}_{sk}e^{-jky'_{0n}}\bar{C}^{\kappa}_{1}\bar{I}^{\lambda}_{R_n 2}\bar{I}_{1}\right\} \tag{3.158}$$

$$T_{21} = -dw'\Re\left\{\sum_{\chi}\frac{3\mu_0}{gl}K^{\lambda}_{pR_n}K^{\lambda}_{sk}e^{-jly'_{0n}}\bar{C}^{\lambda}_{2}\bar{I}^{\kappa}_{R_n 1}\bar{I}_{2}\right\} \tag{3.159}$$

The expressions for torque, in conjunction with the voltage equations, completely describe the electro-mechanical operation of the BDFM under the influence of inter-bar currents within the limits of the assumptions made. Specifically, the motor was assumed to have a smooth air-gap, be unsaturated, and the inter-bar currents were assumed to flow between adjacent rotor bars in specific locations. The validity of the model under these assumptions is discussed in the next chapter.

Chapter 4

Experimental Verification and Investigation

This chapter presents the results of experiments performed on a BDFM using a rotor fabricated in such a way as to ensure the flow of significant inter-bar currents between the rotor bars. The experimental results not only demonstrate that the inter-bar resistance phenomenon causes degraded performance, but also serve to validate the inter-bar resistance model presented in Chapter 3. The correlation between measured and predicted results suggests that the model is a sufficiently accurate tool for predicting the inter-bar current effects in a BDFM.

4.1 Rotor Test Results

The presence of inter-bar currents in a rotor implies that the resistance between the rotor bars and rotor iron is relatively low in comparison to the bar resistance. In order to achieve this result, a rotor was constructed in which the rotor bars were hammered into the rotor slots. This resulted in a good contact between the rotor bars and the rotor iron. The rotor was skewed one rotor slot (10°) in order to facilitate electrical contact between the rotor bars and the rotor iron.

Before welding the end-connections to the bars, the inter-bar resistance was measured between all pairs of adjacent bars. A fixed dc current (10-20 A) was injected into one bar and extracted from the other and the voltage between them

Chapter 4

Experimental Verification and Investigation

This chapter presents the results of experiments performed on a BDFM using a rotor fabricated in such a way as to ensure the flow of significant inter-bar currents between the rotor bars. The experimental results not only demonstrate that the inter-bar resistance phenomenon causes degraded performance, but also serve to validate the inter-bar resistance model presented in Chapter 3. The correlation between measured and predicted results suggests that the model is a sufficiently accurate tool for predicting the inter-bar current effects in a BDFM.

4.1 Rotor Test Results

The presence of inter-bar currents in a rotor implies that the resistance between the rotor bars and rotor iron is relatively low in comparison to the bar resistance. In order to achieve this result, a rotor was constructed in which the rotor bars were hammered into the rotor slots. This resulted in a good contact between the rotor bars and the rotor iron. The rotor was skewed one rotor slot (10°) in order to facilitate electrical contact between the rotor bars and the rotor iron.

Before welding the end-connections to the bars, the inter-bar resistance was measured between all pairs of adjacent bars. A fixed dc current (10-20 A) was injected into one bar and extracted from the other and the voltage between them

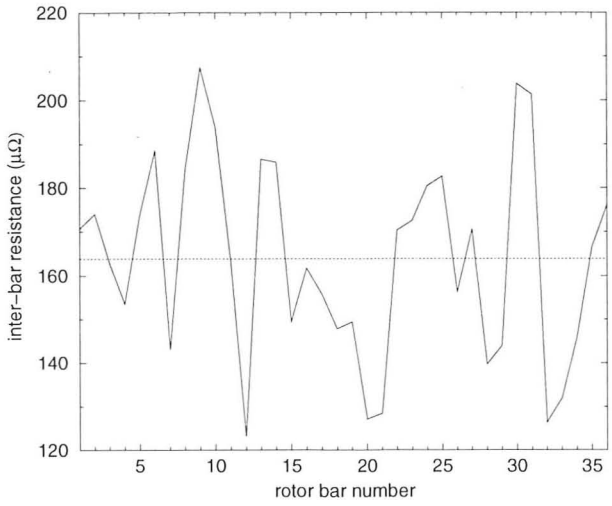

Figure 4.1: Measured values of inter-bar resistance around the rotor between adjacent bars assuming five cuts.

measured. This data provided an estimate of the inter-bar resistance. More detail concerning the calculation of the inter-bar resistance and experimental methods is given in Appendix C.

For the purposes of this work, the inter-bar resistance is assumed to be uniform (although the model is capable of representing non-uniformity) modelled by a fixed number of cuts represented by lumped resistances, as described in Chapter 3. In actuality, because of the inconsistencies in the bar to iron contact, the resistance between adjacent bars varies. Fig. 4.1 shows the variation in the measured values of inter-bar resistance assuming five cuts. The average value of inter-bar resistance is 164 $\mu\Omega$, with a standard deviation of 22.9 $\mu\Omega$. Error due to measurement equipment suggests a maximum error of ± 3 $\mu\Omega$. This is far less than the standard deviation showing that the variation measured is truly due to variations in the bar to iron contact resistance.

Further investigations were carried out to determine whether the inter-bar resistance was dominated by the contact resistance between the rotor bar and rotor iron, or whether it was dominated by the resistance of the iron. In order to answer this question, current was injected between non-adjacent bars.

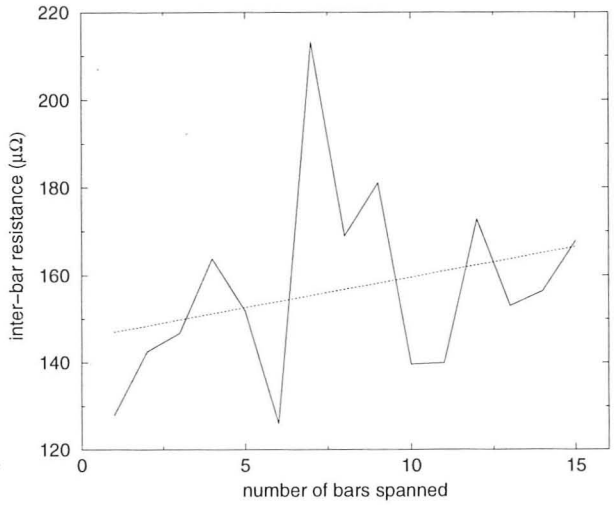

Figure 4.2: Measured values of inter-bar resistance between non-adjacent bars assuming five cuts.

Figure 4.2 shows the inter-bar resistance between bars with successively greater spacing, up to a span of 15 bars, along with a best-fit linear relationship between resistance and span. There is a slight upward trend in resistance as the span between the bars increases, owing to a component of resistance due to the rotor iron resistivity. However, if the iron resistance were to dominate, the increase would be linear with near unity slope. This is not the case, implying that the bar-iron contact resistance dominates.

4.2 Machine Test Results

The validity of the inter-bar resistance model was tested in four stages, each relying on the accuracy of the model in different ways. The first stage involved no-load induction motor tests where only one winding was excited at a time. In this situation, the BDFM behaves like an induction motor with a modified cage rotor. The second stage involved performance modeling of a machine with an insulated rotor as well as comparisons with the predicted results of the harmonic model presented in [23]. The third stage involved locked-rotor induction motor

tests. The final stage involved tests to verify the ability of the model to represent inter-bar currents as well as accommodate the cross-coupling between the stator windings. This involved simulating and measuring the performance of the BDFM under normal, synchronised operation.

All quantities mentioned are phase quantities. For predictions, the model includes 10 spatial harmonics in addition to the fundamental for each winding. This number was determined by trial and error while observing the effect of the number of harmonics on the precision of the predicted results.

It should be kept in mind that the purpose of this work is to establish the existence of inter-bar currents and to determine whether degraded performance can actually be attributed to this phenomenon. This work is neither attempting to espouse the benefits of the BDFM, nor diminish the commercial potential of the BDFM. The tests were performed on a BDFM that was *not* optimised and which is not claimed to be representative of a well designed machine. The detailed test results described are not indicative of a purpose-designed BDFM, however they do portray the general behaviour that can be expected from a BDFM.

4.2.1 Test Configuration

Throughout the experimental verification process the same test equipment was used in order to help maintain repeatability of the tests. The experimental configuration, shown in block form in Fig. 4.3, is used for tests where both windings are excited. In this case, the first winding is referred to as the power winding and the second as the control winding. For single winding excitation, one of the windings is left disconnected and the other is line excited via an autotransformer. For all the tests, the line frequency is 50 Hz.

When the BDFM is doubly-fed, the power winding is line-excited via an autotransformer and the control winding is excited by a synchronous generator. Frequency control of the second winding is achieved by varying the speed of the synchronous generator with a Ward-Leonard set. The control winding voltage level is controlled by adjustment of the synchronous generator field voltage. The torque on the BDFM is varied with a DC dynamometer which is controlled with another Ward-Leonard set. The torque is measured using a torque transducer.

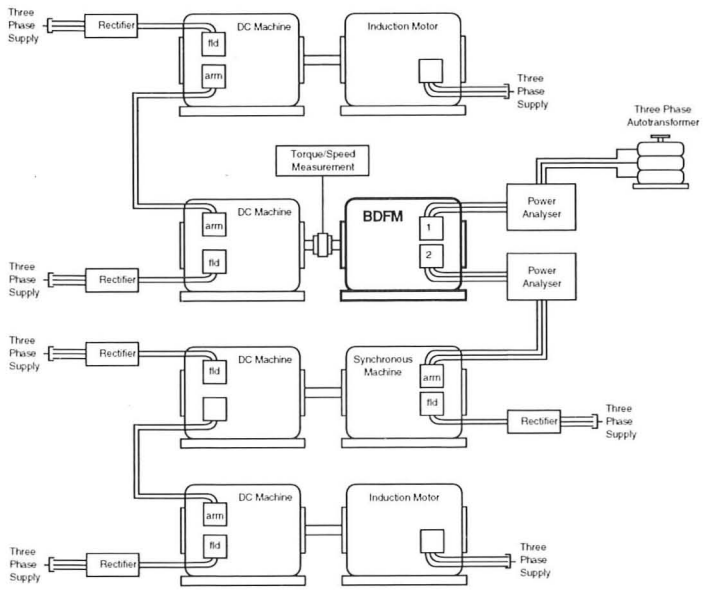

Figure 4.3: Test configuration for double excitation with variable frequency.

Positive torque signifies motoring action of the BDFM and negative torque generating action. Ward-Leonard sets were used because suitable power-electronic drives were not available. The significant drawback to is that the speed of the set varies with the load demand due to the presence of the induction motor. This makes testing at constant speeds difficult and introduces error into the test results.

The BDFM under investigation has a 4 pole power winding and an 8 pole control winding. Details of the BDFM are given in Table 4.1. The rotor is a Type I configuration (Creedy) with no common end-ring (see Fig. 3.4). Pertinent loop specifications are given in Table 4.2.

Two rotors are considered in the experiments, one with insulated rotor bars (the subject of the investigations described in [24]) and one of similar construction specially fabricated to promote rotor bar to iron contact. The rotor with no insulation is identical in all respects to the rotor with insulated bars except for the lack of insulation and the introduction of skew of one rotor slot (10°). The skew was required to provide a tight fit of the rotor bars. Although larger bars may have precluded the need to skew the rotor, they were not available at the time the rotor was being fabricated.

Table 4.1: BDFM Specifications

Dimensions		
stator slots	48	
air-gap (mm)	0.5	
stack length (mm)	27.3	
diameter (mm)	164.6	
stator slot mouth (mm)	3.04	
rotor slot mouth (mm)	2.54	
Stator	**Power Winding**	**Control Winding**
number of layers	1	1
span (slots)	12	6
turns per coil	8	15
phase resistance (Ω)	0.32	0.70
leakage inductance (mH)	1.44	2.69
Rotor		
number of nests	6	
loops per nest	3	
type	Type I (Creedy)	

Table 4.2: Rotor Loop Specifications

Quantity	**Inner Loop**	**Middle Loop**	**Outer Loop**
span (mm)	14.364	43.092	71.820
bar resistance ($\mu\Omega$)	54.48	57.78	59.16
end segment resistance ($\mu\Omega$)	2.87	9.12	15.56
bar leakage inductance (μH)	0.575	0.575	0.575

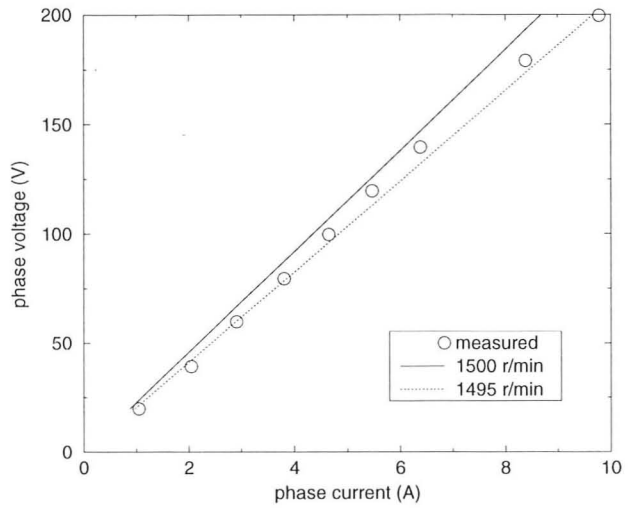

Figure 4.4: No load test results with the power winding (4 poles) excited and the other winding left open.

4.2.2 No-Load Tests

The no-load test is performed to determine whether the stator quantities calculated by the inter-bar model are sufficiently accurate. The shaft of the motor is maintained at the synchronous speed of the winding under test, 1500 r/min for the power winding (4 poles) and 750 r/min for the control winding (8 poles). Because only one winding is excited and the rotor is rotating at the synchronous speed with respect to the excited winding, there are no currents induced in the rotor. Nevertheless, the model employed five inter-bar resistances, each of 164 $\mu\Omega$, between adjacent bars. Figure 4.4 shows the results of the no-load test for the power winding.

During the test, the measured speed of the motor varied by up to 5 r/min. The tachometer used to measure the speed was accurate to ± 1 r/min. The remaining error was due to speed variations in the dynamometer. Consequently, predicted results for a speed of 1495 r/min are also shown. The predictions for 1505 r/min (not shown) are similar.

The measured values are bracketed by the predictions for 1500 r/min and for 1495 r/min shaft speeds, which suggests that the predicted values were within the

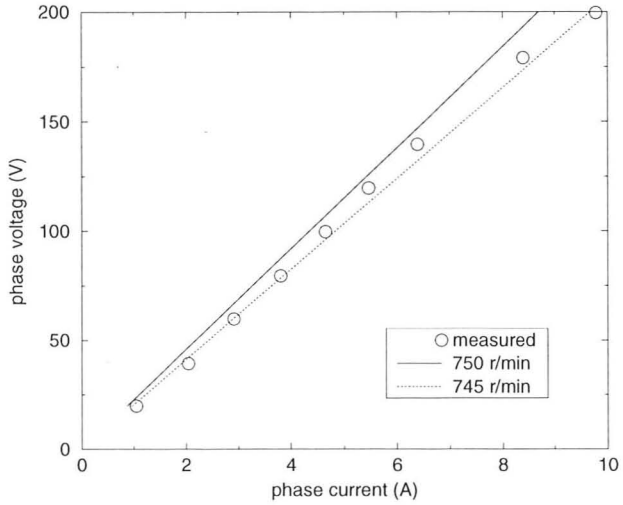

Figure 4.5: No load test results with the control winding (8 poles) excited and the power winding left open.

measurement error. The motor begins to saturate at voltages above 150 V.

Fig. 4.5 shows the results for the control winding (8 poles) under the same test. Predictions were made for 745 r/min to account for the speed variation of the dynamometer witnessed during the experiment. Similar predictions result for a speed of 755 r/min. The measured results are bracketed by the two predictions. The motor saturates beyond 175 V.

Even though the predicted and measured results for both windings do not coincide precisely, the level of correlations suggests that the stator quantity predictions are sufficiently accurate.

4.2.3 Insulated Rotor Test

The next step in verifying the proposed inter-bar current model is to check its accuracy against results generated by a model ignoring inter-bar currents (such as that proposed in [23]) and also those obtained by measurement for an insulated cage rotor. Because the distributed effect of current flow between adjacent bars is modelled by lumped resistances placed at specific locations along the axis of

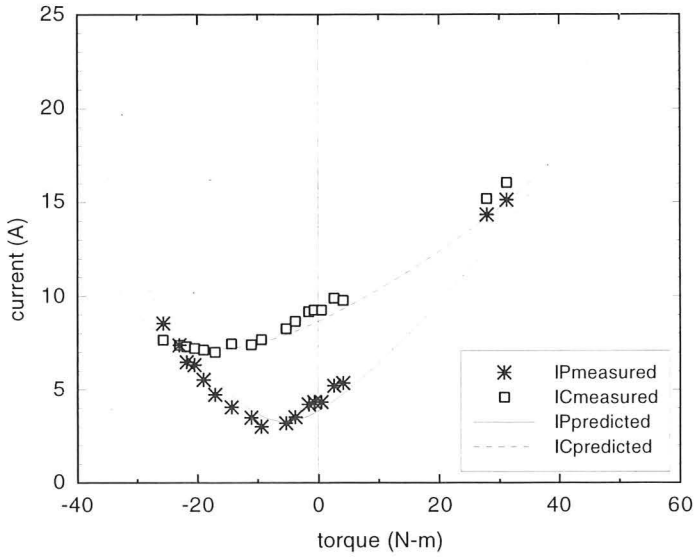

Figure 4.6: Power-winding and control-winding phase current at 400 r/min for $V_1 = 50$ V and $V_2 = 20$ V plotted against torque for a machine with an insulated rotor.

the rotor, called cuts, setting the value of the resistances to an appropriate value can model different levels of insulation between the rotor bars and rotor iron. The situation when the rotor bars are insulated from the iron can be modelled by increasing the level of lumped resistance to a large value in comparison to the value of rotor bar resistance. Through trial and error, a value of 1000 Ω between the bars in five locations was found to be sufficient.

When using the above value of resistance, the inter-bar current model is able to generate the same predictions of performance, to several decimal places[1], as the insulated bar model presented in [23]. The insulated bar model has itself been verified experimentally using the same stator, but using a rotor with an insulated cage. For example, Fig. 4.6 shows the predicted and measured variations of winding current for a power-winding phase voltage (V_1) of 50 V and a control-winding phase voltage (V_2) of 20 V. The power winding was line-excited via the autotransformer and a 10 Hz control-winding voltage was provided via the synchronous generator.

[1]Slightly less accurate predictions (accurate to the first or second decimal point) result when using a value of 1 Ω between adjacent rotor bars

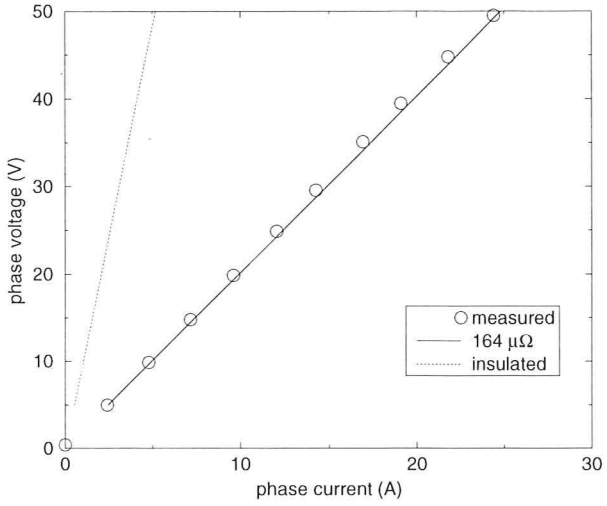

Figure 4.7: Locked rotor test results of the power winding (4 poles) along with predictions for an insulated cage rotor and a rotor with an inter-bar resistance of 164 $\mu\Omega$.

4.2.4 Locked Rotor Tests

Under locked rotor conditions, the rotor resistance becomes very important and the effect of the inter-bar currents should be clearly present. This set of tests determines the accuracy of the model in predicting the behaviour of the BDFM in the absence of cross-coupling since only one winding is excited at a time.

The model includes ten spatial harmonics in addition to the fundamentals, as in the no-load test. The inter-bar resistance phenomenon is modelled using five axial cuts. Along each cut, connecting adjacent bars, is an assumed inter-bar resistance of 164 $\mu\Omega$. The rotor used in this test is the same as that used in the no-load tests and will be the same rotor used in all subsequent tests. The number of harmonics and cuts were determined through trial and error.

Figures 4.7 and 4.8 show the test results for both windings. Predictions for an insulated cage are also shown to illustrate the effect inter-bar currents have on the stator currents. There is a high degree of correlation between the measured and predicted results. The inter-bar current paths have caused higher levels of stator current to flow in order to provide the additional losses presented by the inter-bar resistances.

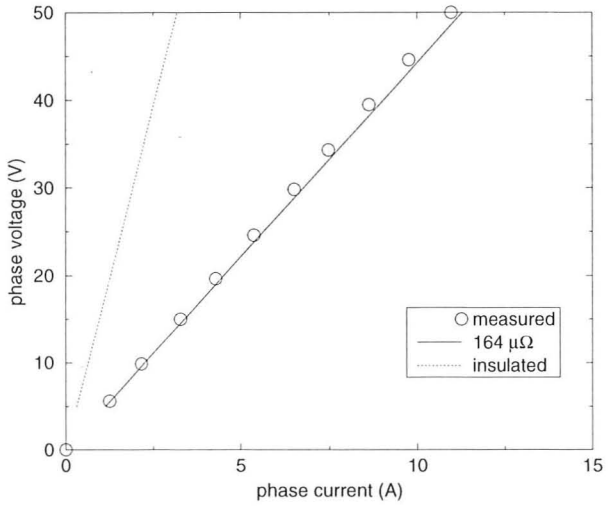

Figure 4.8: Locked rotor test results of the control winding (8 poles) along with predictions for an insulated cage rotor and a rotor with an inter-bar resistance of 164 $\mu\Omega$.

The locked rotor tests suggest that the model is performing as expected and that the model parameters are sufficiently accurate. However, the question of the validity of using 164 $\mu\Omega$ for an inter-bar resistance value as opposed to a different value remains.

Figure 4.9 shows locked rotor predictions on the power winding (4 poles) for different values of inter-bar resistance along with the measured results. The level of correlation between results and measurements suggests that a value of 164 $\mu\Omega$ is sufficiently accurate.

4.2.5 Doubly-Fed Tests

The foregoing tests suggest that the model provides an acceptable level of accuracy using an inter-bar resistance value of 164 $\mu\Omega$. Each of the previous tests validated different aspects of the model. The accuracy of the model when the BDFM, while using an uninsulated rotor, is doubly-fed still remains. Two separate tests are performed, one at 400 r/min and another at 600 r/min. Both speeds correspond to applied control-winding frequencies of 10 Hz, negative sequence ex-

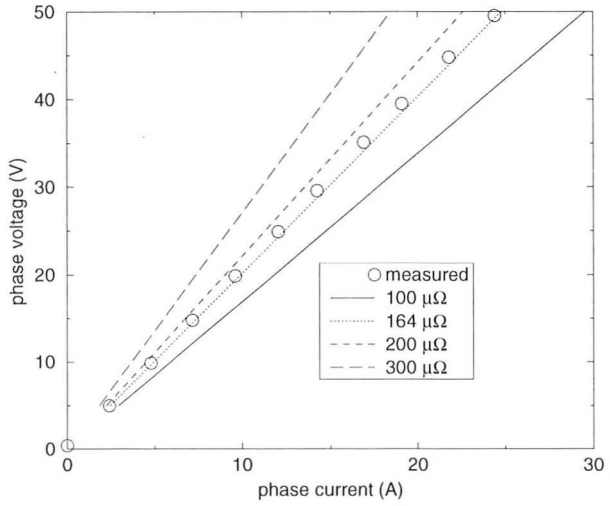

Figure 4.9: Locked rotor test results of the power winding (4 pole) along with predictions for inter-bar resistance links of 100, 164, 200, and 300 $\mu\Omega$.

citation for the former speed and positive excitation for the latter speed. Tests at the same frequency are performed to determine the effect of phase sequence on the predictions.

Tests at 400 r/min

In order to operate the BDFM at 400 r/min, the control winding is excited at a frequency of 10 Hz in opposite phase sequence to that of the power winding (of frequency 50 Hz). Tests are carried out to determine the ability of the inter-bar model to predict the performance of the BDFM with both windings excited. The control-winding voltage is supplied via the synchronous generator connected to the Ward-Leonard set (see Fig. 4.3). Low values of voltage are used in the tests in an attempt to avoid saturation of this BDFM.

Figure 4.10 shows the predicted and measured variations of power-winding current with applied torque for a power-winding phase voltage (V_1) of 50 V and a control-winding phase voltage (V_2) of 20 V. Figure 4.11 shows the predicted current in the control winding for the same conditions. Both graphs also include the predictions for insulated bars in the same (skewed) rotor.

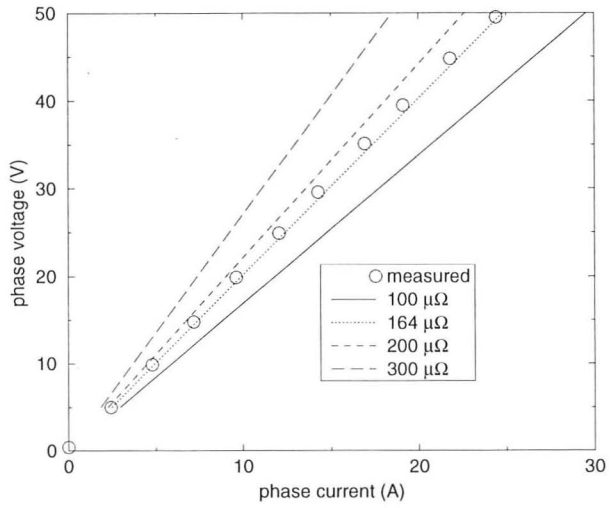

Figure 4.9: Locked rotor test results of the power winding (4 pole) along with predictions for inter-bar resistance links of 100, 164, 200, and 300 $\mu\Omega$.

citation for the former speed and positive excitation for the latter speed. Tests at the same frequency are performed to determine the effect of phase sequence on the predictions.

Tests at 400 r/min

In order to operate the BDFM at 400 r/min, the control winding is excited at a frequency of 10 Hz in opposite phase sequence to that of the power winding (of frequency 50 Hz). Tests are carried out to determine the ability of the inter-bar model to predict the performance of the BDFM with both windings excited. The control-winding voltage is supplied via the synchronous generator connected to the Ward-Leonard set (see Fig. 4.3). Low values of voltage are used in the tests in an attempt to avoid saturation of this BDFM.

Figure 4.10 shows the predicted and measured variations of power-winding current with applied torque for a power-winding phase voltage (V_1) of 50 V and a control-winding phase voltage (V_2) of 20 V. Figure 4.11 shows the predicted current in the control winding for the same conditions. Both graphs also include the predictions for insulated bars in the same (skewed) rotor.

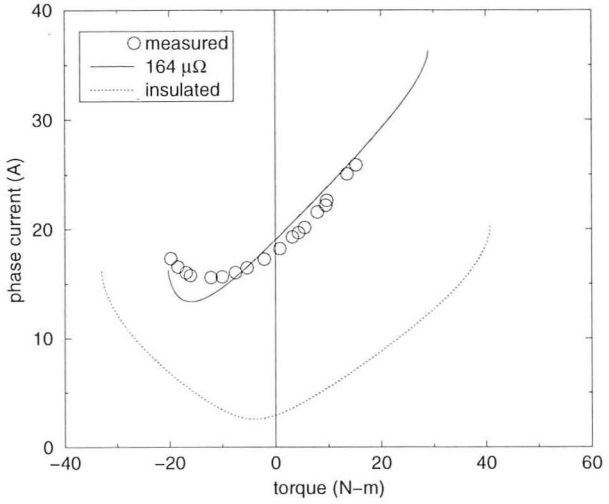

Figure 4.10: Power-winding phase current at 400 r/min for $V_1 = 50$ V and $V_2 = 20$ V plotted against torque.

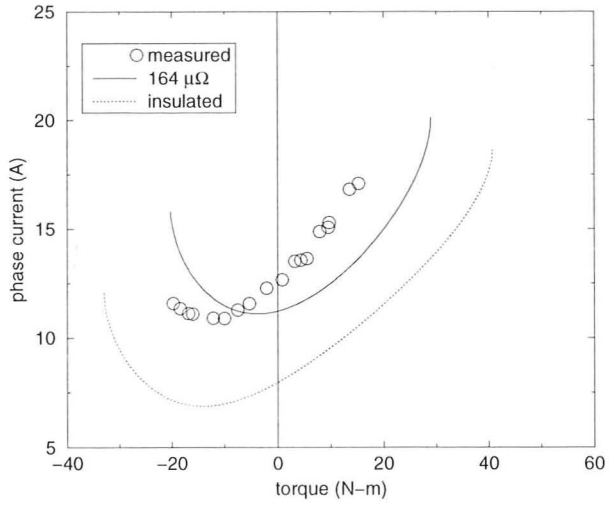

Figure 4.11: Control-winding phase current at 400 r/min for $V_1 = 50$ V and $V_2 = 20$ V plotted against torque.

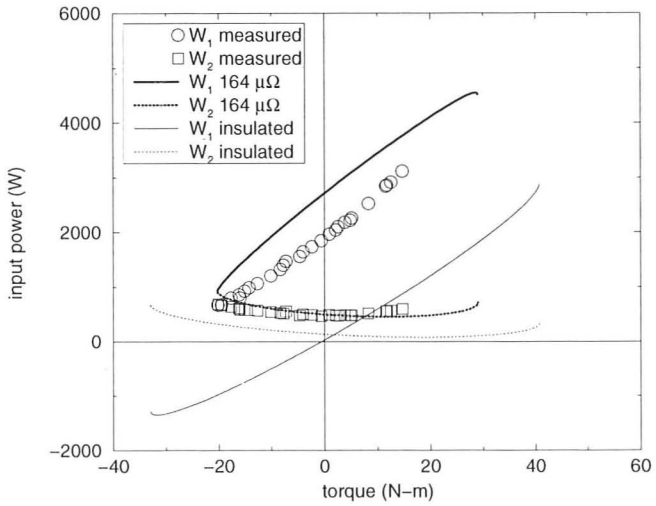

Figure 4.12: Input power to both windings at 400 r/min for $V_1 = 50$ V and $V_2 = 20$ V plotted against torque.

Two observations can be made from these graphs. Firstly, the inter-bar current model clearly predicts the main effects of bar to iron contact. Secondly, the bar to iron contact is seen to have two effects: the current required (in both windings) to produce a given torque is increased—indicating a reduction in efficiency—and the range of available torques is reduced.

Investigation of the input power to the windings further reveals the significant impact the inter-bar current paths have on performance. Figure 4.12 shows the variations of the two stator winding input powers, along with those of an insulated rotor, with load torque. Firstly, the input power is significantly more positive at the same torque levels. This again indicates increased losses and reduced efficiency. Secondly, the input power is *always positive* for this operating condition regardless of whether the torque is positive or negative. The presence of the BDFM inter-bar currents has prevented the BDFM from acting as a generator when mechanical power flow is into the machine. All the energy flowing into the machine is dissipated as heat.

Figure 4.13 shows the efficiency of the machine under the same test conditions. The presence of the inter-bar currents has clearly reduced the efficiency of the

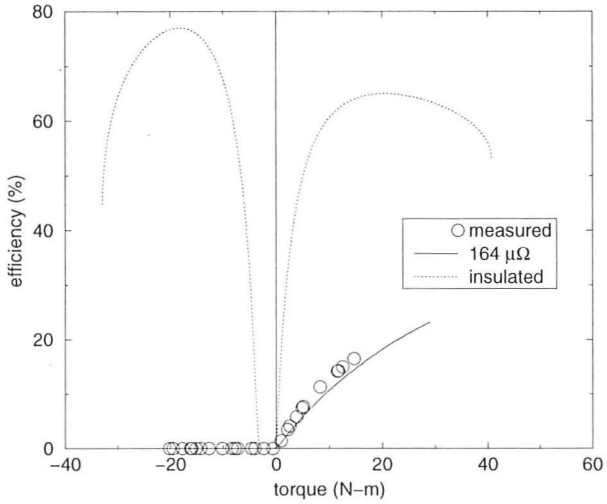

Figure 4.13: Efficiency at 400 r/min for $V_1 = 50$ V and $V_2 = 20$ V plotted against torque.

machine in comparison to a machine using an insulated cage rotor. Indeed, the inter-bar currents have prevented the machine from acting as a generator since the efficiency is zero when attempting to generate, which is equivalent to positive electrical input power for negative input torque as shown in Fig. 4.12.

Even though the predicted efficiency calculations only consider resistive losses, a good agreement exists between predicted and measured results. In fact, the predicted efficiency is less than that measured. Since iron losses are not included, which would lower the predicted efficiency further if included, it can be concluded that the loss in the rotor due to the inter-bar currents is being over-estimated. However, the level of correlation suggests that the trend is predicted and that the reduction in efficiency is due to the flow of inter-bar currents.

Although the accuracy could be improved, the trends are predicted. In an attempt to improve the accuracy, the actual inter-bar resistance values shown in Fig. 4.1 were used between the adjacent bars as well as both slightly larger and slightly smaller values of average inter-bar resistance. The changes on the predictions were minimal, which suggested that the value of inter-bar resistance was most likely not the cause of the error in predictions. Thus, the errors are due

to phenomena not considered in the model.

The most likely cause of the inaccuracies is due to not modelling the flow of inter-bar currents between non-adjacent bars. No attempt was made to model this flow because the results are accurate enough to show that inter-bar currents significantly impact the performance of the BDFM—the goal of this analysis. Because of the extent of the observed performance degradation, despite the inaccuracies in the model, it is clear that the rotor bars must be insulated from the rotor iron if satisfactory operation is to be expected.

Tests at 600 r/min

To operate the BDFM at 600 r/min, the control winding is excited with a voltage at 10 Hz in the same sequence as the power winding. The tests at 600 r/min are performed with the same level of applied voltages as used in the tests at 400 r/min. The purpose of the tests is to determine if the accuracy of the model is affected by the sequence of the control-winding voltage. Figure 4.14 shows the predicted and measured variations in power-winding current for varying load torque. Fig. 4.15 shows the results for the control winding. Also shown are the predicted results for an insulated cage-rotor. Both graphs show that the current is increased for the same torque due to the flow of inter-bar currents. However, for this operating condition, the torque limits are not appreciably reduced when inter-bar currents flow.

The accuracy of predictions has worsened for the power winding and improved for the control winding in comparison to the test results at 400 r/min. Predictions were made using the actual measured inter-bar resistances between the bars, instead of an average value of 164 $\mu\Omega$, to see if the accuracy improves. The predicted results were similar to those predicted using the average value—no improvement in accuracy was obtained. As was concluded for the tests at 400 r/min, the discrepancies are most likely due to the flow of inter-bar currents between non-adjacent rotor bars. Nevertheless, the trends are clearly predicted.

Potentially, the discrepancy could be due to saturation. Hunt suggests in the discussion of his paper that "it is only necessary to make the [stator] iron sufficient to take the flux of the field having the smaller number of poles" [2,

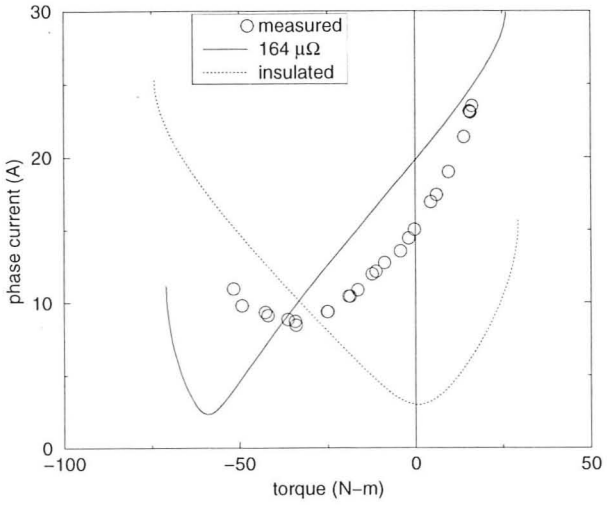

Figure 4.14: Power-winding phase current at 600 r/min for $V_1 = 50$ V and $V_2 = 20$ V plotted against torque.

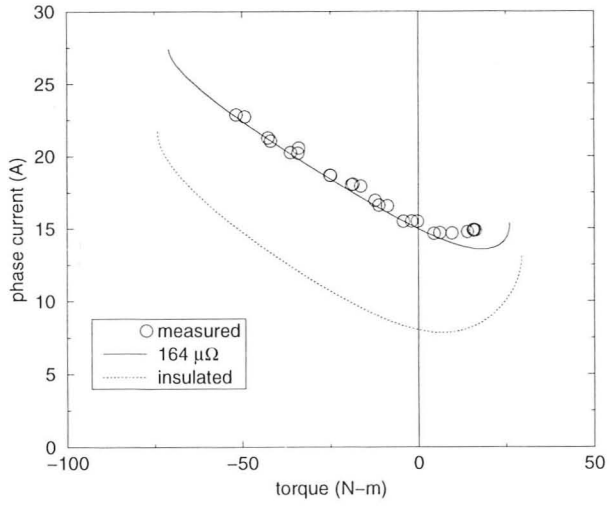

Figure 4.15: Control-winding phase current at 600 r/min for $V_1 = 50$ V and $V_2 = 20$ V plotted against torque.

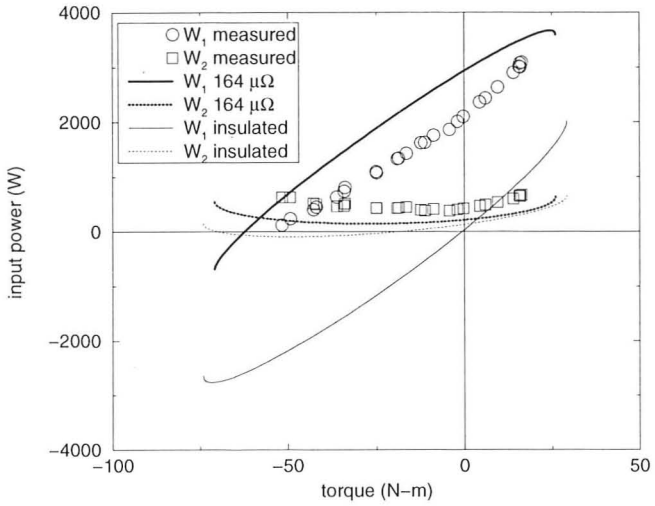

Figure 4.16: Input power to both windings at 600 r/min for $V_1 = 50$ V and $V_2 = 20$ V plotted against torque.

pg. 674 (Discussion)]. His work suggests that the stator winding with the larger number of poles may be more susceptible to saturation of the teeth than the other winding. Conversely, the one with the lower number of poles will be more susceptible to saturation of the stator core. Unfortunately, the inter-bar current model does not take into account saturation so this hypothesis could not be tested. Nevertheless, the low values of voltage suggest saturation is not likely.

Figure 4.16 shows the input power to the windings for an uninsulated rotor as well as for an insulated rotor. Once again, the input power is more positive than that for an insulated rotor for all torque levels. During the measurements, the load torque was not increased appreciably beyond 50 N · m, which was the rated torque limit of the transducer, for fear of damaging the equipment. Therefore, although predictions showed that the motor would eventually generate above 60 N · m, this could not be verified. Nevertheless, the predictions and tests have shown that the inter-bar currents have significantly degraded the performance of the machine.

The efficiency of the machine, both predicted and measured, is shown in Fig. 4.17. For the uninsulated cage, the efficiency is greatly reduced in comparison to a machine with insulated rotor bars. Even though only resistive losses

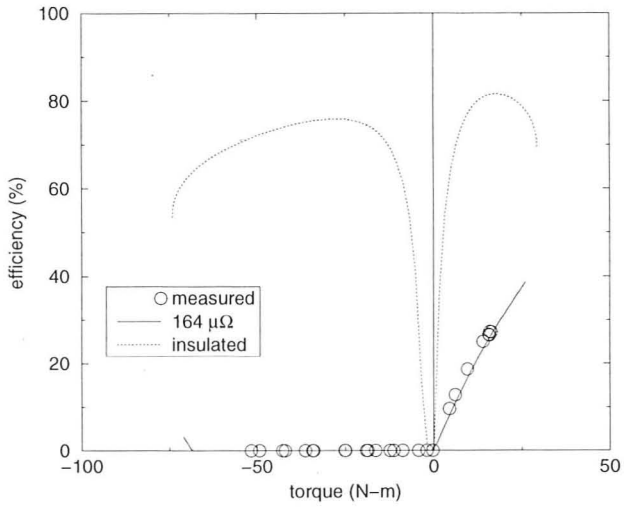

Figure 4.17: Efficiency at 600 r/min for $V_1 = 50$ V and $V_2 = 20$ V plotted against torque.

are considered in the predictions, the correlation between measured and predicted results quite good. The inter-bar current paths prevent the BDFM from generating any output power when supplied with a generating torque, signified by a zero efficiency.

As in the tests at 400 r/min, the predicted efficiency would be less if rotor losses were included in the model. This suggests an over-estimate of the copper losses in the rotor due to the inter-bar currents, most likely due to having too low a value of inter-bar resistance. If a higher value of resistance were used, there would be less current flow between the bars and hence, less losses. However, despite this over-estimate, the trend is predicted.

4.3 Investigations

4.3.1 Threshold Resistance

The results achieved during the tests are encouraging and suggest that the model can be used to make predictions with some level of confidence. In this section

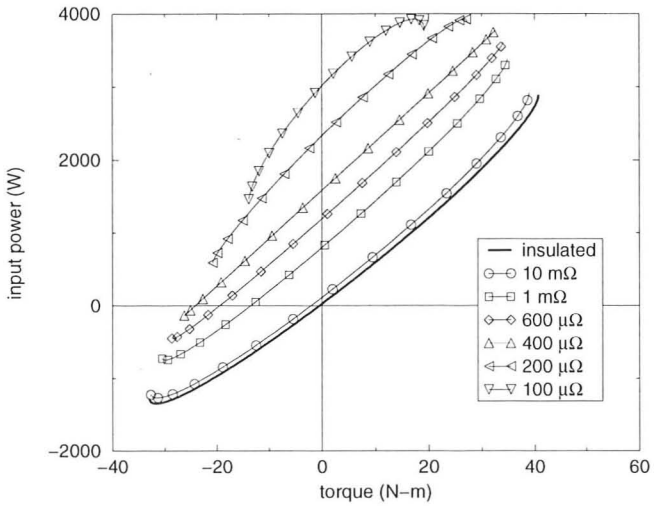

Figure 4.18: Predicted input power of the power winding for different values of inter-bar resistance at the following conditions: 400 r/min, $V_1 = 50$ V, $V_2 = 20$ V.

differing levels of inter-bar resistance are used in order to answer the question, "How good should the rotor insulation be?"

Figure 4.18 shows the effect of different inter-bar resistances on the input power of the power winding under the same supply conditions as used in the experimental work. The control-winding input power is not shown since the performance will be dominated by the power flow through the power winding.

When attempting to generate, the machine will not start to produce any output power until the equivalent inter-bar resistance has increased to nearly 400 $\mu\Omega$. However, in order to get performance close to that of an insulated machine, the inter-bar resistance should be greater than about 10 mΩ—an increase of about two orders of magnitude. Measurements made on a similarly sized die-cast rotor of an induction motor showed the equivalent inter-bar resistance to be around 3 mΩ [32]. This is an order of magnitude improvement, but still needs to be increased.

The corresponding plot of the efficiency, Fig. 4.19, displays the effects of the varying inter-bar resistances in a different manner. As can be seen, any value of inter-bar resistance causes a reduction in the efficiency due to increased losses. For reducing values of inter-bar resistance, the efficiency decreases. With negative

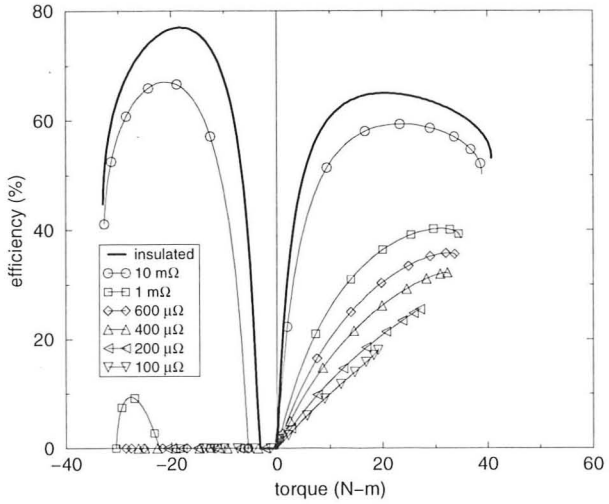

Figure 4.19: Predicted efficiency for different values of inter-bar resistance at the following conditions: 400 r/min, $V_1 = 50$ V, $V_2 = 20$ V.

torque inputs (attempting to generate), the machine produces no output power, signified by zero efficiency.

Similar investigations can be performed at 600 r/min under the same supply conditions, except with the sequence of control-winding voltages reversed. Figure 4.20 shows the input power of the power winding plotted against torque for different values of inter-bar resistance. Figure 4.21 shows the corresponding efficiency.

The input power is increasingly more positive for aa given value of torque with reducing inter-bar resistance. Furthermore, the machine has significantly reduced efficiency for any value of inter-bar resistance less than around 10 mΩ. In contrast to the operation at 400 r/min, the torque limits first increase and then decrease with reducing values of inter-bar resistance. Unfortunately, this increase in torque capability is at the expense of increased losses resulting in worsened performance.

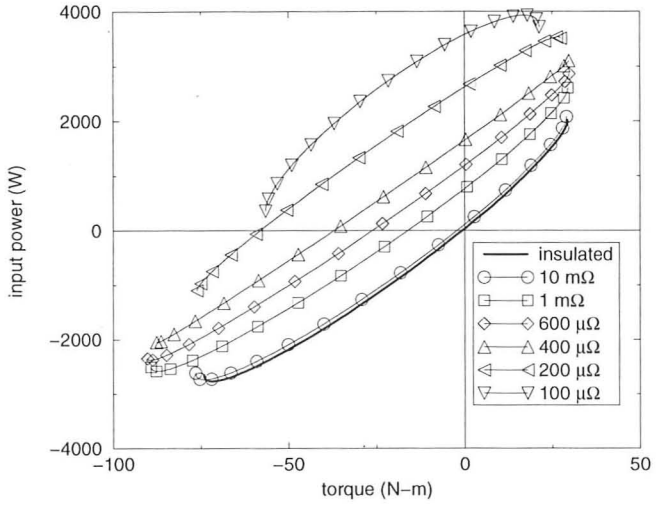

Figure 4.20: Predicted input power of the power winding for different values of inter-bar resistance at the following conditions: 600 r/min, $V_1 = 50$ V, $V_2 = 20$ V.

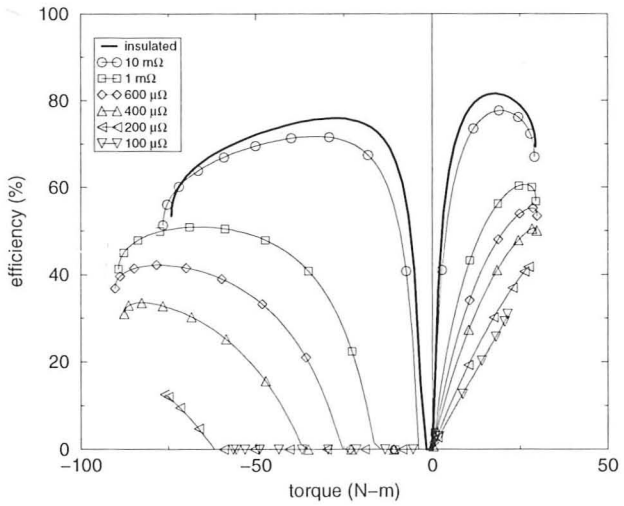

Figure 4.21: Predicted efficiency for different values of inter-bar resistance at the following conditions: 600 r/min, $V_1 = 50$ V, $V_2 = 20$ V.

4.3.2 Torque Limits

When considering the use of the BDFM in a variable speed application, it is useful to know what limits of torque the machine can produce for different speeds. Obviously, these limits will be dependent on the voltages applied to each of the windings. These torque limits have been addressed for an insulated rotor without skew by Ferreira in [31] and by Williamson, Ferreira and Wallace in [24]. However, examining the effect of inter-bar resistances on the torque limits is worthwhile to see the overall effect they have on the torque capability of the machine.

Consider a BDFM with the power winding connected to a supply with voltage V_1 and frequency f_1. The control winding is connected to a variable voltage and variable frequency supply. The maximum voltage that can be produced by the control winding is V_{2max}. Both of the stator winding currents, because of thermal considerations, must be less than the values I_{1max} and I_{2max}. The determination of the torque limits will now involve searching for the optimum value of excitation (V_2 or I_2) and torque angle for a given value of speed.

Figure 4.22 shows the results of the search for the torque limits for both the insulated and uninsulated rotors ($R_{ib} = 164\ \mu\Omega$) used previously in the experimental verification. The phase voltage of the power winding was fixed at 100 V, which also acted as the control-winding voltage limit. Both winding currents were limited to 20 A. The frequency of the control winding was allowed to vary up to 100 Hz while the power-winding frequency was fixed at 50 Hz. In order to achieve speeds less than the natural speed of $N_r = 60\frac{f_1}{P_1+P_2} = 500$ r/min, negative sequence excitation was allowed for the control winding. Speeds below 0 r/min were allowed in this simulation in order to show the shape of the envelope.

For the insulated rotor, the torque is relatively constant around the speed of 500 r/min, corresponding to dc excitation. Beyond a certain point, the torque limits decrease non-linearly. The flat portion of the curve is a result of the imposed current limits while the sloping regions of the curve are due to voltage limitations. The torque limits decrease to zero at the synchronous speed of the power winding, $f_1/P_1 = 1500$ r/min, a result of the induction motor aspects of the machine. For decreasing speeds (including those in the opposite direction of rotation) the torque appears like that experienced during field weakening, owing to the voltage limit.

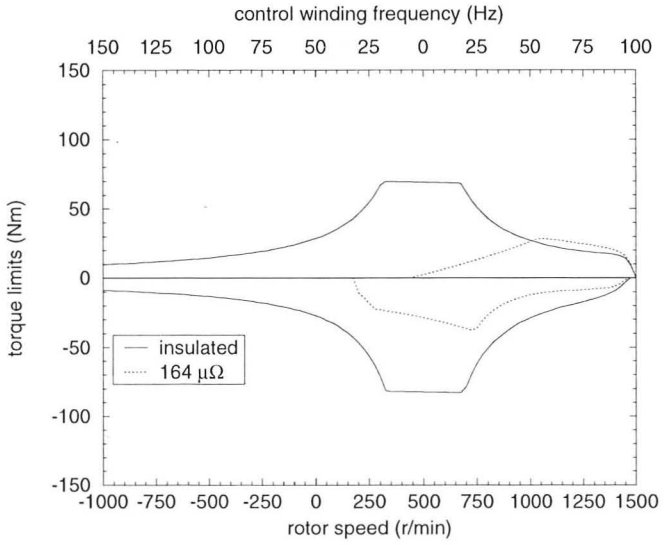

Figure 4.22: Torque limits versus speed for both the insulated rotor and uninsulated rotor with an inter-bar resistance value of 164 $\mu\Omega$ under the following constraints: $V_1 =$ 100 V, $V_2 \leq 100$ V, $I_1 \leq 20$ A, $I_2 \leq 20$ A, $f_1 = 50$ Hz, and $f_2 \leq 150$ Hz

Results achieved when the inter-bar resistance is set to the threshold value of 10 mΩ are not shown since they are similar (with slight reduction of the torque limits) to those of the insulated rotor.

For the uninsulated rotor, clearly, a value of inter-bar resistance of 164 $\mu\Omega$ has a drastic effect on the capability of the machine to produce torque. Not only is the symmetry affected, but the limits are greatly reduced in terms of speed range and torque in comparison to those of an insulated rotor. This graph further reinforces the notion that the inter-bar resistance should be minimised.

Experiments were not carried out at these voltage levels for two reasons. Firstly, the stator currents which would have been measured, based on predictions, would have caused overheating of the motor. Secondly, because of the poor magnetic design of the motor, the voltage levels would have caused the machine to saturate [31].

Chapter 5

Conclusions

5.1 Discussion

This dissertation has presented two different coupled-circuit models of the BDFM. The first model is based on conventional, induction-motor dq analysis and yielded both a transient and steady-state model, the latter being a tool to aid in design. The second model used harmonic analysis to develop a set of equations which were used to predict the performance of the machine under the influence of inter-bar currents.

The dq model is an advancement of the general pole-number model presented in [21]. It provides for the prediction of the overall machine performance as well as the prediction of the individual rotor loop currents. As a dynamic model, it not only predicts the transient behaviour of the machine, but also provides a base for the development of motor controllers.

A competing model to the dq model is the harmonic model developed by Ferreira et al. presented in [23]. This model, like the inter-bar model presented in this dissertation, uses harmonic analysis to derive complex coupling impedances between the different stator and rotor circuits. The foundation for harmonic analysis is the complex conductor density function (see AppendixA), used to describe the non-sinusoidal distribution of the windings about the stator. The result is a more accurate representation of the construction of the machine than that provided by the dq, resulting in slightly more accurate predictions of machine performance.

The development and comprehensive verification of the harmonic model are well documented in [23, 24, 31]. Since it can be shown that the *dq* model and the harmonic models match exactly when only the fundamental spatial harmonics are considered, the verification presented in [23, 24, 31] also acts as a verification of the *dq* model.

Even though the *dq* model is a useful design tool, the competing harmonic model presented in [23] is probably better used in commercial design programs because it provides slightly more accurate performance predictions over the *dq* model. It also allows for the calculation of the electromagnetic fields inside the motor (assuming linearity of the magnetic circuits). Unfortunately it is presently only capable of performing steady-state analysis

Because of the problems experienced in the die-casting of a BDFM rotor, a model needed to be developed which could correctly attribute the performance degradation to inter-bar currents, accurately predict the performance of a machine under the influence of inter-bar currents, and identify a threshold level of resistance that should be attained in the rotor fabrication process which would not seriously degrade machine performance. The second model, presented in Chapter 3, represents the primary focus of this dissertation and was developed to meet these requirements.

The model was made general enough to accommodate any value for the resistance between adjacent bars as well as any value for the bar segment resistances. This flexibility allows the model to predict the performance of a BDFM using an insulated rotor, an uninsulated rotor, or a rotor subject to other imperfections such as those due to broken rotor bars, cracked end-rings (if present), and porosity of the rotor bars. All of these effects can be modelled by adjusting either the inter-bar resistances or the actual bar segment resistances. The effects of porosity in single phase induction motors have recently been investigated in two papers written by Williamson et al. in [27, 28].

The verification of the model proceeded with the fabrication of a rotor where the bar to iron contact was promoted. The inter-bar current paths between adjacent bars were represented by five equal resistances, chosen based on trial and error. The resistance between the bars was measured to be 164 $\mu\Omega$. A series of experiments and simulations were performed to verify the accuracy of the model

and show the performance of the BDFM under the influence of inter-bar currents. Results showed that the inter-bar currents cause an increase in the rotor losses. This leads to an increase in the magnitude of the winding currents (for some operating conditions), a reduction in efficiency, and an increase in the power supplied to the windings. Experiments showed that, when attempting to generate, the BDFM with the fabricated, uninsulated rotor would not produce any output power even though it would remain synchronised when applied with mechanical input power. The presence of the inter-bar currents virtually precluded the operation of the BDFM as a generator. The inter-bar currents also significantly decreased the peak torque capability of the machine, as indicated in Fig. 4.22.

The accuracy of the predictions changed with the sequence of the voltages applied to the control winding. For negative sequence excitation, the power-winding current predictions were more accurate than those of the control winding. Conversely, for positive sequence excitation, the control-winding current predictions were more accurate than those of the power winding. Yet, the predictions for a BDFM using an insulated rotor were correct for both windings under the same supply conditions. This suggests that the cause of this discrepancy is most likely due to the flow of inter-bar currents between non-adjacent rotor bars since the voltages were too low for the machine to be appreciably saturated. Nevertheless, the degree of correlation between the predicted and measured results showed conclusively that inter-bar currents significantly degraded machine performance.

Computer simulations were performed using the model to identify a threshold level of resistance necessary to obtain satisfactory performance. The results showed that the inter-bar resistance needed to be increased to a value greater than 10 mΩ in order to achieve performance close to that obtained using an insulated rotor. Resistance measurements on a die-cast induction motor rotor of similar size, as reported by Gersh, Smith and Samuelson in [32], showed that the equivalent resistance (for five equal resistances between adjacent rotor bars) was approximately 3 mΩ, an order of magnitude worse than that which should be achieved. In conclusion, if the benefits associated with using a BDFM are to be realised, special precautions must be taken to insulate the rotor bars from the rotor iron.

5.2 Future Work

From the author's experience in the BDFM, the following topics need further attention if the BDFM is to become a commercial product: design, saturation, starting, rotor manufacture, capability curves, dynamic response and generator operation. Each of these items is addressed in the following paragraphs.

5.2.1 Design

There are three good models to facilitate the design of the steady state performance of the BDFM: the *dq* model and inter-bar current models presented here and the harmonic model in [23]. Although all are accurate and capable, none have been used to design a special purpose BDFM that has been built and tested.

Research to date has always carried the caveat that the machine studied is "sub-optimal." In order to demonstrate the viability of the BDFM as a marketable item, an optimally designed BDFM should be constructed and tested, thus demonstrating the benefits of low converter rating, high speed range capability, and power factor control. Of course, each of these interrelated aims may be mutually exclusive, therefore some sort of balance must be sought. Indeed, the concept of an *optimum design* must be defined based on the perceived application of the machine.

As for the choice of models, the author recommends using the model presented by Ferreira et al. for design purposes, which was briefly described in [23] and fully described in [31]. The inter-bar current model should be reserved for studies of rotor anomalies since the results presented here compel a manufacturer to ensure the rotor bars are insulated if acceptable performance is to be achieved. If dynamic studies are conducted, the *dq* model should be used, making use of the impedance formulae given in [31].

5.2.2 Saturation

Saturation is a problem that has plagued the experimental motors developed both at the University of Cambridge and at Oregon State University. As was found through the development effort, two three-phase windings on the same stator cause

problems in the design of the motor magnetics. The design programs developed thus far have not adequately addressed the effects of saturation and the demands on the stator iron.

To predict the effects of saturation, Ferreira developed a two-dimensional finite element model in his Ph.D. thesis [31]. Although successful, the solutions were computationally intensive, requiring several days to extract a single data point. For design purposes, the computational time needs to be shortened.

One possible method of modelling saturation is to use saturation factors, as is done in conventional induction machine analysis. This, although seemingly straightforward, is actually complicated by the fact that the two stator windings are of different pole numbers. This will require modifications to the published methods of calculation of saturation factors. This author recommends more research be performed in the development of these factors.

5.2.3 Starting

Very little research has been conducted to determine acceptable methods of starting the BDFM. One possible method is to start the BDFM synchronously from standstill and gradually increase the frequency of the control-winding voltages in order to raise the speed of the motor. The drawback to using this method is that the converter rating may become larger than necessary, i.e. more expensive, making the drive commercially less attractive. Another method is to start the BDFM as an induction machine with only the power winding excited. As the machine approaches the lower limit of the speed range, the second winding is engaged so as to synchronise the BDFM on-the-fly. The research group at Oregon State University uses this technique with some success [33]. However, more research is needed on this topic in order to prescribe a method that can be shown to work in all situations.

5.2.4 Rotor Manufacture

As was shown in this dissertation, the rotor bars must be insulated from the rotor iron in order to achieve satisfactory performance. One way to ensure this is to fabricate the rotor, taking care to insulate the rotor bars. This is time consuming

and expensive, suitable only to low levels of machine production. If the BDFM is to be produced in larger quantities, a method needs to be devised to insulate the bars of the die-cast rotor from the rotor iron.

This problem is currently being tackled by the power engineering group at Oregon State University, headed by Professor Alan Wallace. Professor Wallace suggests that the die-casting process can be modified so as to provide a higher level of insulation, greater than the threshold amount, by applying a coating to the rotor iron prior to pouring the molten aluminium alloy into the rotor. Preliminary tests show this to be possible. If true then the technique developed will be applicable for all types of die-cast rotors. The details of their results have yet to be published, although it appears that they may be presented during the October 1997 meeting of the IEEE Industry Applications Society Annual Meeting to be held in New Orleans, Louisiana.

5.2.5 Capability Curves

The limits of torque capability were plotted with respect to the speed of the machine. This graph, a form of capability curve, is very useful in the specification of the BDFM for particular applications. The curves enable the suitability of the BDFM for a particular application to be quickly determined. Although the curve presented in this dissertation shows the absolute maximum values of torque production, the limits can be decreased in order to show the achievable limits when considering stability of the motor—the ability of the motor to maintain synchronism. Further research needs to be conducted to determine what are the suitable stability limits.

5.2.6 Dynamic Response

Currently, the only simplified model capable of predicting dynamic performance is the *dq* model. It would be useful if the harmonic model could be refined to allow it to be used in dynamic analysis, which would offer an improvement in accuracy.

5.2.7 Generator Operation

The BDFM has been proposed as a wind generator as well as an automotive alternator. The author has also performed some preliminary studies of the BDFM for use as a generator in airplanes. The BDFM appears attractive in this role because of its power factor control and reduced rating converter. Although analysed as a stand-alone piece of equipment, it is yet to be determined how the BDFM will perform as part of a larger power system.

Appendix A

Conductor Density Function

The conductor density function is a very powerful concept which facilitates the calculation of machine inductances. It has been presented by Williamson et al. in [23, 25]. However, since it is crucial to the development of the inter-bar current model, it is presented here for the sake of completeness. It's abilities are demonstrated here where it is used to develop a mathematical description of a balanced three-phase stator winding.

A.1 Single Coil

An electric machine is composed of a series of coils set into slots. A coil of T turns carries current down one coil side and back through the other coil side. Harmonic analysis is used to describe this coil as a complex Fourier series.

The coil description is the conductor density function. Since the machine is round, the conductor density is periodic, a necessity for using a Fourier series description. The conductors are assumed to be evenly distributed across the mouth of a slot of width b.

The conductor density function is a vector function and points in the direction of assumed positive current flow. Positive current flow is represented by positive turns per metre (density), T/b. Negative current flow is signified by a negative density. Figure A.1 shows a coil of T turns, with span α, placed in the stator slots along with the associated density function ($f(y)$). The coil is centred at a

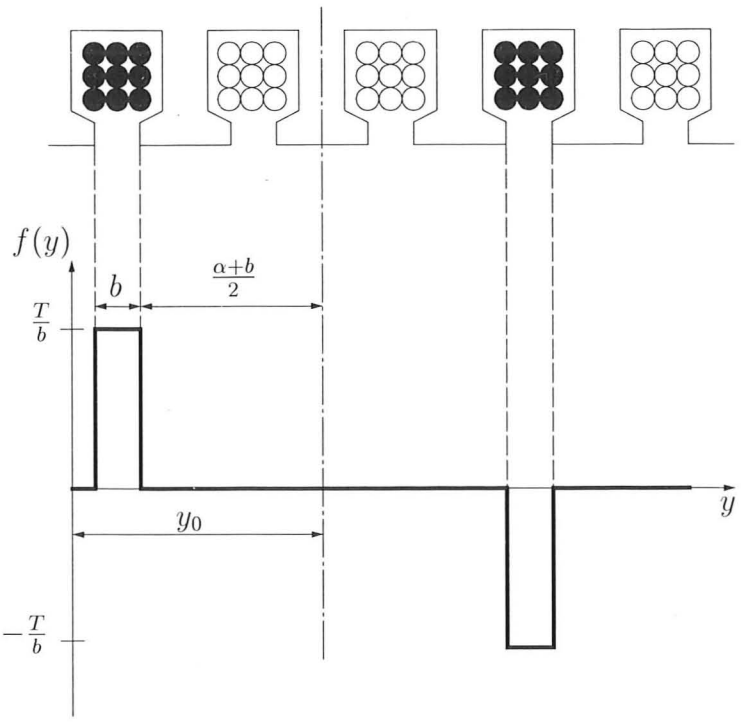

Figure A.1: Diagram of the conductor density function for a coil.

position y_0 from the origin, measured circumferentially. The coil density function is represented by the complex Fourier series

$$\vec{c}(y) = \sum_{\kappa=-\infty}^{\infty} \bar{C}^{\kappa} e^{-jky}\, \hat{a}_x \tag{A.1}$$

where it is assumed that the coil is directed along the x-axis, signified by the unit direction vector, $\hat{a}_x$. κ is the harmonic number and takes on integer values.

Circumferential distance, y, is converted to an angle through use of the wave number, k. The wave number accounts for periodicity in the fields and is defined

$$k = \frac{2\kappa}{d} \tag{A.2}$$

The value of $\bar{C}^{\kappa}$, the Fourier coefficient, is given as

$$\bar{C}^{\kappa} = \frac{1}{\pi d} \int_0^{\pi d} f(y) e^{jky}\, dy \tag{A.3}$$

where the values of $f(y)$ can be extracted from Fig. A.1:

$$f(y) = \begin{cases} \frac{T}{b} & y_0 - \frac{\alpha}{2} - \frac{b}{2} \leq y \leq y_0 - \frac{\alpha}{2} + \frac{b}{2}, \\ -\frac{T}{b} & y_0 + \frac{\alpha}{2} - \frac{b}{2} \leq y \leq y_0 + \frac{\alpha}{2} + \frac{b}{2}. \end{cases} \tag{A.4}$$

Integrating (A.3) with the limits and function values given in (A.4) yields

$$\bar{C}^{\kappa} = -j\frac{2T}{\pi d} K_b^{\kappa} K_p^{\kappa} e^{jky_0} \tag{A.5}$$

K_b^{κ} is termed the slot width factor and K_p^{κ} is the coil pitch factor as defined in (A.6) and (A.7), respectively. The slot width factor accounts for the distribution of the conductors across the slot mouth. If the coil sides are considered point conductors ($b = 0$) the slot width factor (taking the limit and using L'Hospital's Rule) becomes unity.

$$K_b^{\kappa} = \frac{\sin\left(\frac{kb}{2}\right)}{\left(\frac{kb}{2}\right)} \tag{A.6}$$

$$K_p^{\kappa} = \sin\left(\frac{k\alpha}{2}\right) \tag{A.7}$$

At this point, there is no constraint on the harmonics used in the summation. However, it should be noted that $\vec{c}(y) = 0$ for $\kappa = 0$.

A.2 Coil Group

In a phase winding, the coils are arranged in groups of coils, called a coil group. For a three-phase stator winding of P pole-pairs, there are $\frac{N_s}{6P}$ coils per coil group, where N_s is the number of stator slots. In a double layer winding, each coil group is separated by $\frac{\pi d}{2P}$, where d is the diameter to the air-gap. Figure A.2 shows two poles of a double layer winding with the coils that comprise one coil group (three coils) highlighted. Direction of the coils is indicated and the associated conductor density shown.

The conductor density can be determined by summing the individual coil density functions. Let the centre of the n-th coil in the coil group, y_n, be

$$y_n = y_0 + (n-1)\frac{\pi d}{N_s} \tag{A.8}$$

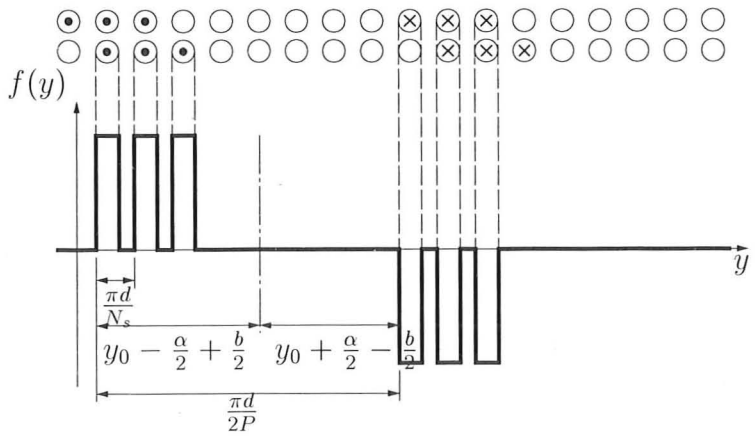

Figure A.2: Conductor density function for a coil group with appropriate dimensions marked (only two poles are shown).

Summing the coil group densities results in the coil group density, $\vec{c}_{cg}(y)$, where

$$\vec{c}_{cg}(y) = \sum_{n=1}^{\frac{N_s}{6P}} \sum_{\kappa=-\infty}^{\infty} \bar{C}^{\kappa} e^{jky_{0n}} e^{-jky} \hat{a}_x \tag{A.9}$$

The first summation in (A.9) concerns only on the exponential in y_n; the remaining terms in the equation do not depend on n. A geometric progression, shown in (A.10) for a general variable x, exists for the exponential in y_{0n}.

$$\begin{aligned} \sum_{n=1}^{N} x^{n-1} &= 1 + x + x^2 + \cdots + x^{N-1} \\ &= \frac{1 - x^N}{1 - x} \end{aligned} \tag{A.10}$$

Using (A.10), and simplifying the exponential term yields

$$\begin{aligned}
\sum_{n=1}^{\frac{N_s}{6P}} e^{jky_n} &= \sum_{n=1}^{\frac{N_s}{6P}} e^{jky_0} e^{jk\frac{\pi d}{N_s}(n-1)} \\
&= e^{jky_0}\left(\frac{1-e^{j\frac{k\pi d}{6P}}}{1-e^{j\frac{k\pi d}{N_s}}}\right) \\
&= e^{jky_0}\left(\frac{1-e^{j\frac{2\pi\kappa}{6P}}}{1-e^{j\frac{2\pi\kappa}{N_s}}}\right) \\
&= e^{jky_0}\left(\frac{e^{j\frac{\pi\kappa}{6P}}\left(e^{-j\frac{\pi\kappa}{6P}}-e^{j\frac{\pi\kappa}{6P}}\right)}{e^{j\frac{\pi\kappa}{N_s}}\left(e^{-j\frac{\pi\kappa}{N_s}}-e^{j\frac{\pi\kappa}{N_s}}\right)}\right) \\
&= e^{jky_0}\left(e^{j\left(\frac{\pi\kappa}{6P}-\frac{\pi\kappa}{N_s}\right)}\frac{\sin\left(\frac{\pi\kappa}{6P}\right)}{\sin\left(\frac{\pi\kappa}{N_s}\right)}\right)
\end{aligned} \tag{A.11}$$

where the algebraic steps taken in the simplification are shown for clarity.

Substituting (A.11) into (A.9) yields the simplified form of the coil group conductor density function,

$$\vec{c}_{cg}(y) = \sum_{\kappa=-\infty}^{\infty} \bar{C}^{\kappa} e^{-jky}\hat{a}_x \tag{A.12}$$

where $\bar{C}^{\kappa}$ is re-defined as

$$\bar{C}^{\kappa} = -j\frac{2TN_s}{6\pi dP}K_{bs}^{\kappa}K_p^{\kappa}K_d^{\kappa}e^{j\left(\frac{\pi\kappa}{6P}-\frac{\pi\kappa}{N_s}\right)}e^{jky_0} \tag{A.13}$$

which makes use of the harmonic distribution factor, K_d^{κ}, such that

$$K_d^{\kappa} = \frac{\sin\left(\frac{\pi\kappa}{6P}\right)}{\frac{N_s}{6P}\sin\left(\frac{\pi\kappa}{N_s}\right)} \tag{A.14}$$

The next stage in the process of describing the stator winding, is to assemble the coil groups to form a phase winding.

A.3 Phase Winding

A phase winding is composed of coil groups. For a double layer winding, such as that shown in Fig. A.2, the P coil groups are separated by $\frac{\pi d}{2P}$, each group with

a different polarity. Coil groups of the same polarity are separated by $\frac{\pi d}{P}$. The conductor density for a phase winding, $\vec{c}_{ph}(y)$, is found by summing the density functions for the appropriate coil groups:

$$\begin{aligned}\vec{c}_{ph}(y) &= \vec{c}_{cg}(y)\left(1 - e^{jk\frac{\pi d}{2P}} + e^{jk2\frac{\pi d}{2P}} - e^{jk3\frac{\pi d}{2P}} \cdots - e^{j(2P-1)k\frac{\pi d}{2P}}\right) \\ &= \vec{c}_{cg}(y)\left(1 - e^{jk\frac{\pi d}{2P}}\right)\sum_{n=1}^{P} e^{j(n-1)k\frac{\pi d}{P}} \\ &= \vec{c}_{cg}(y)\left(1 - e^{jk\frac{\pi d}{2P}}\right)\frac{1 - e^{2\pi\kappa}}{1 - e^{j2\kappa\pi/P}}\end{aligned} \tag{A.15}$$

The last term in (A.15) is zero unless $\kappa = qP$, where q is any integer. With this constraint on κ,

$$\begin{aligned}\vec{c}_{ph}(y) &= \vec{c}_{cg}(y)\left(1 - e^{jk\frac{\pi d}{2P}}\right)P \\ &= \vec{c}_{cg}(y)P\left(-j2\sin(\frac{q\pi}{2})e^{j\frac{q\pi}{2}}\right)\end{aligned} \tag{A.16}$$

Further simplifications are achieved by considering the value of the parenthesised function when q takes on different values, shown in Table A.1. The table shows that only odd harmonics are present and result in a value of two; even harmonics result in a value of zero. Therefore, κ can be constrained

$$\kappa = (2q + 1)\,P \tag{A.17}$$

Using the results from Table A.1 and recognising that the number of turns per phase, $N_{ph} = \frac{TN_s}{3}$, (A.13) can now be defined as

$$\bar{C}^{\kappa} = -j\frac{2N_{ph}}{\pi d}K_b^{\kappa}K_p^{\kappa}K_d^{\kappa}e^{j\left(\frac{\pi\kappa}{6P} - \frac{\pi\kappa}{N_s}\right)}e^{jky_0} \tag{A.18}$$

such that

$$\vec{c}_{ph}(y) = \sum_{\kappa=-\infty}^{\infty} \bar{C}^{\kappa}e^{-jky}\hat{a}_x \tag{A.19}$$

If the winding is single layer, the coil groups are spaced $\frac{\pi d}{P}$ apart and are of the same polarity. The resulting equation has the same form. However, the correct number of turns per phase for a single layer winding is used: $N_{ph} = \frac{TN_s}{6}$.

Table A.1: Simplification of $\vec{c}_{ph}(y)$ in (A.16) based on q.

q	$-j2\sin(\frac{q\pi}{2})e^{j\frac{q\pi}{2}}$
-3	$(-j2)(1)(j) = 2$
-2	$(-j2)(0)(-1) = 0$
-1	$(-j2)(-1)(-j) = 2$
$+0$	$(-j2)(0)(1) = 0$
$+1$	$(-j2)(1)(j) = 2$
$+2$	$(-j2)(0)(j) = 0$
$+3$	$(-j2)(-1)(-j) = 2$

Equation (A.18) gives the expression for a single phase of a three-phase winding. Let this be the A-phase so that

$$\vec{c}_A(y) = \vec{c}_{ph}(y) \tag{A.20}$$

For a three-phase winding, the other two phases are displaced $\frac{2\pi d}{6P}$ from each other. Therefore,

$$\vec{c}_B(y) = \vec{c}_A(y)e^{jk\frac{2\pi d}{6P}} \tag{A.21}$$

$$\vec{c}_C(y) = \vec{c}_A(y)e^{-jk\frac{2\pi d}{6P}} \tag{A.22}$$

Equations (A.20)–(A.22) define the stator windings by a complex Fourier series where only odd space harmonics are present. This type of definition of the windings is the basis for harmonic analysis. Even though the technique was applied to a three-phase winding, any winding configuration could be accommodated by appropriate combinations of the coil density functions.

Appendix B

Torque Calculation

The electromagnetic torque produced by the BDFM under the influence of inter-bar currents which flow between adjacent rotor bars will be shown to be the sum of four components, two due to direct coupling of the rotor currents with the stator windings and two due to cross coupling of the rotor currents with the stator windings. The expressions for torque due to these components is derived from the expression for the force exerted by the stator winding fields on an individual rotor current-loop. It is assumed that only those rotor current-loops that couple with the main air-gap flux contribute to the torque produced by the machine.

B.1 General Expression

Consider a representative rotor current-loop, the n-th, as depicted in Fig. B.1, subjected to a stator flux density, $\vec{b}_s(y', t)$, with a rotor current $i_{R_n}(t)$ flowing in the rotor loop. Interaction of the rotor current and rotor flux density will not produce torque, therefore only the stator flux density is considered.

The reference rotor loop has a width σ_n in the circumferential direction and an associated depth w' in the axial direction. The coordinate system used is described earlier in section 3.1.2. Briefly, the (x', y') coordinates form the standard rotor reference frame (RRF) coordinate system while (x'', y'') form the skewed RRF, skewed a positive angle γ from the standard RRF. The unit direction vector $\hat{a}_{x''}$ is aligned with the rotor bars. The distributed inter-bar resistance is modelled

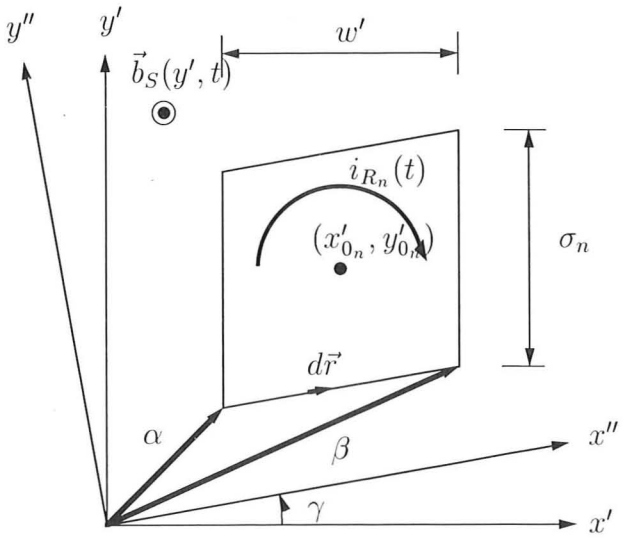

Figure B.1: Reference rotor loop used in the derivation of the torque equation.

by lumped resistance place between adjacent rotor bars along "cuts" made across the rotor bars in the $\hat{a}_{y'}$ direction.

The force on an elemental rotor bar segment, $d\vec{r}$, assuming the rotor bar to be a filament, is given by (B.1) [34] where the negative sign accounts for the current flowing against the direction vector.

$$d\vec{f} = -i_{R_n}(t)\, d\vec{r} \times \vec{b}(y', t) \tag{B.1}$$

The total force on the bar segment will be the line integral of (B.1) from the start of the bar to the end of the bar. Because the variables are vector quantities, they must must be in consistent coordinate systems. This is best achieved by parameterising both $d\vec{r}$ and $b_s(y', t)$. In general form, an equation for a line segment can be written as

$$\vec{r} = \vec{\alpha} + s(\vec{\beta} - \vec{\alpha}) \tag{B.2}$$

where $\vec{\alpha}$ is a vector to the start of the bar, $\vec{\beta}$ is a vector to the end of the bar, and

s is a scalar such that $0 \leq s \leq 1$. $\vec{\alpha}$ can be expressed as

$$\begin{aligned}\vec{\alpha} &= x'_{0n}\,\hat{a}'_x + y'_{0n}\,\hat{a}'_y + \left(-\frac{w'}{2}\,\hat{a}'_x + \left(-\frac{\sigma_n}{2} - \frac{w'}{2}\tan(\gamma)\right)\hat{a}'_y\right) \\ &= \left(x'_{0n} - \frac{w'}{2}\right)\hat{a}'_x + \left(y'_{0n} - \frac{\sigma_n}{2} - \frac{w'}{2}\tan(\gamma)\right)\hat{a}'_y\end{aligned}$$

and $\vec{\beta}$ as

$$\begin{aligned}\vec{\beta} &= x'_{0n}\,\hat{a}'_x + y'_{0n}\,\hat{a}'_y + \left(\frac{w'}{2}\,\hat{a}'_x + \left(-\frac{\sigma_n}{2} + \frac{w'}{2}\tan(\gamma)\right)\hat{a}'_y\right) \\ &= \left(x'_{0n} + \frac{w'}{2}\right)\hat{a}'_x + \left(y'_{0n} - \frac{\sigma_n}{2} + \frac{w'}{2}\tan(\gamma)\right)\hat{a}'_y\end{aligned}$$

The difference of the two is given as

$$\left(\vec{\beta} - \vec{\alpha}\right) = w'\,\hat{a}'_x + w'\tan(\gamma)\,\hat{a}'_y \tag{B.3}$$

The parameterised vector describing the lower bar segment is

$$\vec{r}\,(s) = \left(x'_{0n} - \frac{w'}{2} + sw'\right)\hat{a}_{x'} + \left(y'_{0n} - \frac{\sigma_n}{2} - \frac{w'}{2}\tan(\gamma) + sw'\tan(\gamma)\right)\hat{a}'_y \tag{B.4}$$

Differentiating with respect to s yields an expression for $d\vec{r}(s)$,

$$d\vec{r}\,(s) = w'\,ds\,\hat{a}'_x + w'\tan(\gamma)\,ds\,\hat{a}'_y \tag{B.5}$$

The stator flux density consists of two components, one due to the first winding, $\vec{b}_1(y',t)$, and the other due to the second winding, $\vec{b}_2(y',t)$. Transforming (3.31) into the RRF and substituting for winding specific variables,

$$\vec{b}_1(y',t) = \Re\left\{\sum_{\kappa}\sqrt{2}\bar{B}_1^{\kappa}e^{j\left(\omega'_1 t - ky'\right)}\right\}\hat{a}_z \tag{B.6}$$

and similarly for the second winding,

$$\vec{b}_2(y',t) = \Re\left\{\sum_{\lambda}\sqrt{2}\bar{B}_2^{\lambda}e^{j\left(\omega'_2 t - ly\right)}\right\}\hat{a}_z \tag{B.7}$$

Parameterise by substituting

$$\begin{aligned}y' &= \vec{r}\,(s)\cdot\hat{a}_{y'} \\ &= y'_{0n} - \frac{\sigma_n}{2} - \frac{w'}{2}\tan(\gamma) + sw'\tan(\gamma)\end{aligned}$$

into (B.6) and (B.7) to yield

$$\vec{b}_1(s,t) = \Re\left\{\sum_{\kappa} \sqrt{2}\bar{B}_1^{\kappa} e^{j\omega_1' t} e^{-jk\left(y'_{0n} - \frac{\sigma_n}{2} - \frac{w'}{2}\tan\gamma\right)} e^{-jksw'\tan(\gamma)}\right\}\hat{a}_z \tag{B.8}$$

$$\vec{b}_2(s,t) = \Re\left\{\sum_{\lambda} \sqrt{2}\bar{B}_2^{\lambda} e^{j\omega_2' t} e^{-jl\left(y'_{0n} - \frac{\sigma_n}{2} - \frac{w'}{2}\tan\gamma\right)} e^{-jlsw'\tan(\gamma)}\right\}\hat{a}_z \tag{B.9}$$

Substitute (B.5) into (B.1), which parameterises this equation, to obtain

$$\begin{aligned} d\vec{f} &= -i_{R_n}(t)\, d\vec{r}(s) \times \vec{b}(s,t) \\ &= -i_{R_n}(t)\left(w'\tan(\gamma) b(s,t)\, ds\, \hat{a}_{x'} - w' b(s,t)\, ds\, \hat{a}_{y'}\right) \end{aligned} \tag{B.10}$$

where $b(s,t) = b_1(s,t) + b_2(s,t)$.

As evidenced by (B.10), there are two components of force, one in the longitudinal direction, $\hat{a}_{x'}$, and one in the tangential direction, $\hat{a}_{y'}$. Only the tangential force, which produces useful torque, will be considered. The force on the first bar is computed by integrating (B.10) with respect to s,

$$f_1 = \int_0^1 \left(i_{R_n(p)}(t) + i_{R_n(c)}(t)\right)\left(b_1(s,t) + b_2(s,t)\right) w' ds \tag{B.11}$$

where, similar to the stator flux density, a substitution for the two components of rotor current, $i_{R_n}(t) = i_{R_n 1}(t) + i_{R_n 2}(t)$, has been made. This calculation will result in the integration of four current-flux density products,

$$\begin{aligned} f_1 = &\int_0^1 w' i_{R_n 1}(t) b_1(s)\, ds + \int_0^1 w' i_{R_n 2}(t) b_1(s)\, ds \\ &+ \int_0^1 w' i_{R_n 1}(t) b_2(s)\, ds + \int_0^1 w' i_{R_n 2}(t) b_2(s)\, ds \end{aligned} \tag{B.12}$$

Each involves the integration of the common term,

$$\begin{aligned} \int_0^1 e^{-jksw'\tan(\gamma)} ds &= \frac{j}{w'k\tan(\gamma)}\left[e^{-jksw'\tan(\gamma)}\right]_0^1 \\ &= \frac{j}{w'k\tan(\gamma)}\left(e^{-jkw'\tan(\gamma)} - 1\right) \\ &= \frac{j}{w'k\tan(\gamma)} e^{-jk\frac{w'}{2}\tan(\gamma)}\left(e^{-jk\frac{w'}{2}\tan(\gamma)} - e^{jk\frac{w'}{2}\tan(\gamma)}\right) \\ &= \frac{j e^{-jk\frac{w'}{2}\tan(\gamma)}}{kw'\tan(\gamma)}\left(-2j\sin\left(k\frac{w'}{2}\tan(\gamma)\right)\right) \\ &= e^{-jk\frac{w'}{2}\tan(\gamma)} K_{sk}^{\kappa} \end{aligned} \tag{B.13}$$

which introduces the harmonic skew factor as defined in (3.58). Substituting (B.8) and (B.9) into (B.12) and performing the integration yields

$$
\begin{aligned}
f_1 = w' i_{R_n 1}(t) \Re \left\{ \sum_{\kappa} \sqrt{2} \bar{B}_1^{\kappa} e^{-jky'_{0n}} e^{jk\frac{\sigma_n}{2}} K_{sk}^{\kappa} e^{j\omega'_1 t} \right\} \\
+ w' i_{R_n 2}(t) \Re \left\{ \sum_{\kappa} \sqrt{2} \bar{B}_1^{\kappa} e^{-jky'_{0n}} e^{jk\frac{\sigma_n}{2}} K_{sk}^{\kappa} e^{j\omega'_1 t} \right\} \\
+ w' i_{R_n 1}(t) \Re \left\{ \sum_{\lambda} \sqrt{2} \bar{B}_2^{\lambda} e^{-jly'_{0n}} e^{jl\frac{\sigma_n}{2}} K_{sk}^{\lambda} e^{j\omega'_2 t} \right\} \\
+ w' i_{R_n 2}(t) \Re \left\{ \sum_{\lambda} \sqrt{2} \bar{B}_2^{\lambda} e^{-jly'_{0n}} e^{jl\frac{\sigma_n}{2}} K_{sk}^{\lambda} e^{j\omega'_2 t} \right\}
\end{aligned} \tag{B.14}
$$

At this stage, consider the elemental force on the second rotor bar,

$$
d\vec{f}_2 = i_{R_n}(t)\, d\vec{r}_2 \times \vec{b}(y', t) \tag{B.15}
$$

where $d\vec{r}_2$ is the elemental position vector of the second bar segment. The position vector for the second bar is obtained from that of the first bar,

$$
\vec{r}_2(s) = \vec{r}\,(s) + \sigma_n\, \hat{a}_{y'} \tag{B.16}
$$

The flux density seen by the second bar is a phase shifted version of the original flux density

$$
\vec{b}(s_2) = \vec{b}(s) e^{-jk\sigma_n} \tag{B.17}
$$

After considerable simplification and combination with (B.14), the tangential force on the n-th rotor loop can be expressed as the sum of four components

$$
f_n = f_{11} + f_{12} + f_{21} + f_{22} \tag{B.18}
$$

where the subscripts denote force contributions due to direct-coupled rotor currents ((f_{11} and f_{22}) and cross coupled rotor currents (f_{12} and f_{21}). The force

components are given as

$$f_{11} = w' i_{R_n 1}(t) \Re \left\{ \sum_{\kappa} \sqrt{2}(2j) e^{-jky'_{0n}} K^{\kappa}_{pR_n} K^{\kappa}_{sk} \bar{B}^{\kappa}_1 e^{j\omega'_1 t} \right\} \tag{B.19}$$

$$f_{12} = w' i_{R_n 2}(t) \Re \left\{ \sum_{\kappa} \sqrt{2}(2j) e^{-jky'_{0n}} K^{\kappa}_{pR_n} K^{\kappa}_{sk} \bar{B}^{\kappa}_1 e^{j\omega'_1 t} \right\} \tag{B.20}$$

$$f_{21} = w' i_{R_n 1}(t) \Re \left\{ \sum_{\lambda} \sqrt{2}(2j) e^{-jly'_{0n}} K^{\lambda}_{pR_n} K^{\lambda}_{sk} \bar{B}^{\lambda}_2 e^{j\omega'_2 t} \right\} \tag{B.21}$$

$$f_{22} = w' i_{R_n 2}(t) \Re \left\{ \sum_{\lambda} \sqrt{2}(2j) e^{-jly'_{0n}} K^{\lambda}_{pR_n} K^{\lambda}_{sk} \bar{B}^{\lambda}_2 e^{j\omega'_2 t} \right\} \tag{B.22}$$

where the calculation introduces the harmonic pitch factors of the rotor loops ($K^{\kappa}_{pR_n}$ and $K^{\lambda}_{pR_n}$), as defined in (3.20), along with the factor $(2j)$.

The next step in the analysis is to substitute expressions for the rotor currents into (B.19)–(B.22). In order to simplify the equations and place the quantities under the influence of a single real operator, the identity

$$\Re\left\{\bar{I}\right\} \Re\left\{\bar{B}\right\} = \frac{1}{2}\left(\Re\left\{\bar{I}\bar{B}\right\} + \Re\left\{\bar{I}\bar{B}^*\right\}\right) \tag{B.23}$$

will be used which has the effect of doubling the number of terms in the force equation from four to eight. For bookkeeping sake, the two additional terms will be denoted by subscripts a and b. Performing the substitutions and simplifying gives

$$f_{11a} = \frac{1}{2} w' \Re \left\{ \left(\sum_{\kappa'} \sqrt{2} \bar{I}^{\kappa'}_{R_n 1} \, e^{j(\omega_1 - \kappa' \omega_R)t} \right) \left(\sum_{\kappa} \sqrt{2}(2j) K^{\kappa}_{pR_n} K^{\kappa}_{sk} e^{-jky'_{0n}} \bar{B}^{\kappa}_1 e^{j(\omega_1 - \kappa\omega_R)t} \right) \right\} \tag{B.24}$$

$$f_{11b} = \frac{1}{2} w' \Re \left\{ \left(\sum_{\kappa'} \sqrt{2} \bar{I}^{\kappa'}_{R_n 1} e^{j(\omega_1 - \kappa' \omega_R)t} \right) \left(\sum_{\kappa} \sqrt{2}(-2j) K^{\kappa}_{pR_n} K^{\kappa}_{sk} e^{jky'_{0n}} \bar{B}^{\kappa *}_1 e^{-j(\omega_1 - \kappa\omega_R)t} \right) \right\} \tag{B.25}$$

$$f_{12a} = \frac{1}{2} w' \Re \left\{ \left(\sum_{\lambda'} \sqrt{2} \bar{I}_{R_n 2}^{\lambda'} e^{j(\omega_2 - \lambda' \omega_R)t} \right) \left(\sum_{\kappa} \sqrt{2}(2j) K_{pR_n}^{\kappa} K_{sk}^{\kappa} e^{-jky'_{0n}} \bar{B}_1^{\kappa} e^{j(\omega_1 - \kappa\omega_R)t} \right) \right\} \quad \text{(B.26)}$$

$$f_{12b} = \frac{1}{2} w' \Re \left\{ \left(\sum_{\lambda'} \sqrt{2} \bar{I}_{R_n 2}^{\lambda'} e^{j(\omega_2 - \lambda' \omega_R)t} \right) \left(\sum_{\kappa} \sqrt{2}(-2j) K_{pR_n}^{\kappa} K_{sk}^{\kappa} e^{jky'_{0n}} \bar{B}_1^{\kappa *} e^{-j(\omega_1 - \kappa\omega_R)t} \right) \right\} \quad \text{(B.27)}$$

$$f_{21a} = \frac{1}{2} w' \Re \left\{ \left(\sum_{\kappa'} \sqrt{2} \bar{I}_{R_n 1}^{\kappa'} e^{j(\omega_1 - \kappa' \omega_R)t} \right) \left(\sum_{\lambda} \sqrt{2}(2j) K_{pR_n}^{\lambda} K_{sk}^{\lambda} e^{-jly'_{0n}} \bar{B}_2^{\lambda} e^{j(\omega_2 - \lambda\omega_R)t} \right) \right\} \quad \text{(B.28)}$$

$$f_{21b} = \frac{1}{2} w' \Re \left\{ \left(\sum_{\kappa'} \sqrt{2} \bar{I}_{R_n 1}^{\kappa'} e^{j(\omega_1 - \kappa' \omega_R)t} \right) \left(\sum_{\lambda} \sqrt{2}(-2j) K_{pR_n}^{\lambda} K_{sk}^{\lambda} e^{jly'_{0n}} \bar{B}_2^{\lambda *} e^{-j(\omega_2 - \lambda\omega_R)t} \right) \right\} \quad \text{(B.29)}$$

$$f_{22a} = \frac{1}{2} w' \Re \left\{ \left(\sum_{\lambda'} \sqrt{2} \bar{I}_{R_n 2}^{\lambda'} e^{j(\omega_2 - \lambda' \omega_R)t} \right) \left(\sum_{\lambda} \sqrt{2}(-2j) K_{pR_n}^{\lambda} K_{sk}^{\lambda} e^{-jly'_{0n}} \bar{B}_2^{\lambda} e^{j(\omega_2 - \lambda\omega_R)t} \right) \right\} \quad \text{(B.30)}$$

$$f_{22b} = \frac{1}{2} w' \Re \left\{ \left(\sum_{\lambda'} \sqrt{2} \bar{I}_{R_n 2}^{\lambda'} e^{j(\omega_2 - \lambda' \omega_R)t} \right) \left(\sum_{\lambda} \sqrt{2}(-2j) K_{pR_n}^{\lambda} K_{sk}^{\lambda} e^{jly'_{0n}} \bar{B}_2^{\lambda *} e^{-j(\omega_2 - \lambda\omega_R)t} \right) \right\} \quad \text{(B.31)}$$

where the frequency of the different elements has been expanded and the the harmonic subscripts κ' and λ' are used in the expressions for the rotor currents instead of the original un-primed quantities.

The primed quantities are used to differentiate between the two different stator produced harmonics. The harmonics are determined from (3.28), where the appropriate substitution for q is made.

The torque on the rotor loop is calculated by multiplication of the force equations by the radius of the machine, $\frac{d}{2}$,

$$T = \frac{d}{2}\left(f_{11a} + f_{11b} + f_{12a} + f_{12b} + f_{21a} + f_{21b} + f_{22a} + f_{22b}\right) \tag{B.32}$$

Inspection of the subscripts shows that there are four components due to direct coupling and four due to cross coupling.

B.2 Direct Coupling

The force components due to direct coupling of the rotor currents are those given in (B.24), (B.25), (B.30) and (B.31). Of the four terms, not all terms will produce steady-state torque at all speeds of operation. In order to determine which terms produce steady-state torque, the frequencies of the current and flux density are inspected in each term of the product in order to determine which contribute to steady-state torque.

Consider the first force component, (B.24). Add the two frequencies (a result of the multiplication on a term by term basis) and set to zero,

$$(\omega_1 - \kappa'\omega_R) + (\omega_1 - \kappa\omega_R) = 0 \tag{B.33}$$

Substituting $\kappa' = (6q' + 1)\kappa_1$ and $\kappa = (6q + 1)\kappa_1$, it is seen that a steady-state torque will be produced only when

$$\omega_R = \frac{\omega_1/\kappa_1}{3(q' + q) + 1} \tag{B.34}$$

At the different speeds dictated by the values of q and q', the torque produced is that normally associated with the synchronous cusps of torque in an induction machine. Nevertheless, the effect of these torques will be ignored. This means that

neither (B.24) nor (B.30) (by similar analysis) will produce any useful torque—only pulsating torque.

However, by inspection, both (B.25) and (B.31) will produce steady-state torque when $\kappa' = \kappa$, other harmonics producing pulsating torque. Applying this constraint and using the radius of the machine,

$$T_{11} = \frac{d}{2} w' \Re \left\{ \sum_{\kappa} -2j \bar{I}^{\kappa}_{R_n 1} K^{\kappa}_{pR_n} K^{\kappa}_{sk} e^{jky_{0n}} \bar{B}^{\kappa *}_{1} \right\} \tag{B.35}$$

$$T_{22} = \frac{d}{2} w' \Re \left\{ \sum_{\lambda} -2j \bar{I}^{\lambda}_{R_n 2} K^{\lambda}_{pR_n} K^{\lambda}_{sk} e^{jly_{0n}} \bar{B}^{\lambda *}_{2} \right\} \tag{B.36}$$

Further simplification is achieved by substituting for the values of the stator flux density coefficients, $\bar{B}^{\kappa}_{1}$ and $\bar{B}^{\lambda}_{2}$, which by using (3.32) are given as

$$\bar{B}^{\kappa}_{1} = j \frac{3\mu_0}{gk} \bar{C}^{\kappa}_{1} \bar{I}_1 \tag{B.37}$$

$$\bar{B}^{\lambda}_{2} = j \frac{3\mu_0}{gl} \bar{C}^{\lambda}_{1} \bar{I}_2 \tag{B.38}$$

Conjugating and substituting into (B.35) and (B.36) yields

$$T_{11} = -dw' \Re \left\{ \sum_{\kappa} \frac{3\mu_0}{gk} K^{\kappa}_{pR_n} K^{\kappa}_{sk} e^{jky_{0n}} \bar{C}^{\kappa *}_{1} \bar{I}^{\kappa}_{R_n 1} \bar{I}^{*}_{1} \right\} \tag{B.39}$$

$$T_{22} = -dw' \Re \left\{ \sum_{\lambda} \frac{3\mu_0}{gl} K^{\lambda}_{pR_n} K^{\lambda}_{sk} e^{jly_{0n}} \bar{C}^{\lambda *}_{2} \bar{I}^{\lambda}_{R_n 2} \bar{I}^{*}_{2} \right\} \tag{B.40}$$

It should be noted that either expression, (B.39) or (B.40), taken individually is the torque produced by an equivalent induction machine. However, in the BDFM, the cross coupling produces additional components of torque which must also be considered in the analysis.

B.3 Cross Coupling

Cross coupling is the coupling that occurs when rotor currents, induced by one stator winding, induce voltages in the other stator winding at that other winding's supply frequency. Cross coupling only occurs for some of the stator harmonics.

Depending on the sequence of the control-winding voltage, some of the cross coupled torque terms will produce steady-state torque and some will not. Cross coupling is briefly described in sections 3.3.6 and 1.2 with more mathematical detail given in section 3.4.

In order to determine which components of force contribute to steady-state torque, the frequency of the rotor current and stator flux density are added together, the sum set to zero, and the rotor speed is isolated. By association with the proper speed equation, a constraint on the primed harmonic numbers is determined. For the force term given by (B.26), steady-state torque is generated when

$$(\omega_2 - \lambda'\omega_R) + (\omega_1 - \kappa\omega_R) = 0 \tag{B.41}$$

which corresponds to a rotor speed of

$$\omega_R = \frac{\omega_1 + \omega_2}{\kappa + \lambda'} \tag{B.42}$$

Cross coupling will occur if $\lambda' = \lambda$ and the BDFM is excited with positive sequence excitation. For the force term given in (B.28), steady-state torque is produced when

$$(\omega_1 - \kappa'\omega_R) + (\omega_2 - \lambda\omega_R) = 0 \tag{B.43}$$

which corresponds to a rotor speed

$$\omega_R = \frac{\omega_1 + \omega_2}{\kappa' + \lambda} \tag{B.44}$$

Clearly, cross coupling will occur when $\kappa' = \kappa$. Substituting both of these constraints into the expressions for force given in (B.27) and (B.29) and simplifying, the torque due to positive sequence excitation may be expressed

$$T_{12} = -dw'\Re\left\{\sum_{\chi}\frac{3\mu_0}{gk}K^{\kappa}_{pR_n}K^{\kappa}_{sk}e^{-jky'_{0n}}\bar{C}^{\kappa}_{1}\bar{I}^{\lambda}_{R_n 2}\bar{I}_1\right\} \tag{B.45}$$

$$T_{21} = dw'\Re\left\{\sum_{\chi}\frac{3\mu_0}{gl}K^{\lambda}_{pR_n}K^{\lambda}_{sk}e^{-jly'_{0n}}\bar{C}^{\lambda}_{2}\bar{I}^{\kappa}_{R_n 1}\bar{I}_2\right\} \tag{B.46}$$

where χ represents the set of cross coupling harmonics (κ, λ) which must satisfy the constrain given in (3.113). Harmonics which do not satisfy this constraint result in the production of pulsating torque.

It can be shown that expressions for torque due to negative sequence excitation will be produced by the force components (B.26) and (B.28). After simplification,

$$T_{12} = -dw'\Re\left\{\sum_{\chi}\frac{3\mu_0}{gk}K^{\kappa}_{pR_n}K^{\kappa}_{sk}e^{jky'_{0n}}\bar{C}^{\prime\kappa *}_{1}\bar{I}^{\lambda}_{R_n 2}\bar{I}^{*}_{1}\right\} \tag{B.47}$$

$$T_{21} = dw'\Re\left\{\sum_{\chi}\frac{3\mu_0}{gl}K^{\lambda}_{pR_n}K^{\lambda}_{sk}e^{-jly'_{0n}}\bar{C}^{\prime\lambda *}_{2}\bar{I}^{\kappa}_{R_n 1}\bar{I}^{*}_{2}\right\} \tag{B.48}$$

where the summation index χ indicates that only those harmonics which satisfy (3.113) are included in the summation.

Appendix C

Resistance Measurements

In order to verify the inter-bar current model presented in Chapter 3, a rotor was constructed which promoted the bar to iron contact. Several different measurements were made on the rotor in order to determine the value of inter bar resistance between the bars and the iron.

The rotor is constructed of 36 bars evenly spaced around the circumference of the periphery. The rotor was skewed 10°, equivalent to one rotor slot. Because of the availability of materials and the lack of insulation, the rotor slot was larger than the rotor bar. Thus, skew was necessary in order to ensure a tight fit between the bars and the iron. A profile of a rotor bar is shown in Fig. C.1.

C.1 Bar Resistance

The resistance per unit length of a rotor bar was determined in two ways, by measurement and by calculation. In the measurements, a current was injected in one end of the bar and extracted from the other end. The voltage was measured between points a known distance apart. The data obtained was then used to calculate the resistance per unit length. Six different combinations of measuring and current injection points were used. Not only was the voltage measured at the point of injection, or near it, it was also measured between two points on the surface of the bar.

Using an injected current of 10 A, a value of 42.8 $\mu\Omega$ was measured for the

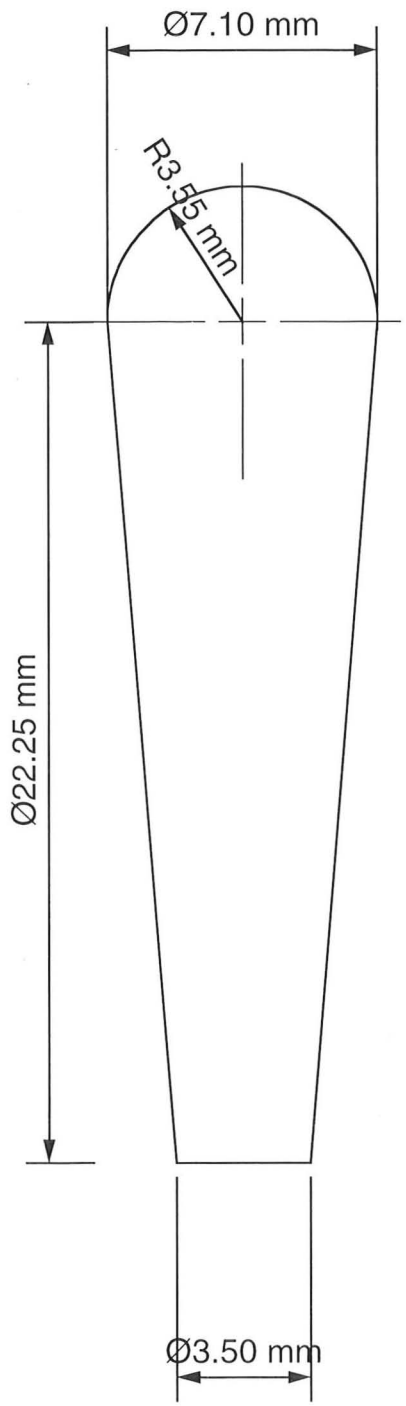

Figure C.1: Profile of a typical rotor bar used to fabricate the rotor.

sample rotor bar with a standard deviation of 1.87 $\mu\Omega$. Using 20 A, the resistance was measured to be 43.3 $\mu\Omega$ with a standard deviation of 1.64 $\mu\Omega$. This was well within the predicted random error due to the equipment of 3.1 $\mu\Omega$ for a 10 A current and 0.44 $\mu\Omega$ for a 20 A current.

The second method of resistance calculation involved using the density of copper and computing the resistance from the relationship,

$$R = \frac{\rho l}{A} \tag{C.1}$$

where ρ is the resistivity of the material, l is the length of the bar, and A is the cross sectional area of the bar. The area of the bar was computed based on the dimensions of the bar profile given in Fig. C.1 and by weighing the bar and using the density of copper to estimate the area. The area was calculated to be 118.4 ± 0.7 mm^2 using the density of copper and 118.8 ± 0.1 mm^2 by measurement. A value of 118.8 mm^2 is used since the measurement technique was subjected to less error. The final result is a resistance of 43.3 $\mu\Omega$ for the sample bar.

Based on the good agreement between the results achieved by both calculation and measurement, the measurement technique of applying a current and measuring the voltage was deemed acceptable. This technique was subsequently used to measure the resistance between adjacent rotor bars.

C.2 Resistance Between Adjacent Bars

C.2.1 Method

Once the rotor bars were inserted into the rotor and cut to the proper lengths to accept the end connections, measurements were made to determine the resistance between adjacent bars. There exist two different methods for applying current through the bars. The first method, illustrated in Fig. C.2, is to inject a current in one bar and extract it from the adjacent bar at the same end of the rotor. The second method, shown in Fig. C.3, is to inject current into a bar at one end and extract it from the adjacent bar at the other end of the rotor.

When performing the measurements, the voltage was measured in four locations, as illustrated in both Figs. C.2 and C.3. The two readings near each

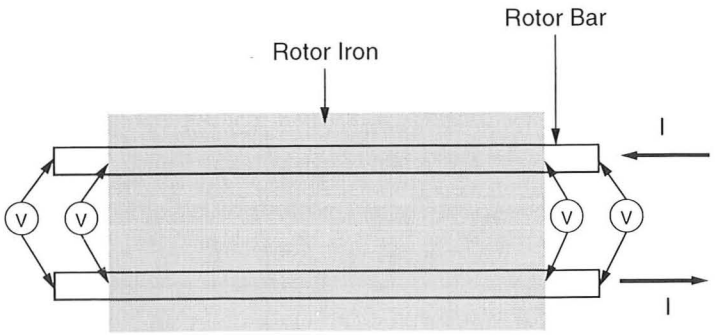

Figure C.2: The first method used in measuring the resistance between adjacent rotor bars showing the points where current is injected and extracted.

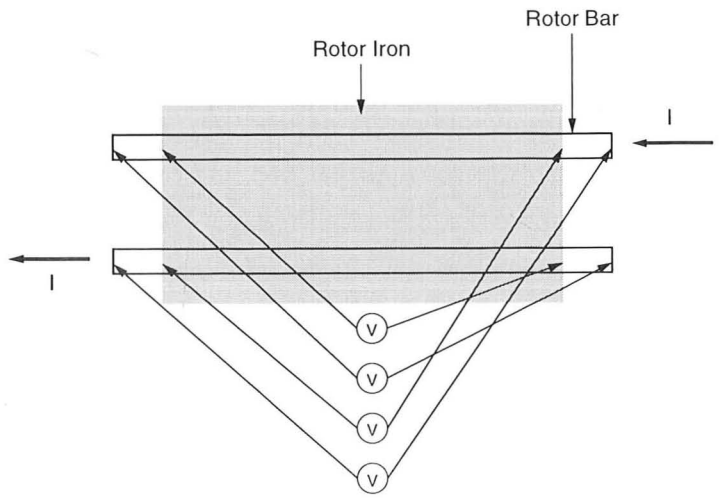

Figure C.3: The second method used in measuring the resistance between adjacent rotor bars showing the points where current is injected and extracted.

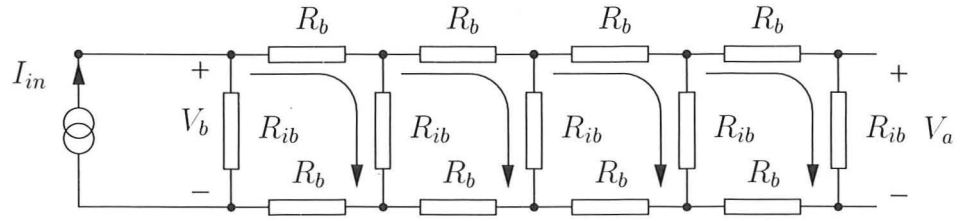

Figure C.4: Equivalent circuit used to determine the inter-bar resistance between adjacent bars when current is injected and extracted from adjacent bars at the same end of the rotor.

other are averaged, resulting in two sets of voltage readings. Using the voltage and current, the value of inter-bar resistance for a specific number of cuts can be determined.

C.2.2 Resistance Calculation

For the first method of measurement, the equivalent circuit shown in C.4 where V_a is the voltage measured opposite to where the current is injected, V_b is the voltage near the injection point, R_{ib} is the value of inter-bar resistance (five cuts assumed), and R_b is the resistance of each bar segment.

When the value of $R_{ib} \gg R_b$, the bar resistance may be neglected. In this case, $V_a = V_b$ and $R_{ib} = \frac{V_a}{IN_c}$, where N_c is the number of cuts. However, the measurements showed that the two voltages were much different from each other which meant that the value of the resistances in the equivalent circuit were similar in value. In this case, the calculation for R_{ib} becomes non-trivial.

In order to calculate R_{ib}, a set of mesh current equations is written using state variables defined

$$\mathbf{x}^{\mathbf{T}} = \begin{bmatrix} R_{ib} & I_2 & I_3 & I_4 & I_5 \end{bmatrix} \tag{C.2}$$

where the currents are those that flow clockwise in the "windows" of the equivalent circuit, numbered sequentially (starting with 2) from left to right, shown in

Fig.C.4. The set of mesh current equations forms a non-linear vector equation,

$$\begin{bmatrix} -Ix_1 - x_3x_1 + 2R_bx_2 + 2x_1x_2 \\ -x_1x_2 - x_4x_1 + 2R_bx_3 + 2x_1x_3 \\ -x_1x_3 - x_5x_1 + 2R_bx_4 + 2x_1x_4 \\ -x_1x_4 + 2R_bx_5 + 2x_1x_5 \\ x_1x_5 - V_a \end{bmatrix} = \mathbf{0} \tag{C.3}$$

This system of equations can be solved for $x_1 = R_{ib}$ by using Newton's Method (Taylor Series), which is widely known as the Newton-Raphson non-linear root finding algorithm:

$$\begin{gathered} \text{Guess } \mathbf{x}^0 \text{as an initial estimate of } \mathbf{x}^* \\ \text{Solve } \mathbf{F}'(\mathbf{x}^{k-1})\mathbf{z} = -\mathbf{F}(\mathbf{x}^{k-1}) \\ \text{Set } \mathbf{x}^{(k)} = \mathbf{x}^{(k-1)} + \mathbf{z} \end{gathered}$$

where $\mathbf{F}(\mathbf{x})$ is the matrix equation in (C.3) and $\mathbf{F}'(\mathbf{x})$ is the derivative of $\mathbf{F}(\mathbf{x})$.

If the value of V_b is used instead of V_a, then the last row of (C.3) is changed to

$$Ix_1 - x_2x_1 - V_b = 0 \tag{C.4}$$

The second method of measurement shown in Fig. C.3 can be represented by the equivalent circuit shown in Fig. C.4. For this situation, the vector equation is given as

$$\begin{bmatrix} 2R_bx_2 + 2x_1x_2 - x_1I - x_3x_1 - IR_b \\ 2R_bx_3 + 2x_1x_3 - x_2x_1 - x_4x_1 - IR_b \\ 2R_bx_4 + 2x_1x_4 - x_3x_1 - x_5x_1 - IR_b \\ 2R_bx_5 + 2x_1x_5 - x_4x_1 - IR_b \\ x_2R_b + x_3R_b + x_4R_b + x_5R_b + x_1x_2 - Ix_1 - V_a \end{bmatrix} = \mathbf{0} \tag{C.5}$$

If V_b is used instead of V_a the last row of the equation is changed to

$$x_2R_b + x_3R_b + x_4R_b + x_5R_b + x_1x_5 - V_b = 0 \tag{C.6}$$

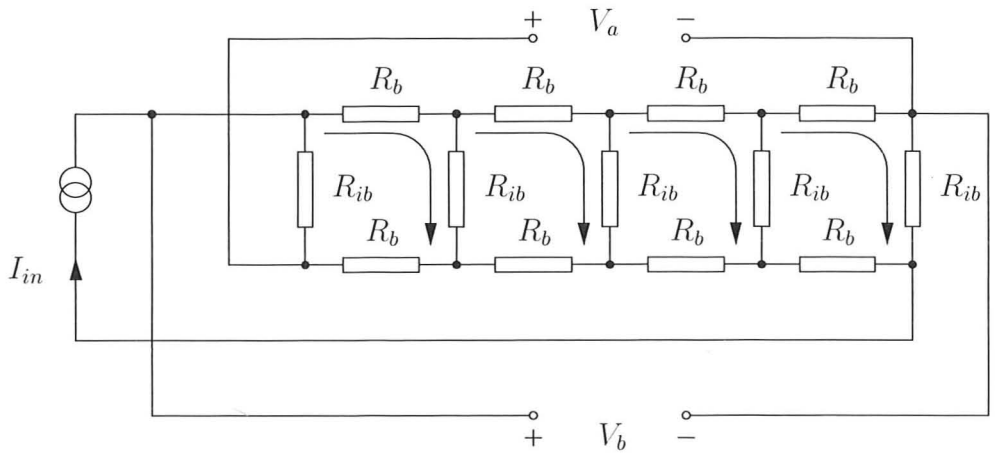

Figure C.5: Equivalent circuit used to determine the inter-bar resistance between adjacent bars when current is injected into one end of a bar and extracted from the other end of an adjacent bar.

Appendix D

Transformation Trigonometric Identities

The calculation of the different elements of the impedance matrix given in (2.48) involves the multiplication of a series of trigonometric functions. However, by using complex notation and simplifying, certain trigonometric relationships have been determined.

For the following, $N_n = P_1 + P_2$ is the number of nests, which is also the number of elements in the series as well as the number of phases in the rotor loop system. Each rotor nest is displaced $\frac{2\pi}{N_n}$ mechanical radian from its neighbour. Hence, the electrical angles between rotor nests are

$$\beta_1 = -P_1 \frac{2\pi}{N_n} = -P_1 \frac{2\pi}{P_1 + P_2} \tag{D.1}$$

$$\beta_2 = -P_2 \frac{2\pi}{N_n} = -P_2 \frac{2\pi}{P_1 + P_2} \tag{D.2}$$

The following relationships hold:

$$\cos \beta_1 = \cos \beta_2 \tag{D.3}$$

$$\sin \beta_1 = -\sin \beta_2 \tag{D.4}$$

$$\sum_{n=1}^{N_n} \cos(n-1)\beta_1 \cos(n-1)\beta_2 = \frac{N_n}{2} \tag{D.5}$$

$$\sum_{n=1}^{N_n} \sin(n-1)\beta_1 \sin(n-1)\beta_2 = -\frac{N_n}{2} \tag{D.6}$$

$$\sum_{n=1}^{N_n} \cos^2(n-1)\beta_1 = \frac{N_n}{2} \tag{D.7}$$

$$\sum_{n=1}^{N_n} \cos^2(n-1)\beta_2 = \frac{N_n}{2} \tag{D.8}$$

$$\sum_{n=1}^{N_n} \sin(n-1)\beta_1 \cos(n-1)\beta_1 = 0 \tag{D.9}$$

$$\sum_{n=1}^{N_n} \sin(n-1)\beta_2 \cos(n-1)\beta_2 = 0 \tag{D.10}$$

$$\sum_{n=1}^{N_n} \sin(n-1)\beta_1 \cos(n-1)\beta_2 = 0 \tag{D.11}$$

$$\sum_{n=1}^{N_n} \cos(n-1)\beta_1 \sin(n-1)\beta_2 = 0 \tag{D.12}$$

$$\sum_{n=0}^{N_n-1} \cos n\beta_1 \left(\cos(n-1)\beta_1 + \cos(n+1)\beta_1\right) = N_n \cos\beta_1 = N_n \cos\beta_2 \tag{D.13}$$

$$\sum_{n=0}^{N_n-1} \cos n\beta_2 \left(\cos(n-1)\beta_2 + \cos(n+1)\beta_2\right) = N_n \cos\beta_1 = N_n \cos\beta_2 \tag{D.14}$$

$$\sum_{n=0}^{N_n-1} \sin n\beta_1 \left(\sin(n-1)\beta_1 + \sin(n+1)\beta_1\right) = N_n \cos\beta_1 = N_n \cos\beta_2 \tag{D.15}$$

$$\sum_{n=0}^{N_n-1} \sin n\beta_2 \left(\sin(n-1)\beta_2 + \sin(n+1)\beta_2\right) = N_n \cos\beta_1 = N_n \cos\beta_2 \tag{D.16}$$

$$\sum_{n=0}^{N_n-1} \sin n\beta_1 \left(\cos(n-1)\beta_1 + \cos(n+1)\beta_1\right) = 0 \tag{D.17}$$

$$\sum_{n=0}^{N_n-1} \cos n\beta_1 \left(\sin(n-1)\beta_1 + \sin(n+1)\beta_1\right) = 0 \tag{D.18}$$

$$\sum_{n=0}^{N_n-1} \sin n\beta_2 \left(\cos(n-1)\beta_2 + \cos(n+1)\beta_2\right) = 0 \tag{D.19}$$

$$\sum_{n=0}^{N_n-1} \cos n\beta_2 \left(\sin(n-1)\beta_2 + \sin(n+1)\beta_2\right) = 0 \tag{D.20}$$

Other relationships that prove useful come directly from [29] and are given here for reference. For x and y arbitrary angles:

$$\sum_{n=1}^{3} \cos\left(x - (n-1)\frac{2\pi}{3}\right) = 0 \tag{D.21}$$

$$\sum_{n=1}^{3} \sin\left(x - (n-1)\frac{2\pi}{3}\right) = 0 \tag{D.22}$$

$$\sum_{n=1}^{3} \cos^2\left(x - (n-1)\frac{2\pi}{3}\right) = \frac{3}{2} \tag{D.23}$$

$$\sum_{n=1}^{3} \sin^2\left(x - (n-1)\frac{2\pi}{3}\right) = \frac{3}{2} \tag{D.24}$$

$$\sum_{n=1}^{3} \sin\left(x - (n-1)\frac{2\pi}{3}\right) \cos\left(x - (n-1)\frac{2\pi}{3}\right) = 0 \tag{D.25}$$

$$\sum_{n=1}^{3} \sin\left(x - (n-1)\frac{2\pi}{3}\right) \cos\left(y - (n-1)\frac{2\pi}{3}\right) = \frac{3}{2}\sin(x-y) \tag{D.26}$$

$$\sum_{n=1}^{3} \sin\left(x-(n-1)\frac{2\pi}{3}\right)\sin\left(y-(n-1)\frac{2\pi}{3}\right)=\frac{3}{2}\cos(x-y) \tag{D.27}$$

$$\sum_{n=1}^{3} \cos\left(x-(n-1)\frac{2\pi}{3}\right)\sin\left(y-(n-1)\frac{2\pi}{3}\right)=-\frac{3}{2}\sin(x-y) \tag{D.28}$$

$$\sum_{n=1}^{3} \cos\left(x-(n-1)\frac{2\pi}{3}\right)\cos\left(y-(n-1)\frac{2\pi}{3}\right)=\frac{3}{2}\cos(x-y) \tag{D.29}$$

$$\sum_{n=1}^{3} \sin\left(x+(n-1)\frac{2\pi}{3}\right)\cos\left(y-(n-1)\frac{2\pi}{3}\right)=\frac{3}{2}\sin(x+y) \tag{D.30}$$

$$\sum_{n=1}^{3} \sin\left(x+(n-1)\frac{2\pi}{3}\right)\sin\left(y-(n-1)\frac{2\pi}{3}\right)=-\frac{3}{2}\cos(x+y) \tag{D.31}$$

$$\sum_{n=1}^{3} \cos\left(x+(n-1)\frac{2\pi}{3}\right)\sin\left(y-(n-1)\frac{2\pi}{3}\right)=\frac{3}{2}\sin(x+y) \tag{D.32}$$

$$\sum_{n=1}^{3} \cos\left(x+(n-1)\frac{2\pi}{3}\right)\cos\left(y-(n-1)\frac{2\pi}{3}\right)=\frac{3}{2}\cos(x+y) \tag{D.33}$$

Appendix E

Equivalent Rotor Current in the *dq* Model

The rotor currents in the *dq* model of Chapter 2 consist of two components. One component of currents is induced by the first stator winding and the the other is induced by the second winding. For analyses where it is unimportant to calculate the separate effects due to direct and cross coupling, it is worthwhile combining the rotor currents into an equivalent rotor current, thus reducing the number of equations.

E.1 Voltage Equation

Using the nomenclature defined in Chapter 2, the currents in the i-th rotor loop system system can be related to their two axis quantities by the relationship,

$$\mathbf{i_{R_i}} = \mathbf{C^T_{R1_i}} \mathbf{i'_{R1_i}} + \mathbf{C^T_{R2_i}} \mathbf{i'_{R2_i}} \tag{E.1}$$

where use is made of the general transformation relationship given in (2.21). Expanding (E.1),

$$\begin{bmatrix} (i_{R_i})_1 \\ (i_{R_i})_2 \\ \vdots \\ (i_{R_i})_{N_n} \end{bmatrix} = \sqrt{\frac{2}{N_n}} \begin{bmatrix} 1 & 0 \\ \cos\beta_1 & \sin\beta_1 \\ \vdots & \vdots \\ \cos(N_n-1)\beta_1 & \sin(N_n-1)\beta_1 \end{bmatrix} \begin{bmatrix} i_{qR1_i} \\ i_{dR1_i} \end{bmatrix}$$
$$+ \sqrt{\frac{2}{N_n}} \begin{bmatrix} 1 & 0 \\ \cos\beta_2 & \sin\beta_2 \\ \vdots & \vdots \\ \cos(N_n-1)\beta_2 & \sin(N_n-1)\beta_2 \end{bmatrix} \begin{bmatrix} i_{qR2_i} \\ i_{dR2_i} \end{bmatrix} \quad \text{(E.2)}$$

By inspection, the first row of the equation is given as

$$(i_{R_i})_1 = \sqrt{\frac{2}{N_n}}(i_{qR1_i} + i_{qR2_i}) \quad \text{(E.3)}$$

Combining the q axis currents into one quantity leads to the definition for an equivalent q axis current,

$$i_{qR_i} \equiv i_{qR1_i} + i_{qR2_i} \quad \text{(E.4)}$$

By a similar approach, the second row of (E.2) is given as

$$(i_{R_i})_2 = \sqrt{\frac{2}{N_n}}(\cos\beta_1 i_{qR_i} + \sin\beta_1(i_{dR1_i} - i_{dR2_i})) \quad \text{(E.5)}$$

where use is made of the the definition for the q axis rotor current in (E.4) and the trigonometric relationships given in (D.3) and (D.4). This leads to the definition of the d axis rotor current,

$$i_{dR_i} = i_{dR1_i} - i_{dR2_i} \quad \text{(E.6)}$$

Equations (E.4) and (E.6) combine the two components of rotor current into one equivalent rotor current that includes the effects due to both windings. The voltage equation can now be written as

$$\begin{bmatrix} \mathbf{v}'_1 \\ \mathbf{v}'_2 \\ \mathbf{0} \end{bmatrix} = \begin{bmatrix} \mathbf{Z}'_{11} & \mathbf{0} & \mathbf{Z}'_{1R} \\ \mathbf{0} & \mathbf{Z}'_{22} & \mathbf{Z}'_{2R} \\ \mathbf{Z}'_{R1} & \mathbf{Z}'_{R2} & \mathbf{Z}'_{RR} \end{bmatrix} \begin{bmatrix} \mathbf{i}'_1 \\ \mathbf{i}'_2 \\ \mathbf{i}'_R \end{bmatrix} \quad \text{(E.7)}$$

where each of the matrices representing the coupling have been combined into equivalent matrices.

Many of the matrices are unchanged from those given in Chapter 2. However, the matrices $\mathbf{Z'_{1R1}}$ and $\mathbf{Z'_{1R2}}$ have been combined into an equivalent matrix, $\mathbf{Z'_{1R}}$. Similarly, the matrices $\mathbf{Z'_{2R2}}$ and $\mathbf{Z'_{2R1}}$ have been combined into an equivalent matrix, $\mathbf{Z'_{2R}}$. Even though the sign of some of the matrix elements changes, the form of the matrices remains the same. For the i-th rotor loop system,

$$\mathbf{Z'_{1R_i}} = \begin{bmatrix} M'_{1R_i}\frac{d}{dt} \\ P_1\omega_R M'_{1R_i} - P_1\omega_R M'_{1R_i} \quad M'_{1R_i}\frac{d}{dt} \end{bmatrix} \tag{E.8}$$

$$\mathbf{Z'_{2R_i}} = \begin{bmatrix} M'_{2R_i}\frac{d}{dt} \\ -P_2\omega_R M'_{2R_i} - P_1\omega_R M'_{2R_i} \quad -M'_{2R_i}\frac{d}{dt} \end{bmatrix} \tag{E.9}$$

This alternative system of equations can be used in transient analysis. The two components of rotor currents have been combined into one equivalent rotor current. This is at the cost of losing the identity of the direct and cross coupled quantities with the benefit being a reduced number of equations.

E.2 Torque Equation

The torque of the BDFM can be expressed in terms of the single equivalent rotor current by using (E.4) and (E.6). After considerable simplification of (2.82), the torque may be expressed

$$\begin{aligned} T_e = P_1 \sum_{i=1}^{N_l} M_{1R_i} \left(i_{q1}(i_{dR1_i} - i_{dR2_i}) - i_{d1}(i_{qR1_i} + i_{qR2_i})\right) \\ - P_2 \sum_{i=1}^{N_l} M_{2R_i} \left(i_{q2}(i_{dR1_i} - i_{dR2_i}) + i_{d2}(i_{qR1_i} + i_{qR2_i})\right) \end{aligned} \tag{E.10}$$

Substituting for the equivalent rotor currents,

$$T_e = P_1 \sum_{i=1}^{N_l} M_{1R_i} \left(i_{q1} i_{dR_i} - i_{d1} i_{qR_i}\right) - P_2 \sum_{i=1}^{N_l} M_{2R_i} \left(i_{q2} i_{dR_i} + i_{d2} i_{qR_i}\right) \tag{E.11}$$

This equation is used in conjunction with the voltage equation given in the previous section, thus providing a complete transient model of the BDFM.

Bibliography

[1] A. K. Wallace, R. Speé, and H. K. Lauw, "The potential of brushless doubly-fed machines for adjustable speed drives," in *Proceedings of the IEEE Industry Applications Society Pulp and Paper Industry Annual Meeting*, pp. 45–50, June 1990.

[2] L. J. Hunt, "A new type of induction motor," *Journal of the Institution of Electrical Engineers*, vol. 39, pp. 648–667, 1907.

[3] L. J. Hunt, "The "cascade" induction motor," *Journal of the Institution of Electrical Engineers*, vol. 52, pp. 406–426, 1914.

[4] F. Creedy, "Some developments in multi-speed cascade induction motors," *Journal of the Institution of Electrical Engineers*, vol. 59, pp. 511–521, 1921.

[5] B. H. Smith, "Theory and performance of a twin stator induction machine," *IEEE Transactions of PAS*, vol. PAS-85, pp. 123–131, Feb. 1966.

[6] B. H. Smith, "Synchronous behavior of doubly-fed twin stator induction machine," *IEEE Transactions of PAS*, vol. PAS-86, pp. 1227–1236, Oct. 1967.

[7] C. D. Cook and B. H. Smith, "Stability and stabilisation of doubly-fed single-frame cascade induction machines," *Proceedings of IEE*, vol. 126, pp. 1168–1174, Nov. 1979.

[8] B. S. P. Perera and B. H. Smith, "Experimental determination of equivalent circuit parameters of single-frame cascaded induction machines having phase-wound rotors," in *Electric Energy Conference 1987*, (Adelaide), Oct. 1987.

[9] B. S. P. Perera and B. H. Smith, "A novel model for single-frame cascaded induction machines having a multi-circuit rotor winding," *Electric Machines and Power Systems*, vol. 21, pp. 783–802, 1993.

[10] A. R. W. Broadway and L. Burbridge, "Self-cascaded machine: a low-speed motor or high-frequency brushless alternator," *Proceedings of the Institution of Electrical Engineers*, vol. 117, pp. 1277–1290, 1970.

[11] A. Kusko and C. Somuah, "Speed control of a single-frame cascade induction motor with slip-power pump back," *IEEE Transactions on Industry Applications*, vol. IA-14, no. 2, pp. 97–105, 1978.

[12] A. K. Wallace, R. Speé, and H. K. Lauw, "Dynamic modeling of the brushless doubly-fed machine," in *Proceedings of the IEEE Industry Applications Society Annual Meeting*, pp. 329–334, Oct. 1989.

[13] A. K. Wallace, R. Speé, and H. K. Lauw, "Performance simulation of the brushless doubly-fed machines," in *Proceedings of the IEEE Industry Applications Society Annual Meeting*, pp. 738–743, Oct. 1989.

[14] R. Li, A. K. Wallace, R. Speé, and Y. Wang, "Two axis model development of cage rotor brushless doubly-fed machines," *IEEE Transactions on Energy Conversion*, vol. 6, pp. 453–460, Sept. 1991.

[15] R. Li, A. K. Wallace, and R. Speé, "Dynamic simulation of brushless doubly-fed machines," *IEEE Transactions on Energy Conversion*, vol. 6, pp. 445–452, 1991.

[16] R. Li, R. Speé, A. K. Wallace, and G. C. Alexander, "Synchronous drive performance of brushless doubly-fed machines," *IEEE Transactions on Industry Applications*, pp. 963–970, July/August 1991.

[17] H. K. Lauw, J. B. Klaasens, N. G. Butler, and D. B. Seely, "Variable-speed generation with the series resonant converter," *IEEE Transactions on Energy Conversion*, vol. 3, pp. 755–764, 1990.

[18] V. Javadekar, D. K. Ravi, R. Sepé, and A. K. Wallace, "A variable-speed brushless doubly-fed automotive alternator," in *Proceedings of the European Power Electronics Conference*, (Florence, Italy), pp. 99–103, 1991.

[19] A. K. Wallace and R. Speé, "Research, development and applications studies for brushless doubly-fed machines," in *Proceedings of teh Second International Conference on Electrical Machines and Drives*, (Sao Paulo, Brazil), pp. 41–60, 1991.

[20] A. K. Wallace, M. S. Boger, and E. Wiedenbrüg, "Medium- and high-voltage, low-speed drives using low-voltage IGBT converters," in *IEEE-ISIE*, (Athens, Greece), July 1995.

[21] M. S. Boger, A. K. Wallace, R. Speé, and R. Li, "General pole number model of the brushless doubly-fed machine," in *Proceedings of the IEEE Industry Applications Society Annual Meeting*, (Denver), Oct. 1994.

[22] M. S. Boger, A. K. Wallace, A. Kemp, and E. Wiedenbrüg, "The investigation of rotor current distributions in brushless doubly-fed machines," in *Proceedings of the IEEE Industry Applications Society Annual Meeting*, (Orlando, FL), October 1996.

[23] S. Williamson, A. C. Ferreira, and A. K. Wallace, "Generalised theory of the brushless doubly-fed machine. Part 1: Analysis," *IEE Proc.-Electr. Power Appl.*, pp. 111–122, Mar. 1997.

[24] S. Williamson and A. C. Ferreira, "Generalised theory of the brushless doubly-fed machine. part 2: Model verification and performance," *IEE Proc.-Electr. Power Appl.*, pp. 123–129, Mar. 1997.

[25] S. Williamson, "Power factor improvement in cage-rotor induction motors," *Proceedings of the IEEE*, vol. 130, no. 2, pp. 121–129, 1983.

[26] S. Williamson and E. R. Laithwaite, "Generalised harmonic analysis for the stead-state performance of sinusoidally excited cage induction motors," *Proc. IEE Electr. Power Appl.*, vol. 132, no. 3, pp. 157–163, 1985.

[27] S. W. Williamson, R. C. Healey, and J. D. Loyd, "Rotor cage anomalies and unbalanced magnetic pull in single phase induction motors. Part I. Analysis," in *Proceedings of the IEEE Industry Applications Society Annual Meeting*, (San Diego, CA), Oct. 1996.

[28] S. W. Williamson, R. C. Healey, and J. Tevaarwerk, "Rotor cage anomalies and unbalanced magnetic pull in single phase induction motors. Part II. Experimental and theoretical studies," in *Proceedings of the IEEE Industry Applications Society Annual Meeting*, (San Diego, CA), Oct. 1996.

[29] P. C. Krause, *Analysis of Electric Machinery.* McGraw Hill, 1986.

[30] C. V. Jones, *The Unified Theory of Electrical Machines.* London: Butterworths, 1967.

[31] A. C. Ferreira, *Analysis of Brushless Doubly-Fed Induction Machines.* PhD thesis, University of Cambridge, Sept. 1996.

[32] D. Gersh, A. C. Smith, and A. Samuelson, "Measurement of inter-bar resistancein cage rotors," in *Eighth International Conference on Electrical Machines and Drives*, (Cambridge, UK), Sept. 1997.

[33] B. Gorti, D. Zhou, G. C. Alexander, R. Speé, and A. K. Wallace, "Development of a brushless doubly-fed machine for a limited-speed pump drive in a waste water treatment plant," in *Proceedings of the IEEE Industry Applications Society Annual Meeting*, (Denver, CO), pp. 523–529, Oct. 1994.

[34] P. Lorraine, D. Corson, and F. Lorrain, *Electromagnetic Fields and Waves.* New York: W. H. Freeman and Company, third ed., 1988.